The role of RIPK1 auto-phosphorylation at S166 in cell death and inflammatory signaling

Inaugural-Dissertation

zur

Erlangung des Doktorgrades

der Mathematisch-Naturwissenschaftlichen Fakultät

der Universität zu Köln

vorgelegt von

Lucie Henriette Laurien

aus Braunschweig

Köln, 2021

Berichterstatter:

Prof. Dr. Manolis Pasparakis

Prof. Dr. Hamid Kashkar

Prof. Dr. Matthias Hammerschmidt

Tag der mündlichen Prüfung: 08.03.21

Zusammenfassung

Receptor-Interacting Protein Kinase 1 (RIPK1) ist ein Schlüsselprotein in Signalwegen der angeborenen Immunantwort, die in Folge von Aktivierung verschiedener Rezeptoren wie Tumor necrosis factor receptor 1 (TNFR1) und Toll-like receptors (TLRs) ablaufen. In diesen Signalwegen fördert RIPK1 die Lebensfähigkeit von Zellen sowie Gewebshomöostase unabhängig von seiner Kinaseaktivität, wobei seine katalytische Aktivität Zelltod vermittelt. Von Bedeutung ist, dass sich die Kinaseaktivität von RIPK1 als Treiber von Zelltod und Entzündung in Mausmodellen herausgestellt hat und mit der Pathogenese von humanen entzündlichen und degenerativen Erkrankungen in Verbindung gebracht wird. RIPK1 autophosphoryliert an mehreren Aminosäureresten, zu denen Serin (S) 14/15, S161, S166 und Threonin (T)169 gehört und zur Zeit nimmt man an, dass Autophosphorylierung die hauptsächliche Funktion der Kinaseaktivität von RIPK1 ist. Obwohl Autophosphorylierung an Stelle 166 routinemäßig als Biomarker für RIPK1 Aktivierung eingesetzt wird, wurden die funktionelle Bedeutung und physiologische Relevanz dieser Position bisher nicht untersucht. Ziel dieser Arbeit war, die Rolle der RIPK1-Autophosphorylierung an S166 für die RIPK1-vermittelte Signalübertragung zu untersuchen. Zu diesem Zweck wurden Mäuse generiert, die RIPK1 mit nicht-phosphorylierbarer Serin zu Alanin Mutation an Position 166 vom endogenen *Ripk1*-Locus exprimieren (*Ripk1*$^{S166A/S166A}$-Mäuse). Wir konnten zeigen, dass die RIPK1S166A-Mutation die Kinaseaktivitäts-unabhängige Funktion von RIPK1 nicht beeinträchtigt, um pro-entzündliche und überlebensfördernde Signale stromabwärts von TNFR1, TLR 3 und 4 zu induzieren. Andererseits beobachten wir eine teilweise Inhibierung der TNFR1-induzierten, RIPK1-Kinaseaktivitäts-abhängigen Apoptose und Nekroptose sowie der TLR 3- und 4-induzierte Nekroptose in *Ripk1*$^{S166A/S166A}$-Zellen, was zeigt, dass die RIPK1-Autophosphorylierung an Position S166 die von der katalytischen Aktivität abhängige Funktion von RIPK1, Zelltod zu induzieren, steuert. Bemerkenswerterweise schützte die RIPK1S166A-Mutation Mäuse vollständig vor RIPK1 Kinaseaktivitäts-abhängigen entzündlichen Pathologien in Dickdarm, Leber und Haut und verringerte die Letalität in einem Modell systemischer Entzündung, was zeigt, dass in vivo die RIPK1-Autophosphorylierung an S166 essentiell ist, Zelltod und Entzündung zu fördern. In Bezug auf den zugrundeliegenden Mechanismus, beobachteten wir eine Inhibierung der Bildung von Zelltod-induzierenden Komplexen stromabwärts von TNFR1 sowie TLR 3 und 4 durch die RIPK1S166A-Mutation, was zeigt, dass die Autophosphorylierung an S166 die Einfügung von RIPK1 in zytotoxische Komplexe ermöglicht. Darüber hinaus legen unsere Ergebnisse nahe, dass die RIPK1-Autophosphorylierung an S166 als Treiber der Kinaseaktivität wirkt und die Autophosphorylierung an anderen Stellen erleichtert. Zusammengenommen zeigen die in dieser Arbeit präsentierten Daten, dass die Autophosphorylierung an S166 die RIPK1-

Kinaseaktivität lizenziert die nachgeschaltete Signalübertragung zu induzieren und den Zelltod zu fördern. Daher rechtfertigen unsere Ergebnisse die Verwendung der S166-Phosphorylierung als Marker für die Aktivierung von RIPK1, was die Gliederung menschlicher Patienten unterstützen kann, die von einer Behandlung mit RIPK1-Kinase-Inhibitoren profitieren können.

Abstract

Receptor-Interacting Protein Kinase 1 (RIPK1) functions as a key player downstream of innate immune receptors such as Tumor necrosis factor receptor 1 (TNFR1) and Toll-like receptors (TLRs). In these signaling pathways, RIPK1 promotes cell survival and tissue homeostasis in a manner independent of its catalytic function, whereas its kinase activity mediates cell death. Importantly, RIPK1 kinase activity has emerged as a driver of cell death and inflammation in mouse models and has been implicated in the pathogenesis of human inflammatory and degenerative diseases. RIPK1 auto-phosphorylates at multiple sites, including Serine (S) 14/15, S161, S166 and Threonine (T)169 and to date, auto-phosphorylation is believed to be the main function of its kinase activity. Whereas auto-phosphorylation at S166 is routinely used as a biomarker for RIPK1 activation, its functional importance and physiological relevance have not been investigated. In this work, we aimed to shed light on the role of RIPK1 auto-phosphorylation at S166 for RIPK1-mediated signaling. To this aim, we generated mice expressing RIPK1 with non-phosphorylatable serine to alanine mutation at position 166 from the endogenous *Ripk1* locus (*Ripk1*$^{S166A/S166A}$ mice). We show that RIPK1S166A mutation does not impair the kinase activity-independent function of RIPK1 to induce pro-inflammatory and pro-survival signaling downstream of TNFR1, TLR 3 and 4. On the other hand, we observed a partial protection from TNFR1-induced, RIPK1 kinase activity-dependent apoptosis and necroptosis as well as from TLR 3- and 4-induced necroptosis in *Ripk1*$^{S166A/S166A}$ cells, showing that RIPK1 auto-phosphorylation at S166 drives its catalytic activity-dependent function to induce cell death. Strikingly, RIPK1S166A mutation completely protected mice from RIPK1 kinase activity-dependent inflammatory pathologies in the colon, liver and skin and decreased lethality in a model of systemic inflammation, showing that in vivo, RIPK1 auto-phosphorylation at S166 is essential to drive cell death and inflammation. Mechanistically, RIPK1S166A mutation inhibited the formation of cell death-inducing complexes downstream of TNFR1 as well as TLR 3 and 4, demonstrating that auto-phosphorylation at S166 enables engagement of RIPK1 in cytotoxic complexes. Furthermore, our data suggest that RIPK1 auto-phosphorylation at S166 acts as a driver of kinase activity and facilitates auto-phosphorylation at other sites. Taken together, the data presented in this thesis show that auto-phosphorylation at S166 licenses RIPK1 kinase activity to induce downstream signaling and promote cell death. Therefore, our results warrant the use of S166 phosphorylation as a marker for RIPK1 activation, which can aid in the stratification of human patients that may benefit from treatment with RIPK1 kinase inhibitors.

Table of contents

Abbreviations

IκBα	Inhibitor of NF-κB alpha
A20	Tumor necrosis factor alpha induced protein 3
Alfp	α-fetoprotein enhancer
ALS	Amyotrophic lateral sclerosis
BMDMs	Bone marrow-derived macrophages
cFLIP	Cellular FLICE-like inhibitory protein
CHX	Cycloheximide
cIAP 1/2	Cellular inhibitor of apoptosis protein 1/2
Cre	Causes recombination
CRISPR	Clustered regularly interspaced short palindromic repeats
CYLD	Cylindromatosis
DD	Death domain
ddH_20	Double-distilled water
DED	Death effector domain
DFs	Dermal fibroblasts
DMEM	Dulbecco's Modified Eagle Medium
DMSO	Dimethyl sulfoxide
DNA	Desoxyribonucleic acid
EDTA	Etylene Diamine Tetraacetate
ERK	Extracellular signal-regulated kinase
FADD	Fas-associated protein with death domain
HCC	Hepatocellular carcinoma
HEPES	2-[4-(2-hydroxyethyl)piperazin-1-yl]ethanesulfonic acid
HOIL-1	Heme-Oxidized IRP2 ubiquitin ligase 1 homolog
HOIP	HOIL-1 interacting protein
HRP	Horseradish peroxidase
IHC	Immunohistochemistry
IKK1/2	IκB kinase 1/2
IRAK	Interleukin-1 receptor associated kinase
JNK	c-Jun N-terminal kinase
LFs	Lung fibroblasts
LPC	Liver parenchymal cell
LUBAC	Linear ubiquitin chain assembly complex
MAPK	Mitogen-activated protein kinase
MEFs	Murine embryonic fibroblasts

MLKL	Mixed lineage kinase like
MyD88	Myeloid differentiation primary response 88
Nec-1s	Necrostatin 1s
NEMO	Nuclear factor-κB essential modulator
NF-κB	Nuclear factor “kappa-light-chain-enhancer” of activated B cells
p38	p38 mitogen-activated protein kinase
PCR	Polymerase chain reaction
PRR	Pattern recognition receptor
RHIM	RIP homotypic interaction motif
RIPK1/3	Receptor-Interacting Protein Kinase 1/3
RNA	Ribonucleic acid
SDS	Sodium dodecyl sulfate
SHARPIN	SHANK associated RH domain interactor
SMAC	Second mitochondrial activator of caspase
TAB 2/3	TAK1-binding protein 2/3
TAK1	Transforming growth factor beta-activated kinase 1
TBK1	TANK-binding kinase 1
TEMED	Tetramethylethylenediamine
Tg	transgenic
TLR	Toll-like receptor
TNF	Tumor necrosis factor
TNFR1	Tumor necrosis factor receptor 1
TRADD	Tumor necrosis factor receptor type1-associated death domain protein
TRAF2	TNF receptor-associated factor 2
TRIF	TIR-domain-containing adapter-inducing interferon-β
Wt	Wild type
XIAP	X-linked inhibitor of apoptosis
ZBP1	Z-DNA-binding protein 1
zVAD-fmk	carbobenzoxy-valyl-alanyl-aspartyl-[O-methyl]-fluoromethylketone

Abbreviations of units

%	percent
°C	Degree Celsius
A	Ampere
bp	base pair
G, mg, μg, ng	gram, milligram, microgram, nanogram
h, min, sec	hours, minutes, seconds
kDa	kilo Dalton
l, ml, μl	liter, milliliter, microliter
M, mM, μM, nM	molar, millimolar, micromolar, nanomolar
rpm	rounds per minute
V	Volt

Table of Figures

List of Tables

1. Introduction

1.1 Cell death and its role in Inflammation

To cope with threats such as injury and infection, organisms rely on well-coordinated immune responses. Inflammation is an integral part of the innate immune response that serves the defense against pathogens or tissue damage and involves the action of immune cells, blood vessels and molecular mediators. While the physiological purpose of an inflammatory reaction is protection from infection or restoration of injury, sustained inflammation can lead to tissue damage. In addition, tissue inflammation has early on been described to be accompanied by cell death (Wallach et al., 2014).

Inflammation is initiated by resident immune cells such as macrophages and neutrophils that express pattern recognition receptors (PRRs) which sense molecular motifs associated with damage or infection, termed damage-associated molecular patterns (DAMPs) and pathogen-associated molecular patterns (PAMPs), respectively (Kumar et al., 2011; Takeuchi and Akira, 2010). Downstream of PRRs, signaling pathways activate transcriptional programs, that serve the induction of inflammatory mediators, such as cytokines and chemokines. These small proteins in turn act on surface receptors on their target cells to propagate the inflammatory response and often form amplification loops that ramp up the expression of inflammatory messengers. Of particular importance for the induction of inflammatory as well as pro-survival pathways are the family of mitogen activated protein kinases (MAPKs) and the transcription factor nuclear factor 'kappa-light-chain-enhancer' of activated B-cells (NF-κB) (Kumar et al., 2011; Zhang et al., 2017a) (MAPK reference). In order to evade host immunity, pathogens have on the other hand evolved strategies to inhibit innate immune signaling pathways and stall immune reactions (Reddick and Alto, 2014). In this case, an infected cell becomes a double-liability for the host as it is restrained from inducing an inflammatory response and furthermore serves as a replicative niche for the pathogen. Within the co-evolution of pathogen and host immunity, signaling pathways have evolved ways to allow for elimination of an infected cell. In keeping with this concept, besides inducing pro-inflammatory and pro-survival signaling, many innate immune receptors can also trigger cell death (Pasparakis and Vandenabeele, 2015; Peltzer and Walczak, 2019). Furthermore, cell death is considered to play a role in promoting tissue repair and homeostasis by influencing the immune response (Legrand et al., 2019).

Conclusively, rather than being only a secondary, passive consequence of inflammation, cell death has emerged as an active modulator of the immune response initiated in response to cellular stress (Green, 2019; Legrand et al., 2019).

1.2 Regulated cell death as trigger of immune responses

Cells may undergo various forms of cell death, which have been classified according to morphological, biochemical and functional properties. Apoptosis is the prime example and earliest recognized form of a molecularly controlled, regulated type of cell death (Kerr et al., 1972; Pasparakis and Vandenabeele, 2015). This form of cell death has important functions in development, tissue homeostasis as well as in the immune system. Morphologically, apoptosis is characterized by a regulated disassembly of the cell, involving cytoplasmic shrinkage, chromatin condensation, nuclear fragmentation, blebbing of the plasma membrane and apoptotic body formation (Pasparakis and Vandenabeele, 2015). Thereby, apoptosis is in its morphology distinct from necrosis, a form of cell death that is characterized by swelling of organelles, cellular swelling and permeabilization of the plasma membrane (Pasparakis and Vandenabeele, 2015). Based on its “violent” morphology, necrosis has long been considered an uncontrolled, passive or “accidental cell death” (Pasparakis and Vandenabeele, 2015; Wallach et al., 2014) caused by external factors such as injury or trauma. It later became clear that there are multiple forms of necrotic cell death that occur in a regulated manner, such as necroptosis, pyroptosis and ferroptosis.

Dying cells in a tissue trigger effects in their surrounding which can include the compensatory proliferation of neighboring cells, as well as the induction or inhibition of an immune response (Green, 2019). In context of the latter, cell death that triggers an adaptive immune response is described as immunogenic, while cell death that triggers an innate inflammatory response is termed inflammatory cell death (Yatim et al., 2017). While cell death may breach barrier tissues and cause inflammation by triggering contact of immune cells with microbes and PAMP-driven immune responses, cell death can also induce inflammation under sterile conditions. In this context, the impact of cell death on the immune response is considered to be influenced by DAMPs released from the dying cell. DAMPs are a poorly defined class of molecules that are only released from cells upon plasma membrane rupture into the extracellular space. They can be recognized by sentinel cells of the immune system such as macrophages and dendritic cells and induce an inflammatory and in some cases an adaptive immune response. DAMPs include molecules that are present in living cells such as High-Mobility-Group-Protein B1 (HMGB1) and adenosine triphosphate (ATP) as well as proteins that are induced upon cell death initiation such as proteins of the Interleukin (IL) 1 family (Legrand et al., 2019; Yatim et al., 2017).

In concordance with its morphology which encompasses the formation of apoptotic bodies that can be rapidly removed by phagocytes before DAMP release occurs, apoptosis is generally believed to be immunologically silent. Necrosis on the other hand is associated with a bursting of the cellular membrane and release of DAMPs into the extracellular space, therefore is generally though to induce an immune reaction. However, in certain settings, also apoptosis

can be inflammatory (Kumari et al., 2014; Vlantis et al., 2016) or immunogenic (Krysko et al., 2012) and the traditional concepts of the immune-stimulatory effect of apoptotic and necroptotic cell death are currently under debate (Green, 2019; Pasparakis and Vandenabeele, 2015). How the death of a cell affects the immune system may be largely influenced by the cellular communication between dying cells and immune cells as well as their tissue microenvironment (Legrand et al., 2019). Nevertheless, the effect of specific types of cell death on the immune response to date remains incompletely understood.

1.3 RIPK1 as a key player in innate immune signaling pathways

1.3.1. TNFR1 signaling

1.3.1.1. TNFR1-induced pro-survival and pro-inflammatory gene expression

Downstream of multiple innate immune receptors, Receptor-Interacting Protein Kinase 1 (RIPK1) has occurred as a key player that has a decisive role in whether a cell undergoes regulated cell death or whether an inflammatory response is induced. For this reason, RIPK1 is crucially involved in mediating immune responses and ensuring tissue homeostasis (Newton, 2020; Pasparakis and Vandenabeele, 2015; Weinlich and Green, 2014).

The function of RIPK1 is best understood in signaling induced by binding of the cytokine tumor necrosis factor (TNF) to TNF Receptor 1 (TNFR1). TNF is a crucial player among various cytokines expressed downstream of innate immune receptors such as PRRs or Interleukin-1 receptor (Takeuchi and Akira, 2010) and is produced by macrophages, monocytes, dendritic cells and activated lymphocytes as well as by non-professional immune cells such as epithelial and endothelial cells. TNF binds two receptors, which are TNFR1 and TNFR2, of which TNFR1 appears to be the key mediator of TNF-induced signaling in most cell types as it is ubiquitously expressed and activated by soluble TNF, whereas TNFR2 is expressed only in certain cell types, and requires membrane bound TNF for full activation (Varfolomeev and Vucic, 2018) .

In general, binding of TNF to TNFR1 triggers inflammation in tissues by inducing pro-inflammatory and pro-survival gene expression through the activation of MAPK and NF-κB signaling. This is achieved by formation of an intracellular membrane-bound signaling complex, termed complex I (Figure 1). Upon ligation of TNFR1, the receptor trimerizes and within seconds triggers the formation of complex I (Ting and Bertrand, 2016; Varfolomeev and Vucic, 2018). In this complex, TNFR1-associated death domain protein (TRADD) and RIPK1 are recruited via homotypic death domain (DD) interactions with TNFR1 (Hsu et al., 1996; Hsu et al., 1995; Micheau and Tschopp, 2003; Pobezinskaya et al., 2008). TRADD contains a TNF-receptor-associated factor 2 (TRAF2) interaction domain and serves as a platform for recruitment of TNF receptor associated factor 2 (TRAF2) and/or TRAF5 (Hsu et al., 1996;

Vince et al., 2009) TRAF2 furthermore attracts the E3 ubiquitin ligases cellular inhibitor of apoptosis 1 and 2 (cIAP1/2) to the complex (Shu et al., 1996) (Figure 1). cIAP1/2 facilitate the addition of K63-, K11- and K48- linked ubiquitin chains to themselves, RIPK1 and possibly other proteins in complex I (Bertrand et al., 2008; Dynek et al., 2010; Varfolomeev et al., 2008), thereby allowing recruitment of the linear ubiquitin chain assembly complex [LUBAC; composed of the E3 ligase HOIL-1 interacting protein (HOIP), haem-oxidized IRP2 ubiquitin ligase-1 (HOIL-1) and SHANK-Associated RH Domain Interactor (Sharpin)] (Gerlach et al., 2011; Haas et al., 2009). LUBAC further adds M1-linked-(linear) ubiquitin chains to RIPK1 and other proteins in this complex such as TRADD, TNFR1 and NF-κB essential modulator (NEMO) (Gerlach et al., 2011; Haas et al., 2009; Tokunaga and Iwai, 2009). There is evidence that LUBAC furthermore extends existing K63-linked chains with M1 linked chains, thereby producing hybrid chains, which are attached to RIPK1 (Emmerich et al., 2016) (Figure 1). The action of cIAPs and LUBAC in complex I finally produce a ubiquitin chain network which acts as a scaffold to allow the recruitment of the key downstream mediators for the induction of NF-κB and MAPK signaling.

One of these key proteins is Transforming growth factor β-activated kinase 1 (TAK1), which is bound to TAK1-binding protein 2 and 3 (TAB2 and 3) and is recruited and activated via K63-linked ubiquitin chains (Kanayama et al., 2004; Wang et al., 2001). TAK1 has an essential function for pro-inflammatory and pro-survival gene expression by activating MAPK signaling. The activated MAPKs include extracellular-signal-regulated kinases 1 and 2 (ERK1/2), Jun N terminal kinase (JNK) and p38, proteins that regulate various cellular programs, including proliferation and survival (Cargnello and Roux, 2011) through gene activation mediated by the transcription factor activator protein 1 (AP-1). On the other hand, TAK1 is required for the activation of the IKK complex, a crucial player for the activation of canonical NF-κB signaling to drive inflammatory and pro-survival signaling. The IκB kinase (IKK) complex consisting of the regulatory subunit NEMO and the catalytic subunits IKK1 and 2 (Ea et al., 2006) and is recruited via affinity of NEMO for linear chains (Clark et al., 2013; Rahighi et al., 2009). The interaction of the IKK complex with K63/M1 hybrid chains might bring it in vicinity to TAK1, which interacts with K63-linked chains, thereby allowing for direct activating phosphorylation of IKK2 by TAK1 (Wang et al., 2001). The active IKK complex subsequently triggers activation of canonical NF-κB signaling through the NF-κB p50/p65 heterodimer, which in the absence of receptor activation, is sequestered in an inactive state in the cytoplasm through binding to inhibitor of κBα (IκBα) (Figure 1). The active IKK complex induces phosphorylation of IκBα inducing and its subsequent proteasomal degradation (Scheidereit, 2006). Consequently, NF-κB p50/p65 is released from its inhibition and free to translocate to the nucleus where it promotes transcription of genes involved in survival and inflammation (Hayden and Ghosh, 2014).

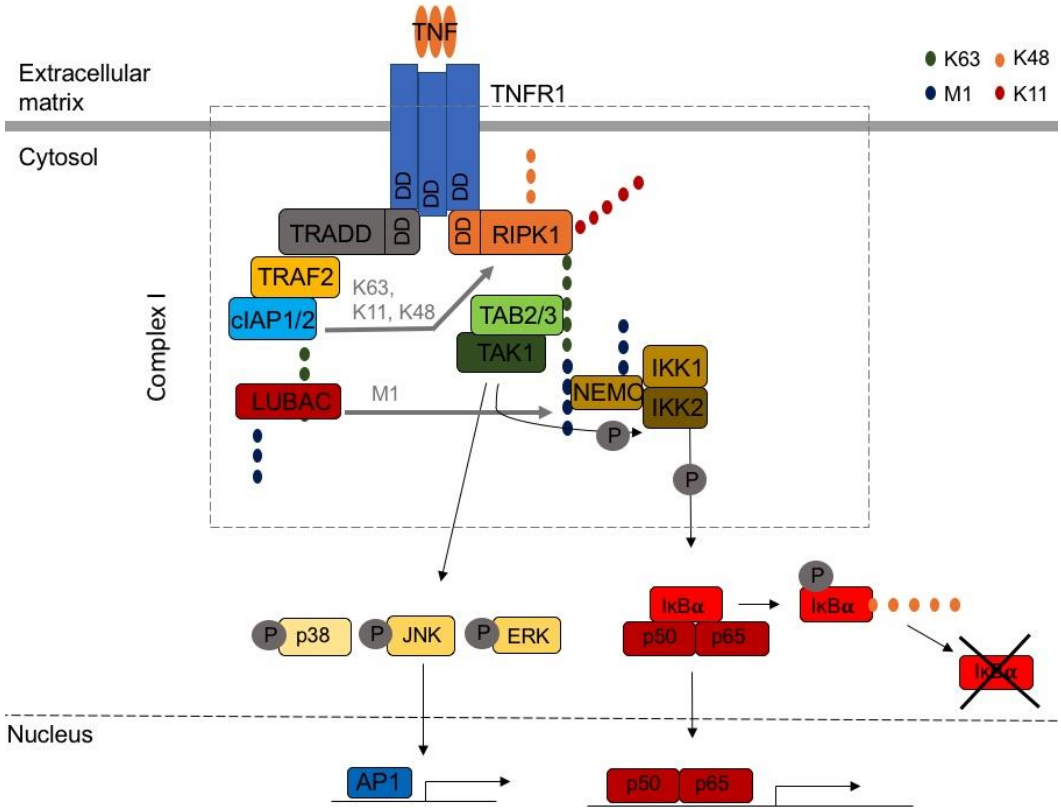

Figure 1: Schematic representation of TNFR1-induced complex I formation.TNF ligation to TNFR1 induces the assembly of a cytosolic, membrane-bound complex, termed complex I. Ubiquitin ligases in this complex such as cIAP1/2 and LUBAC attach ubiquitin chains to RIPK1 that lead to the recruitment of TAK1 and the IKK complex, composed of IKK1/2 and NEMO. TAK1 activates IKK2 by phosphorylation and also induces downstream MAPK activation to promote AP-1 transcription factor activation. The IKK complex subsequently phosphorylates IκBα to induce its degradation, thereby releasing the NF-κB dimer composed of p50 and p65 from its cytosolic inhibition to enter the nucleus. Transcriptional activation by AP-1 and NF-κB eventually leads to the expression of pro-inflammatory and pro-survival genes.

1.3.1.2. TNFR1-induced apoptosis

While the default outcome of TNFR1 ligation is the induction of transcriptional programs promoting cell survival and inflammation, TNF binding to its receptor can also lead to apoptotic cell death under certain conditions. Cell death may be induced by the formation of two distinct cytosolic complexes, which are commonly denominated as IIa and IIb (Figure 2) (Pasparakis and Vandenabeele, 2015; Varfolomeev and Vucic, 2018). Whereas both complex IIa and IIb induce Caspase-8 dependent apoptosis downstream of TNFR1, they functionally differ in their requirement for RIPK1 and its kinase activity. Specifically, while complex IIa does not contain RIPK1 and does not require its catalytic activity for induction of apoptosis, complex IIb formation and cell death signaling depends on RIPK1 and its kinase activity (Polykratis et al., 2014; Wang et al., 2008).

Complex IIa forms in response to TNF receptor ligation under conditions of an impaired NF-κB response, e.g. by suppression of NF-κB nuclear translocation (Micheau and Tschopp,

2003) or inhibition of protein synthesis as in the presence of the translational inhibitor cycloheximide (CHX) (Wang et al., 2008). While the molecular events underlying complex IIa formation are poorly understood, complex IIa requires TRADD binding to Fas-associated DD protein (FADD) via homotypic DD interaction in the cytoplasm (Pobezinskaya et al., 2008). TRADD and FADD association serves as a platform for recruitment of catalytically inactive procaspase-8. Procaspase-8 molecules subsequently oligomerize, which triggers their auto-proteolytic processing. This process involves the generation of a procaspase-8 p43 fragments and ultimately results in the release of p10 and p18 fragments which constitute the enzymatically active protein (Chang et al., 2003; Hughes et al., 2009; Salvesen and Dixit, 1999). The catalytic activity of caspase-8 is modulated by cFLIP in an isoform- and concentration-dependent manner (Hughes et al., 2016).Active procaspase-8 can subsequently engage effector caspases such as Caspase-3 and Caspase-7 which cleave cellular substrates in the cytoplasm and the nucleus to orchestrate apoptotic cell death (Shalini et al., 2015).

Complex IIb on the other hand forms under conditions such as IAP depletion, induced for example by SMAC-mimetics (Wang et al., 2008) or when TAK1 (Dondelinger et al., 2013) or NEMO (Legarda-Addison et al., 2009) are ablated. Complex IIb contains RIPK1, which interacts with the Caspase-8 adaptor Fas-associated DD protein (FADD) via DD-mediated interaction. Importantly, apoptosis mediated via complex IIb critically depends on RIPK1 and its kinase activity (Dondelinger et al., 2013; Polykratis et al., 2014; Wang et al., 2008). FADD possesses a death effector domain (DED) which allows for recruitment of Caspase-8 as well as cFLIP. RIPK3 may be part of this complex as well, as it contributes to RIPK1-dependent apoptosis (Dondelinger et al., 2013). As in complex IIa, activation of caspase-8 in an autocatalytic manner ultimately initiates caspases-3 and -7-mediated apoptosis.

Of note, although the field commonly distinguishes between complex IIa and IIb there might be potential overlap in their formation (Varfolomeev and Vucic, 2018). Furthermore, it remains unclear whether these complexes evolve from a membrane-bound complex I, or form de novo in the cytoplasm.

1.3.1.3. TNFR1-induced necroptosis

Caspase-8 activity may be target of pathogenic inhibition and can be pharmaceutically blocked, e.g. by the pan-caspase inhibitor zVAD-fmk. In case of insufficient caspase activation in complex IIa or IIb, yet another cytosolic complex, termed the necrosome, forms and converts the cell death modality into necroptosis (Pasparakis and Vandenabeele, 2015). The necrosome contains the proteins RIPK1, RIPK3 and mixed lineage kinase like (MLKL) (Figure 2). Similar to complex II, this complex possibly also includes FADD and Caspase-8 (He et al., 2009), which makes it tempting to speculate that the necrosome evolves from an inactive complex II. Importantly, necroptosis downstream of TNFR1 relies on the kinase activities of

RIPK1 and RIPK3 (Berger et al., 2014; Newton et al., 2014; Polykratis et al., 2014; Zhao et al., 2017). In the necrosome, RIPK1 and RIPK3 interact via a common structural motif, termed RIP homotypic interaction motif (RHIM) (Sun et al., 2002) which mediates the assembly of filamentous structures (Li et al., 2012). RIPK3 oligomerization in this complex triggers its autophosphorylation (Orozco et al., 2014; Wu et al., 2014), which allows recruitment and phosphorylation of MLKL within its C-terminal pseudokinase domain (Sun et al., 2012). MLKL phosphorylation induces intramolecular conformational changes exposing its N-terminal 4 helical bundle domain (4HB), promoting its oligomerization and translocation to the plasma membrane (Dondelinger et al., 2014). At the plasma membrane, the 4HB domain is essential to initiate rupture leading to necroptotic cell death. The mechanisms of cell lysis in this context remain incompletely understood, although different mechanisms have been suggested (Cai et al., 2014; Dondelinger et al., 2014).

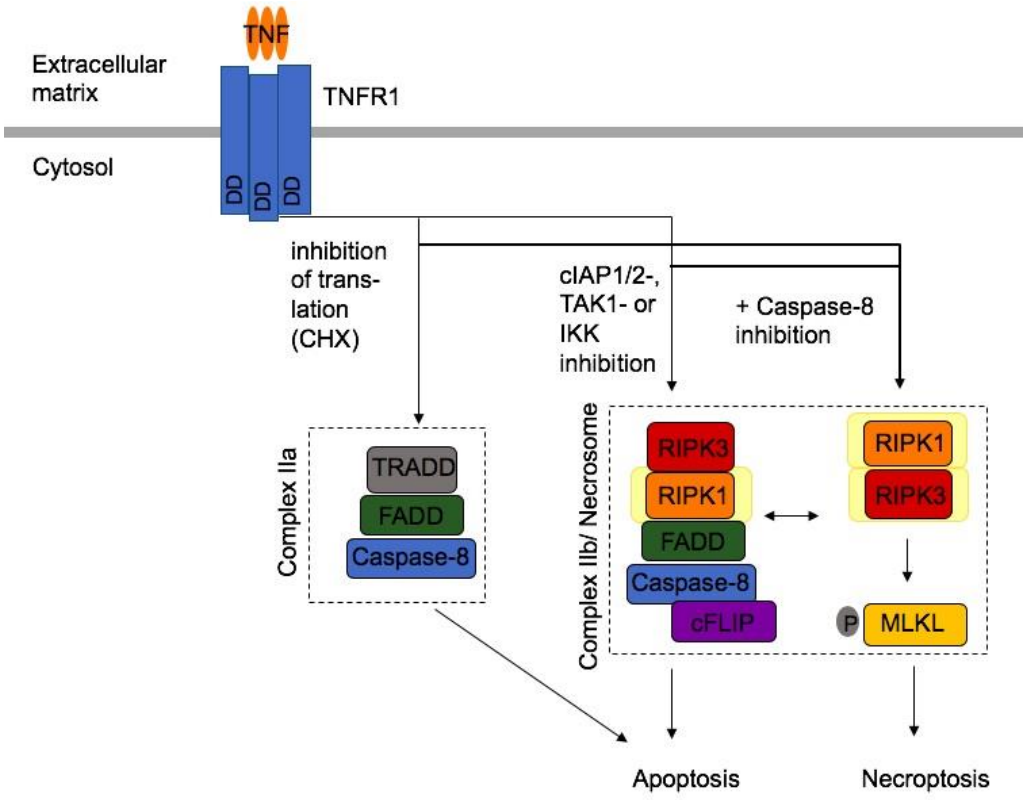

Figure 2: Schematic representation of signaling events downstream of TNFR1 in conditions of compromised complex I signaling or complex I instability. Inhibition of protein translation, such as by cycloheximide (CHX) switches the TNFR1 ligation response to the formation of complex IIa, which induces TRADD- and FADD-dependent, caspase-8-mediated apoptosis. In situations of cIAP1/2, TAK1, or IKK complex inhibition, that lead to complex I destabilization, complex IIb forms and induces RIPK1 kinase activity-dependent apoptosis. In case of caspase inhibition, translational blockade or complex I instability induce the formation of the necrosome in which RIPK1 and RIPK3 interact in a kinase activity-dependent manner leading to MLKL phosphorylation and necroptosis. Complex IIb and the necrosome may evolve from each other depending on Caspase-8 activity. Glowing circles represent kinase activity.

1.3.2. TLR 3 and 4 signaling

RIPK1 is furthermore involved in signaling downstream of Toll like Receptor (TLR) 3 and TLR4. TLRs belong to the family of PRRs and are required for sensing of different PAMPs or DAMPs (Akira and Takeda, 2004). In this line, TLR4 is activated by lipopolysaccharide (LPS), a cell wall component of gram-negative bacteria, while TLR3 is responsive to viral, double stranded RNA. TLRs signal through two different pathways, which depend on the signaling adaptors myeloid differentiation primary response gene (MyD88) and TIR-containing adaptor inducing interferon-beta (TRIF). All TLRs, with the exception of TLR3, employ MyD88 to induce inflammatory responses, while only TLR3 and TLR4 signal via TRIF which can engage RIPK1 for signaling (Cusson-Hermance et al., 2005; Meylan et al., 2004).

MyD88-dependent signaling on the other hand is RIPK1-independent. In brief, MyD88 is recruited to TLR4 through the adaptor protein TIR-containing adaptor protein (TIRAP). MyD88 has a death domain which upon TLR activation initiates the recruitment of members of the IRAK (IL-1 receptor-associated kinase) family of protein kinases (Akira and Takeda, 2004; West et al., 2006) Phosphorylation of IRAK1 and 4 leads to their dissociation from the receptor and their interaction with the E3 ubiquitin ligase TRAF6. TRAF6, together with ubiquitin-conjugating enzyme E2 13 (Ubc13) and ubiquitin-conjugating enzyme E2 variant 1A (Uev1A) subsequently mediates the polyubiquitination of itself and NEMO. This leads to the recruitment and activation of TAB1/2/3 in complex with TAK1, which triggers the activation of the transcription factor AP-1 and NF-κB in an IKK-dependent manner, thereby promoting the expression of pro-survival and inflammatory proteins (Figure 3) (Akira and Takeda, 2004).

On the other hand, TRIF-mediated signaling downstream of TLR3 and TLR4 in RIPK1 proficient cells, proceeds via RIPK1 (Cusson-Hermance et al., 2005; Meylan et al., 2004). In this context, RIPK1 can induce different signaling outcomes ranging from the activation of NF-κB to cell death. TRIF binds to TLR3 directly, while TLR4 requires the adaptor TRIF-related adaptor molecule (TRAM) for its recruitment. TRIF contains a RHIM domain in the C-terminal region to recruit RIPK1 via homotypic RHIM interaction. Furthermore, TRIF also directly binds the E3 ubiquitin ligase TRAF6 via its TRAF6-binding motifs in the N-terminal region (Jiang et al., 2004; Sato et al., 2003) and cIAP1/2. TRAF6 and cIAPs generate K63-linked chains in the complex, leading to the recruitment of TAK1 (Jiang et al., 2004) and the activation of NF-κB signaling. TAK1 is essential in this signaling cascade as TAK1-deficient cells show impaired NF-κB responses downstream of TLR3 (Sato et al., 2005). TAK1 activation in turns seems to rely on RIPK1 and highlighting its crucial role in this pathway, ablation of RIPK1 leads to attenuation of NF-κB activation in response to TLR3 stimulation (Meylan et al., 2004). Furthermore, besides activating NF-κB and AP-1 transcription factors, TLR3 and 4 utilize TRIF to engage TANK binding kinase 1 (TBK1)-containing complexes and activate the transcription factor Interferon regulatory factor 3 (IRF3) (Fitzgerald et al., 2003; Hemmi et al., 2004) which

requires recruitment of TNF-receptor associated factor (TRAF) 3. Activated IRF3 translocates to the nucleus to induce the transcription of Interferon-beta (IFN-beta) to develop an antiviral innate state in the cell, TRAF6 or RIPK1 however are dispensable for this (Cusson-Hermance et al., 2005; Jiang et al., 2004; Meylan et al., 2004).

As in the case of TNF-induced signaling, the default response to TLR3 and 4 ligation is activation of pro-inflammatory signaling, while these receptors can also induce cell death (Figure 3). This response however is less understood than in the case of TNFR1. Whereas MyD88 does not directly promote cell death, TRIF was shown to induce caspase-8-dependent apoptosis, promoted by the absence of cIAPs (Weber et al., 2010). Importantly, RIPK1 was required for apoptosis under these conditions (Estornes et al., 2012; Feoktistova et al., 2011). Similar to TNFR1, caspase inhibition upon ligand binding initiates RIPK3- and MLKL-dependent necroptosis (He et al., 2009; Kaiser et al., 2013). Abrogating RIPK1 kinase activity in this case blocks TRIF-induced necroptosis (Dillon et al., 2014; Polykratis et al., 2014). However, cell death in this situation can proceed in the absence of RIPK1, via a direct interaction of TRIF and RIPK3 through their RHIM domains (Buchrieser et al., 2018; Dillon et al., 2014; Kaiser et al., 2013).

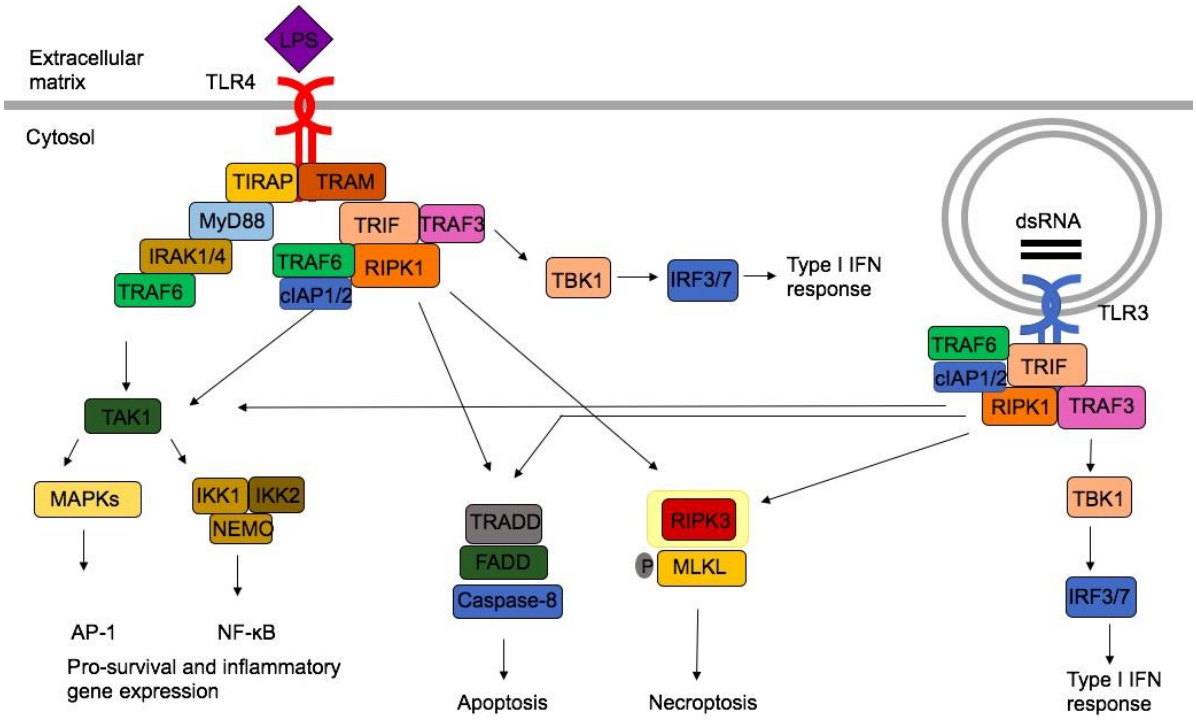

Figure 3: TLR3 and 4 signal for pro-survival and inflammatory gene expression, but can also induce apoptosis or necroptosis. TLR4 employs MyD88 to activate NF-κB and MAPK signaling. TLR3 and 4 signal via TRIF to activate NF-κB and MAPKs in a RIPK1-dependent manner, however may also induce apoptosis under certain conditions. When caspases are inhibited, TLR3 and 4 ligation leads to MLKL-dependent necroptosis, which is blocked when RIPK1 kinase activity is inhibited, but can also proceed in absence of RIPK1. TRIF furthermore induces IRF3/7 transcription factor-mediated expression of type I interferons via TRAF3- and TBK1-dependent signaling.

1.4 RIPK1 protein function

1.4.1. Protein structure of RIPK1

RIPK1 is a serine/threonine-specific protein kinase with a molecular weight of 74 kilo Dalton. It contains an N-terminal kinase domain, a C-terminally located DD and an intermediate domain including a RHIM domain (Figure 4).

The kinase domain of RIPK1 is composed of a canonical kinase fold consisting of an N-terminal lobe and a relatively bigger C-terminal lobe in between which the ATP-binding cleft can be found. The N- and the C-loop in RIPK1 are connected by an activation loop. RIPK1 contains the key structural motifs that are required for optimal phosphotransfer and are therefore strictly conserved among different protein kinases (Huse and Kuriyan, 2002). These include the catalytic triad residues which are lysine (K) 45, glutamic acid (E) 63 and aspartic acid (D) 156 in mouse RIPK1 (Xie et al., 2013). Thereof, K45 in RIPK1 is required to, in cooperation with a glycine rich-region that forms a loop termed the phosphate-binding loop or P-loop, anchor the ATP phosphates to stabilize ATP in the active cleft. Supporting the functional relevance of this site for ATP binding, mice with K45A mutation in RIPK1 express a catalytically inactive version of RIPK1 (Berger et al., 2014; Liu et al., 2017). P-loop residues that are equally required for ATP stabilization and coordination are RIPK1 residues 24-31 (Xie et al., 2013) and disruption of the P-loop by deleting Glycine (G) 26 and Phenylalanine (F) 27 in mice renders RIPK1 kinase inactive (Liu et al., 2017). Another conserved motif in protein kinases is the catalytic loop which executes the transfer of the gamma-phosphate of ATP to a substrate protein. In RIPK1, this catalytic loop comprises the residues 136-143 (Xie et al., 2013) and in line with its functional relevance mutation of D138 to asparagine (N) in mice results in loss of catalytic activity of RIPK1 (Polykratis et al., 2014). RIPK1 furthermore contains an activation loop, comprising residues D156-E196 (Xie et al., 2013) which is a common regulatory element in protein kinases. This loop provides a platform for peptide substrate binding and is required for stabilizing the kinase in a binding-permissive conformation (Huse and Kuriyan, 2002). In addition, it has a remarkable ability to be rearranged by phosphorylation, by which in some kinases it can be transformed to an open and extended conformation to allow substrate engagement.

On the other hand, RIPK1 mediates protein-protein interaction via its RHIM and DD. The RHIM is a unique segment of homologous sequences initially discovered in RIPK1 and RIPK3 (Sun et al., 2002). This motif in RIPK1 mediates homotypic protein interaction with other RHIM-containing proteins, such as RIPK3, the signaling adapter TRIF (Meylan et al., 2004) and the innate immune sensor Z-DNA-binding protein 1 (ZBP1, also called DAI) (Kaiser et al., 2008). While the exact boundaries of the RHIM motif are unclear, the sequence conservation is

centered around the I(V)QI(V)G motif and mutation of these core residues impairs RIPK1-RIPK3 interaction (Li et al., 2012).

The DD is a conserved homotypic interaction motif which is characterized by a six α-helical bundle structural fold. The DD of RIPK1 (residue 583-669, (Park et al., 2013)) is required for its recruitment to a death receptor signaling complex such as TNFR1 (Hsu et al., 1996) as well as to mediate the binding to other DD-containing adaptor proteins such as TRADD and FADD (Park et al., 2013).

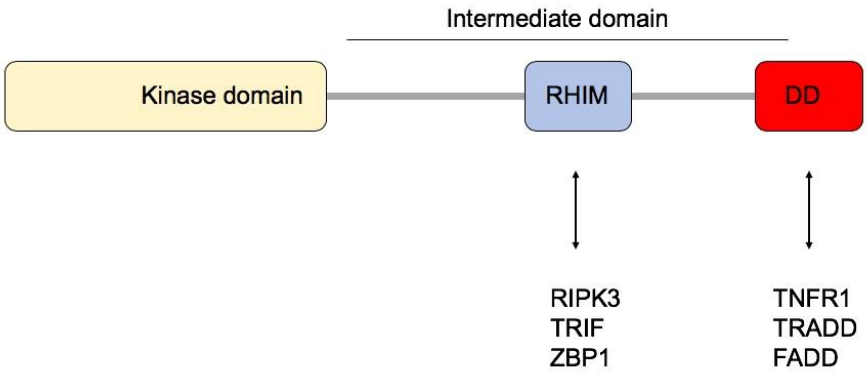

Figure 4: Scheme showing RIPK1 domain structure. RIPK1 contains an N-terminal kinase domain and a C-terminal death domain (DD) which are connected by an intermediate domain containing a RIP homotypic interaction motif (RHIM). Protein-protein interactions mediated by the RHIM or DD are indicated.

1.4.2. RIPK1 kinase-independent function

1.4.2.1. RIPK1 scaffolding function during development

As described above, RIPK1 is a fundamental signaling node in multiple innate immune signaling pathways. The crucial role of RIPK1 for the organism presents itself in the phenotype of mice with full-body deletion of RIPK1. These mice die shortly after birth displaying widespread inflammation and cell death (Kelliher et al., 1998). Later it was found, that the phenotype of *Ripk1*$^{-/-}$ mice is caused by apoptotic and necroptotic cell death, as mice with additional ablation of caspase-8 and RIPK3, but not any of these proteins alone are viable and fertile (Dillon et al., 2014; Kaiser et al., 2014; Rickard et al., 2014b). Studies addressing the upstream activators responsible for cell death induction in absence of RIPK1 have revealed an involvement of different innate immune sensors. Aberrant caspase-8 mediated apoptosis in *Ripk1*$^{-/-}$ mice was promoted by TNFR1, as caspase-8 and TNFR1 deletion are equivalent in their benefit for survival of *Ripk1*$^{-/-}$ mice (Rickard et al., 2014b). RIPK3-induced pathways on the other hand are strongly driven by the interferon-inducible protein ZBP-1 and TRIF, as *Ripk1*$^{-/-}$ *caspase8* $^{-/-}$ *Zbp1*$^{-/-}$ *Trif*$^{-/-}$ mice reach a median survival of 17 weeks (Newton et al., 2016b). *Ripk1*$^{-/-}$ *caspase-8* $^{-/-}$ *Zbp1*$^{-/-}$ mice survive only up to 5 weeks other hand, suggesting that TRIF, which can induce interferon production and drive expression of ZBP1, acts in a

different pathway in inducing lethality in these mice (Ingram et al., 2019). Therefore, these data imply that in the absence of RIPK1, TRIF directly engages RIPK3 for signaling. Conclusively, RIPK1 blocks lethal cell death-inducing pathways engaged by caspase-8 and RIPK3 downstream of multiple innate immune sensors.

These findings prompted studies aimed at delineating the functional importance of the kinase domain as well as the DD and RHIM domain in RIPK1 for inhibiting necroptotic and apoptotic pathways. Interestingly, in contrast to RIPK1-deficient mice, mice that express catalytically inactive RIPK1 are developmentally normal (Berger et al., 2014; Liu et al., 2017; Newton et al., 2014; Polykratis et al., 2014). In line with this, in vitro, RIPK1-deficient cells are more sensitive to TNF-induced cell death than cells expressing kinase-dead RIPK1 (Lee et al., 2004). Furthermore, TLR3- and 4-induced necroptosis in cells is blocked by kinase-inactive RIPK1 (Kaiser et al., 2013; Polykratis et al., 2014), while in the absence of RIPK1 on the other hand, cell death can proceed (Dillon et al., 2014; Kaiser et al., 2013). Taken together, these studies demonstrate that RIPK1 blocks the engagement of lethal cell-death-inducing pathways in a manner independent of its kinase activity. The role of the DD in the pro-survival function of RIPK1 on the other hand remains ambiguous. In *Ripk1*$^{-/-}$ mice, TRADD was shown to form a complex with FADD to mediate Caspase-8 activation and cell death. Furthermore, *Ripk1*$^{-/-}$ *Ripk3*$^{-/-}$ *Tradd*$^{-/-}$ mice survive until weaning or longer (Anderton et al., 2019; Dowling et al., 2019), indicating that TRADD may, similar to FADD, drive apoptosis in absence of RIPK1 and RIPK3. While deletion of TRADD cannot prolong the survival of *Ripk1*$^{-/-}$ mice, it ameliorates inflammation and cell death in these. These data indicate that RIPK1 may block TRADD-FADD interaction via its DD and thereby prevent caspase-8 activation during development (Anderton et al., 2019). Although it remains unclear whether RIPK1-TRADD or RIPK1-FADD interaction is required to inhibit cell death, this study suggests that RIPK1 constitutes an essential brake on caspase-8 mediated apoptosis via its DD. To investigate the role of the DD, Meng et al. mutated a critical lysine residue for DD-mediated homodimerization of RIPK1 (K458) and *Ripk1*$^{K584/K584R}$ mice are viable and healthy (Meng et al., 2018). However, human RIPK1 with K to R mutation of the corresponding residue (K599R) retains the ability to interact with TNFR1, FADD and TRADD and these interactions might be crucial for preventing lethality. Therefore, to date, the role of the DD for the prosurvival function of RIPK1 remains elusive. Mutation of the conserved RHIM motif in RIPK1 (mRHIM) leads to death around birth (Lin et al., 2016; Newton et al., 2016b), mimicking complete absence of RIPK1. TNF-induced NF-κB activation in RHIM mutant mice (*Ripk1*$^{mRHIM/mRHIM}$) is not affected (Lin et al., 2016), indicating that perinatal lethality is not caused by impaired expression of NF-κB-induced pro-survival proteins. Similar to *Ripk1*$^{-/-}$ pups, *Ripk1*$^{mRHIM/mRHIM}$ mice present with dermal inflammation and cell death at embryonic day (E) 18.5. However, while perinatal lethality and skin abnormalities in *Ripk1*$^{-/-}$ mice are driven by both caspase-8- and MLKL-dependent pathways, ablation of RIPK3 or

MLKL in *Ripk1*$^{mRHIM/mRHIM}$ pups alone is sufficient to prevent death and histological lesions (Lin et al., 2016; Newton et al., 2016b). These results show that necroptosis is the main inducer of perinatal lethality in *Ripk1*$^{mRHIM/mRHIM}$ mice. ZBP-1 was identified as the crucial upstream sensor that activates lethal necroptotic pathways in the absence of a functional RIPK1 RHIM, as deletion of ZBP-1 rescued the perinatal lethality in *Ripk1*$^{mRHIM/mRHIM}$ mice (Lin et al., 2016; Newton et al., 2016b). Therefore, the RIPK1 RHIM motif prevents RIPK3-/MLKL-mediated necroptosis induced by ZBP1 during development.

Taken together, the perinatal lethality of *Ripk1*$^{-/-}$ mice can be explained by a pro-survival scaffolding function of RIPK1 which is independent of its kinase activity. The RHIM domain crucially contributes to this function of RIPK1, while the role of its DD remains less clear.

1.4.2.2. RIPK1 scaffolding function in the adult tissue

In addition to its essential function in embryonic development, a vital role for RIPK1 in tissue homeostasis has been established by studies in different tissues, including the hematopoetic compartment, the endothelium, the intestine and the skin (Dannappel et al., 2014; O'Donnell et al., 2018; Roderick et al., 2014; Takahashi et al., 2014).

RIPK1 ablation specifically in intestinal epithelial cells (RIPK1^{IEC-KO}) leads to IEC death and intestinal pathology and results in severe wasting and death of mice within four weeks after birth (Dannappel et al., 2014; Takahashi et al., 2014). The pathology was rescued by simultaneous ablation of FADD and RIPK3 (Dannappel et al., 2014), but not by RIPK3 alone (Dannappel et al., 2014; Takahashi et al., 2014), showing that FADD/caspase-8-dependent apoptosis mediates the pathology. Furthermore, the pathology was reported to at least partially depend on TNFR1, whereas data on the involvement of the microbiota in the phenotype of RIPK1^{IEC-KO} are inconsistent (Dannappel et al., 2014; Takahashi et al., 2014). Interestingly, ablation of all NF-κB subunits in IECs does not phenocopy the intestinal pathology in RIPK1^{IEC-KO} mice (Vlantis et al., 2016) and sustained activation of NF-κB by a constitutively active *Ikk2* transgene rather aggravates the pathology (Dannappel et al., 2014), indicating that IEC apoptosis in RIPK1^{IEC-KO} mice does not result from defective NF-κB signaling. This observation is in line with controversial results on the requirement of RIPK1 for the activation of NF-κB and MAPK signaling (Dannappel et al., 2014; Ea et al., 2006; Lee et al., 2004; Li et al., 2006; Tang et al., 2019; Wong et al., 2010; Zhang et al., 2019c). On the other hand, a degradation of pro-survival, RIPK1-associated proteins such as FLIP, TRAF2 and cIAP1 was observed in RIPK1-deficient intestinal organoids and MEFs, but not in RIPK1 kinase activity-deficient MEFs (Dannappel et al., 2014), showing that the scaffolding function of RIPK1 is required for stabilization of these proteins. In the absence of RIPK1 in the intestinal epithelium, degradation of pro-survival proteins may therefore contribute to IEC apoptosis and intestinal pathology (Dannappel et al., 2014). Considering that RIPK1 kinase activity-deficient mice do not show

any intestinal inflammation, these results demonstrate that RIPK1 acts in IECs in a kinase activity-independent manner and independently of its role in NF-κB signaling to restrain caspase-8-dependent cell death-inducing pathways.

Similarly, epidermis-specific ablation of RIPK1 in RIPK1$^{E\text{-}KO}$ mice results in apoptotic as well as non-apoptotic keratinocyte death and the development of severe skin inflammation starting at around 1 week of age (Dannappel et al., 2014). The phenotype is prevented by concurrent ablation of FADD and RIPK3. However, importantly, also RIPK3 or MLKL deficiency alone is sufficient to block skin inflammation in RIPK1$^{E\text{-}KO}$ mice, although these mice still showed increased levels of keratinocyte apoptosis in their epidermis (Dannappel et al., 2014). These results show that necroptotic cell death drives skin inflammation in RIPK1$^{E\text{-}KO}$ mice, while apoptosis does not trigger inflammation in this context. Furthermore, skin inflammation in this context is suppressed by ablation of ZBP1 (Lin et al., 2016), revealing ZBP-1 as the main driver of necroptosis and inflammation in RIPK1$^{E\text{-}KO}$ mice. RIPK1 therefore prevents RIPK3-driven keratinocyte necroptosis and inflammation downstream of ZBP-1 in the epidermis. The RHIM domain of RIPK1 is considered to be essential for this protective function, based on the observation that mice that express RIPK1 with a mutated RHIM (RIPK1$^{mRHIM/E\text{-}KO}$) in the epidermis show a phenotype similar to RIPK1$^{E\text{-}KO}$ mice (Lin et al., 2016). Taking into account that in contrast to RIPK1$^{E\text{-}KO}$ mice, mice that lack RIPK1 kinase activity do not develop skin lesions (Berger et al., 2014; Liu et al., 2017; Polykratis et al., 2014), these findings demonstrate a kinase activity-independent, RHIM-dependent scaffolding function for RIPK1, that is essential to curb ZBP1-dependent necroptosis in the skin.

Taken together, in the adult tissue such as the skin and the gut, RIPK1 is essential to maintain tissue homeostasis (Figure 5) and prevent excessive caspase-8 and/or RIPK3-driven cell death.

1.4.2.3. RIPK1 function in humans

The importance of understanding RIPK1-mediated signaling has recently been strengthened by reports on immunodeficient patients with mutations in RIPK1 that reveal its fundamental role in human disease pathogenesis. Patients with bi-allelic RIPK1 loss-of function mutations presented with primary immunodeficiencies (Cuchet-Lourenco et al., 2018; Li et al., 2019; Uchiyama et al., 2019), characterized by lymphopenia and susceptibility to infections (Cuchet-Lourenco et al., 2018). Loss of RIPK1 furthermore was reported to result in chronic enteropathies, showing that RIPK1 has a key function to maintain tissue homeostasis in the human intestine (Cuchet-Lourenco et al., 2018; Li et al., 2019; Uchiyama et al., 2019). Additionally, some patients with RIPK1 deficiency suffered from autoimmune clinical features such as progressive polyarthritis (Cuchet-Lourenco et al., 2018). In vitro, patient-derived skin fibroblasts showed impaired MAPK signaling and IL-6 secretion in response to TNF and

Poly(I:C) as well as enhanced sensitivity to TLR3-induced necroptosis compared to healthy-donor-derived cells (Cuchet-Lourenco et al., 2018), suggesting that loss of RIPK1 leads to sensitivity to cell death in primary human cells.

Therefore, similar to the importance of the RIPK1 scaffold to prevent inflammation and maintain tissue homeostasis in mice, these studies show a crucial role for RIPK1 in the human system. Importantly, these findings suggest a functional conservation between RIPK1 in both species and encourage the use of mouse models for the study of RIPK1.

1.4.3. RIPK1 kinase-dependent function

1.4.3.1. RIPK1 kinase activity as a driver of inflammation and cell death

Similar to the substantial amount of studies that document RIPK1's scaffolding function in development and tissue homeostasis, also the kinase-dependent function of RIPK1 has been extensively studied.

In vitro, cells expressing kinase inactive RIPK1 were found to be irresponsive to necroptotic and certain apoptotic stimuli. Primary cells from mice harboring D138N, K45A or $\Delta G_{26}F_{27}$ mutations in RIPK1, that disrupt its catalytic activity, are protected from necroptosis downstream of TNFR1, TLR3 and 4 (Berger et al., 2014; Liu et al., 2017; Polykratis et al., 2014; Shutinoski et al., 2016). Ablation of RIPK1 kinase activity also blunts apoptosis induced by TNF and cIAP1/2 inhibition, but does not affect apoptosis induced by TNF under conditions of inhibited protein synthesis (Berger et al., 2014; Polykratis et al., 2014). In vivo, RIPK1 kinase activity has furthermore been established as a driver of cell death and inflammation in different tissues. In this line, mice with intestinal epithelial cell (IEC)-specific ablation of NEMO ($NEMO^{IEC\text{-}KO}$) spontaneously develop chronic inflammation in the colon and display an intestinal pathology characterized by IEC apoptosis in the colon and ileum and loss of antimicrobial factor-producing Paneth cells in the ileum (Vlantis et al., 2016). Colonic epithelial cell death and colitis are completely prevented by additional ablation of TNFR1, or FADD and RIPK3, while RIPK3-deficiency by itself only provides an ameliorating effect (Vlantis et al., 2016). Importantly, genetic blockade of RIPK1 catalytic activity protects $NEMO^{IEC\text{-}KO}$ mice from developing colitis (Vlantis et al., 2016). These results show that colitis in $NEMO^{IEC\text{-}KO}$ mice is driven by RIPK1 kinase activity-mediated TNF-induced apoptosis. Hepatocyte-specific ablation of NEMO ($NEMO^{LPC\text{-}KO}$) on the other hand leads to spontaneous development of severe liver pathology in mice, characterized by steatohepatitis and hepatocellular carcinoma (HCC). The pathology involves the formation of a RIPK1/FADD/Capase-8 complex in hepatocytes, but is independent of RIPK3 (Kondylis et al., 2015a). Strikingly, ablation of RIPK1 kinase activity completely protects from liver pathology in $NEMO^{LPC\text{-}KO}$ mice (Kondylis et al., 2015a). Therefore, RIPK1 kinase activity drives hepatocyte apoptosis, hepatitis and development of liver cancer in the absence of NEMO. Further evidence for a key role of RIPK1

kinase activity as driver of inflammation and cell death comes from studies that evaluate its function in mice with a chronic proliferative dermatitis mutation in the LUBAC component Sharpin (*Sharpin*$^{cpdm/cpdm}$). Loss of Sharpin in these mice leads to a multiorgan inflammation in tissues such as the skin, liver, lung and spleen (Gijbels et al., 1996; Seymour et al., 2007). Dermatitis in *Sharpin*$^{cpdm/cpdm}$ mice is completely prevented by epidermis-specific deletion of TRADD or ablation of RIPK3 in combination with either FADD or heterozygous ablation of caspase-8, but not by deletion of RIPK3 alone (Kumari et al., 2014; Rickard et al., 2014a), showing that the phenotype is primarily driven by TRADD-and FADD-dependent keratinocyte apoptosis. Importantly, ablation of RIPK1 kinase activity prevents dermatitis in these mice (Berger et al., 2014), showing that in the absence of Sharpin, RIPK1 kinase activity mediates keratinocyte apoptosis and skin inflammation. Thus, whereas RIPK1 suppresses both apoptosis- and necroptosis-inducing signaling in a kinase activity-independent manner (presented under 1.4.2.2.), paradoxically, its catalytic activity promotes activation of these same pathways.

The role of RIPK1 kinase activity has furthermore been evaluated in a wide array of animal models of human inflammatory and degenerative diseases. Necroptosis has been implicated in promoting neuroinflammation in the pathogenesis of several chronic neurodegenerative diseases (Yuan et al., 2019). Indeed, RIPK1 inhibitors have proven effective in mouse models of amyotrophic lateral sclerosis (ALS) (Ito et al., 2016), multiple sclerosis (MS) (Ofengeim et al., 2015) and Alzheimer's disease (AD) (Ofengeim et al., 2017). Inhibition of RIPK1 kinase activity furthermore showed clinical effects in patients with lysosomal storage disorder (LSD) (Cougnoux et al., 2018) and inhibited neural cell death in cells isolated from patients with Parkinson's disease (Iannielli et al., 2018). In addition, RIPK1 kinase activity is involved in acute ischemic injuries in multiple tissues, including brain (Degterev et al., 2005), heart (Koudstaal et al., 2015; Oerlemans et al., 2012; Patel et al., 2020) and kidney (Linkermann et al., 2012; Newton et al., 2016a). In addition, studies revealed a crucial role for RIPK1 kinase activity in systemic inflammatory response syndrome (SIRS), a mouse model of sterile sepsis (Tracey et al., 1986), which is driven by caspase-8- and MLKL/RIPK3-induced signaling (Duprez et al., 2011; Newton et al., 2016a; Polykratis et al., 2014). Benefits of targeting RIPK1 kinase activity for cancer therapy on the other hand have been reported, but remain controversial (Patel et al., 2020; Seifert et al., 2016; Wang et al., 2018).

Conclusively, genetic mouse models of inflammation in different tissues as well as mouse models for human disease have established RIPK1 kinase activity as a driver of cell death and inflammation (Figure 5).

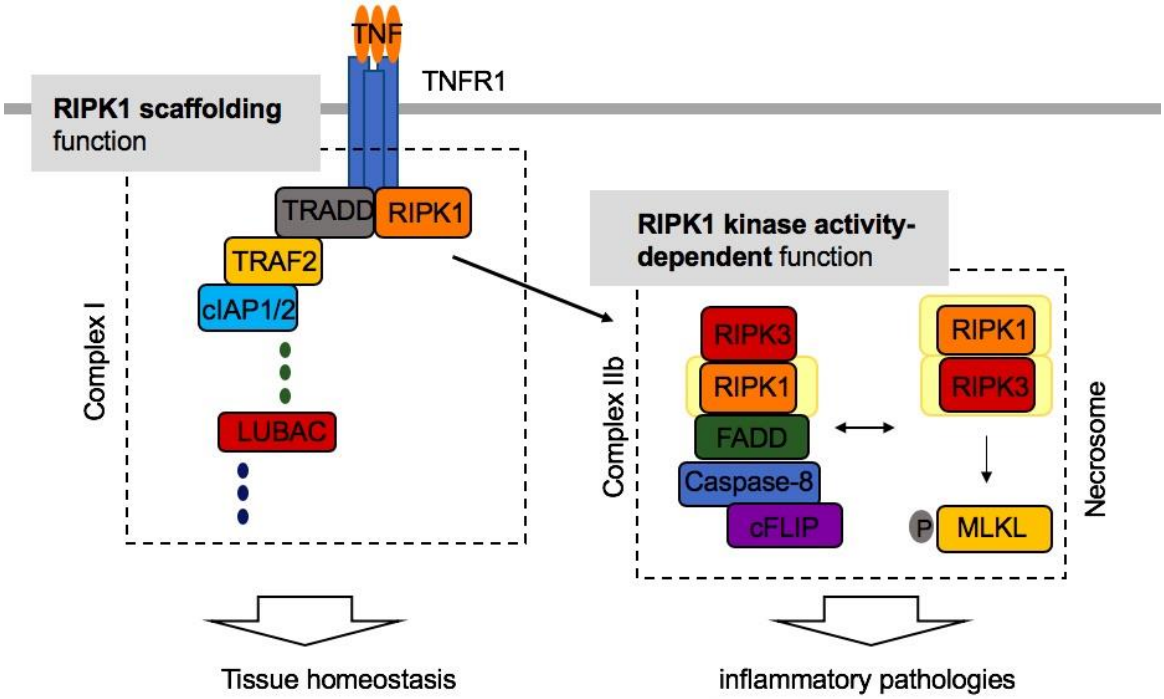

Figure 5: Scheme depicting the requirement for scaffolding and kinase function of RIPK1 in different TNFR1-induced complexes and their roles for organismal health. RIPK1 has a scaffolding role in TNFR1-induced complex I which is essential to maintain tissue homeostasis. On the other hand, RIPK1 exerts a kinase activity-dependent function in complex IIb/necrosome, which has been implicated in multiple inflammatory pathologies.

1.4.3.2. RIPK1 kinase activity-dependent cell death in host immunity

In addition to its role in inflammatory diseases, RIPK1 has emerged as a player in pathogen-host interactions. In this context, both kinase activity-dependent and -independent functions of RIPK1 seem to be important.

Firstly, in a manner independently of its kinase activity, RIPK1 maintains homeostasis and integrity of epithelial tissues (Dannappel et al., 2014; Takahashi et al., 2014), which supports their barrier function (Figure 5). On the other hand, its kinase activity has been reported to directly mediate pathogen-induced cell death. The importance of this mechanism for the host is evident in the context of viral infection, as the evolution of anti-apoptotic mechanisms is a common virulence strategy. In this line, the poxvirus vaccinia virus encodes a caspase inhibitor which inhibits caspase-8. This however results in RIPK3-dependent necroptosis (Cho et al., 2009). *Ripk1*$^{D138N/D138N}$ mice present with increased viral titers compared to wt mice after infection with vaccinia virus, similar to *Ripk3*$^{-/-}$ mice (Cho et al., 2009; Polykratis et al., 2014). Thus, RIPK1 kinase activity-dependent necroptosis is essential for host defense against vaccinia virus infection in vivo. In a bacterial context, RIPK1 kinase activity may, depending on the pathogen involved, be required for pathogenic clearance by triggering death of infected cells, or in other cases contribute to pathogen establishment through elimination of immune cells. In an evolutionary co-adaptation of host and pathogen, some bacteria have evolved virulence mechanisms that interfere with the host immune system to evade an immune

reaction and establish disease. For example, bacteria belonging to the *Yersinia* species express the effector protein *Yersinia* outer protein J (YopJ) that inhibits host cell proteins such as TAK and IKKs and thereby stalls NF-κB and MAPK signaling in the host (Paquette et al., 2012). While these immune responses are inhibited, *Yersinia* infection results in YopJ-dependent cell death in infected cells such as BMDMs. This cell death requires RIPK1 kinase activity (Peterson et al., 2017) and is blocked by ablation of caspase-8 and RIPK3, but not either of these proteins alone (Weng et al., 2014). Therefore, in response to *Yersinia* infection and YopJ-mediated blockade of inflammatory signaling, RIPK1 initiates apoptotic and necroptotic cell death. Importantly, *Ripk1*$^{K45A/K45A}$ mice show an increased lethality in response to *Yersinia* infection (Peterson et al., 2017), showing that RIPK1 kinase activity is required to restrict bacterial loads and control infection in this setting in vivo. On the other hand, studies suggest that other bacteria rather exploit RIPK1- and RIPK3-dependent cell death to establish colonization of the host. For example, inhibition of RIPK1 kinase activity in response to *Salmonella* infection leads to a substantial decrease in macrophage cell death (Robinson et al., 2012). Furthermore, *Ripk3*$^{-/-}$ mice have enhanced control of *Salmonella* bacteria and higher numbers of circulating macrophages compared to wt mice (Robinson et al., 2012). These results indicate that RIPK1- and RIPK3-dependent necroptosis of macrophages in this case might be disadvantageous for the host.

Taken together, although the role of RIPK1 kinase activity in specific pathogenic settings requires more thorough investigation, several studies suggest a functional importance as a modulator of host-pathogen interactions.

1.4.3.3. Therapeutical RIPK1 inhibition

Benefits of RIPK1 inhibition in mouse models as well as studies pointing to a functional conservation of RIPK1 in humans (Cuchet-Lourenco et al., 2018; Li et al., 2019; Uchiyama et al., 2019) have raised hopes for potential clinical effects of RIPK1 kinase inhibition. In line with a conserved pathological function of RIPK1 kinase activity in humans, RIPK1 activation, based on detection of its autophosphorylation at S166 or S14/15 was observed in postmortem pathological samples of patients with AD (Ofengeim et al., 2017) or MS (Ofengeim et al., 2015). Mice which lack RIPK1 kinase activity are healthy and fertile (Berger et al., 2014; Liu et al., 2017; Polykratis et al., 2014), furthermore supporting RIPK1 as a druggable target. The development of RIPK1 inhibitors was initially initiated by discovery of necrostatins, a series of small-molecule inhibitors including Nec-1/Nec-1s that blocked necroptotic cell death (Degterev et al., 2005), which were later found to target RIPK1 (Degterev et al., 2008). The development of RIPK1 inhibitors since has produced a number of small-molecule compounds that predominantly belong to a type II- or as Nec-1s to a type III-class of inhibitors, depending on which conformational state of RIPK1 is targeted (Martens et al., 2020). In the process of

evaluating RIPK1 inhibitors for clinical application, several specific RIPK1 inhibitors have progressed through phase I/II clinical trials, that test pharmacokinetics, safety and tolerability as well as biological effect of a drug. In line with controversial results on the benefit of RIPK1 inhibition in cancer, trials for the compound GSK3145095 in pancreatic cancer have been terminated, while GSK2982772 is currently undergoing clinical trials for the treatment of psoriasis, ulcerative colitis and rheumatoid arthritis (Harris et al., 2017; Mifflin et al., 2020; Weisel et al., 2017). Furthermore, the brain-blood barrier penetrable inhibitor DNL747 has raised hopes for new treatment options in AD, ALS and MS (Sheridan, 2019). Recently, potential applications of RIPK1 inhibitors in COVID-19-infected patients have been suggested (Feng et al., 2020) and safety and effect of the RIPK1 inhibitor SAR443122 (DNL758) was evaluated in a phase I clinical trial in adult patients hospitalized with severe COVID-19.
Taken together, although clinical approval of RIPK1 inhibitors is still pending, these may in the future offer promising treatment options for patients that suffer from inflammatory or degenerative diseases that involve pathogenic activation of RIPK1 kinase activity.

1.5 Regulation of RIPK1

1.5.1. Ubiquitination

The post-translational addition of chains consisting of the small molecule ubiquitin, a process termed ubiquitination, on RIPK1, is believed to be critically involved in cell fate decision upon TNFR1 ligation (Peltzer et al., 2016). While the role of different ubiquitinating enzymes (called E3 ligases) as well as their counterparts, the de-ubiquitinating enzymes (DUBs) remains incompletely understood, it is generally believed that a ubiquitination network on RIPK1 in complex I acts as a scaffold to promote downstream pro-survival signaling and RIPK1 retention in complex I to negatively regulate cell death. Different types of ubiquitin chains are involved in this regulation, which can be distinguished by the ubiquitin residue (lysine (K), with the exception of methionine (M) 1) that mediates linkage to the next ubiquitin protein in a chain. In order to better understand the complexity of RIPK1-modifying ubiquitination and deubiquitinating events, the involved enzymes are currently under intense study.
cIAP1/2 are E3-ubiquitin ligases that mediate K63-, K48-and K11-linked ubiquitination on RIPK1 in TNFR1-induced complex I (Bertrand et al., 2008; Dynek et al., 2010; Mahoney et al., 2008; Varfolomeev et al., 2008) (Figure 6), which was shown to be important for the activation of NF-κB signaling (Dynek et al., 2010; Mahoney et al., 2008; Varfolomeev et al., 2008). Inhibition of cIAP1/2 on the other hand, leads to the induction of cell death via the formation of complex II (Wang et al., 2008). While formally this has not been shown, K376 of RIPK1 may function as an acceptor site for cIAP1/2-mediated K63-linked chains. Supporting this idea, similar to cells in which cIAP1/2 are inhibited, MEFs from *Ripk1*$^{K376R/K376R}$ mice display

excessive complex II formation, RIPK1 kinase activity as well as sensitization to cell death in response to TNF (Tang et al., 2019; Zhang et al., 2019c). In response to TNF treatment in combination with cIAP1/2 inhibitors, *Ripk1*$^{K376R/K376R}$ MEFs however are still more susceptible to cell death than wt cells (Zhang et al., 2019c), arguing that also other E3 ligases might play a role at this site. Mechanistically, MEFs from *Ripk1*$^{K376R/K376R}$ mice fail to properly activate NF-κB signaling (Tang et al., 2019; Zhang et al., 2019c), suggesting that blunted activation of pro-inflammatory and pro-survival gene transcription might sensitize *Ripk1*$^{K376R/K376R}$ MEFs to cell death. Nevertheless, upon blockade of NF-κB signaling, *Ripk1*$^{K376R/K376R}$ MEFs or cells reconstituted with RIPK1 harboring the equivalent human mutation (RIPK1K377R) remain more sensitive to cell death than wt cells (O'Donnell et al., 2007; Tang et al., 2019). These results imply the involvement of NF-κB-dependent and -independent mechanisms of ubiquitin-mediated restriction on RIPK1 activation at this site. Additionally, RIPK1 ubiquitination mediated by cIAP1 has been reported to directly repress RIPK1 kinase activity, independently of the activation of downstream kinases (Annibaldi et al., 2018). Of note, *Ripk1*$^{K376R/K376R}$ mice die during embryonic development due to excessive cell death and inflammation (Tang et al., 2019; Zhang et al., 2019c), highlighting the importance of RIPK1 ubiquitination at K376 as a restrainer of RIPK1-mediated cell death. RIPK1 in complex I is furthermore ubiquitinated with M1-linked chains by LUBAC, which is essential for establishing a balance between TNFR1-mediated gene induction and cell death (Gerlach et al., 2011; Haas et al., 2009; Peltzer et al., 2016; Peltzer et al., 2014) (Figure 6). LUBAC is a tripartite complex consisting of Sharpin, HOIL and the catalytic subunit HOIP and is the only known ubiquitin ligase to generate M1-linked chains under physiological conditions. In line with its crucial role as regulator of RIPK1 function, genetic ablation of LUBAC components has severe consequences for the organism. As mentioned under 1.4.3.1., Sharpin-deficient *Sharpin*$^{cpdm/cpdm}$ mice develop a multi-organ inflammation, which predominantly affects the skin (Gijbels et al., 1996; HogenEsch et al., 1999; Seymour et al., 2007). *Sharpin*$^{cpdm/cpdm}$ mice present with increased cell death in the skin and in line with this, skin lesion development was shown to be driven by TNFR1-induced RIPK1 kinase activity-dependent apoptosis (Berger et al., 2014). These results demonstrate that linear ubiquitination restrains RIPK1 kinase activity from the activation of caspase-8-mediated apoptosis downstream of TNFR1. In contrast to Sharpin-deficient mice, mice that lack HOIP, are not born. HOIP$^{-/-}$ embryos present with excessive cell death in the endothelium and die in utero at around E10.5 (Peltzer et al., 2014) similar to caspase-8, FADD or FLIP-deficient mice (Varfolomeev et al., 1998; Yeh et al., 2000), implicating HOIP in the regulation of cell death signaling. In vitro, Hoip$^{-/-}$ MEFs are sensitized to TNF-induced cell death, as a consequence of increased TNFR1-induced complex II formation (Peltzer et al., 2014). Interestingly, NF-κB signaling in Hoip$^{-/-}$ MEFs is only slightly impaired, suggesting that linear ubiquitination of RIPK1 regulates cell death signaling upstream of NF-κB-induced gene transcription.

Importantly, the ubiquitination of RIPK1 in complex I is modulated by several ubiquitin-specific proteases, so called DUBs, which include Cylindromatosis (CYLD) (Brummelkamp et al., 2003; Kovalenko et al., 2003), TNF-α-induced protein 3 (A20) (Wertz et al., 2004) and Cezanne (Enesa et al., 2008). The M1- and K63-linkage-specific DUB CYLD is recruited to TNFR1 via LUBAC, through interaction with the HOIP-binding adaptor protein SPATA2 (Kupka et al., 2016). CYLD was reported to counteract M1-linked and K63-linked ubiquitination of RIPK1, TRADD and TNFR1 (Draber et al., 2015), thereby sensitizing cells to TNF-induced cell death (Draber et al., 2015; Kupka et al., 2016). In line with this, loss of CYLD blocks complex II formation and apoptosis induction (Wang et al., 2008). The action of CYLD is counteracted by A20, a protein with important anti-inflammatory function, which is highlighted by it being a susceptibility gene in several human inflammatory and autoimmune diseases (Vereecke et al., 2011). A20 is recruited via M1 or K63-linked chains to TNFR1 (Draber et al., 2015; Priem et al., 2019; Wertz et al., 2004) and has been implicated in the negative regulation of NF-κB signaling as part of an inhibitory feedback loop. A20 can function both as a DUB and a ubiquitin ligase and its NF-κB-dampening function has been proposed to be mediated by removal of K63-linked chains off RIPK1 and ubiquitination of RIPK1 with K48-linked chains leading to its proteasomal degradation (Wertz et al., 2004). However, the in vivo importance of its catalytic activity was challenged by the finding that mice that lack the DUB activity of A20 do not display the severe inflammatory pathology and perinatal lethality of *A20*$^{-/-}$ mice (De et al., 2014). On the other hand, mice with mutation of the M1 chain-binding Zinc Finger 7 domain of A20 spontaneously develop progressive polyarthritis, similar to mice with myeloid cell-specific deletion of A20 (*A20*$^{MYC\text{-}KO}$) (Polykratis et al., 2019), suggesting that the main anti-inflammatory function of A20 is independent from its enzymatic activity. Mechanistically, binding of A20 to M1 chains in the TNFR1 complex I is thought to shield these chains from degradation, stabilizing the linear ubiquitin chain network in complex I (Draber et al., 2015; Priem et al., 2019) and inhibiting cell death. In line with this, the inflammatory phenotype of *A20*$^{MYC\text{-}KO}$ mice is driven by RIPK1-RIPK3- and MLKL-dependent necroptosis and inflammasome activation (Polykratis et al., 2019). LUBAC-mediated RIPK1 ubiquitination is balanced by OUT deubiquitinase with linear linkage specificity (OTULIN), which is the only known DUB that specifically cleaves M1 linked chains. OTULIN interacts with LUBAC through HOIP (Draber et al., 2015; Schaeffer et al., 2014), similar to SPATA2, indicating a potential competition between CYLD and OTULIN for LUBAC binding. Currently, the main role of OTULIN is believed to be negative regulation of LUBAC's auto-ubiquitylation. OTULIN is thought to thereby increase stability of LUBAC and TNFR1 complex I, while at the same time preventing complex II formation (Heger et al., 2018).

The concept of RIPK1 ubiquitination as a means to stabilize RIPK1 in complex I is challenged by studies that report RIPK1 ubiquitination in cell death-inducing complexes (de Almagro et

al., 2017; de Almagro et al., 2015). Necrosome-bound RIPK1 is modified with K63 and M1-linked ubiquitin chains and the ubiquitin acceptor site K115 was found to be required for cell death induction (de Almagro et al., 2017; de Almagro et al., 2015).

Therefore, RIPK1 ubiquitination also positively regulates the cell death-inducing potential of RIPK1, suggesting the presence of a “ubiquitin code” of positive and negative regulatory ubiquitination events acting on the cell death inducing function of RIPK1 (Peltzer et al., 2016). In summary, a multitude of ubiquitination and deubiquitination events suggests a high level of regulation on RIPK1 that is required to achieve proper balancing between cell death and inflammation.

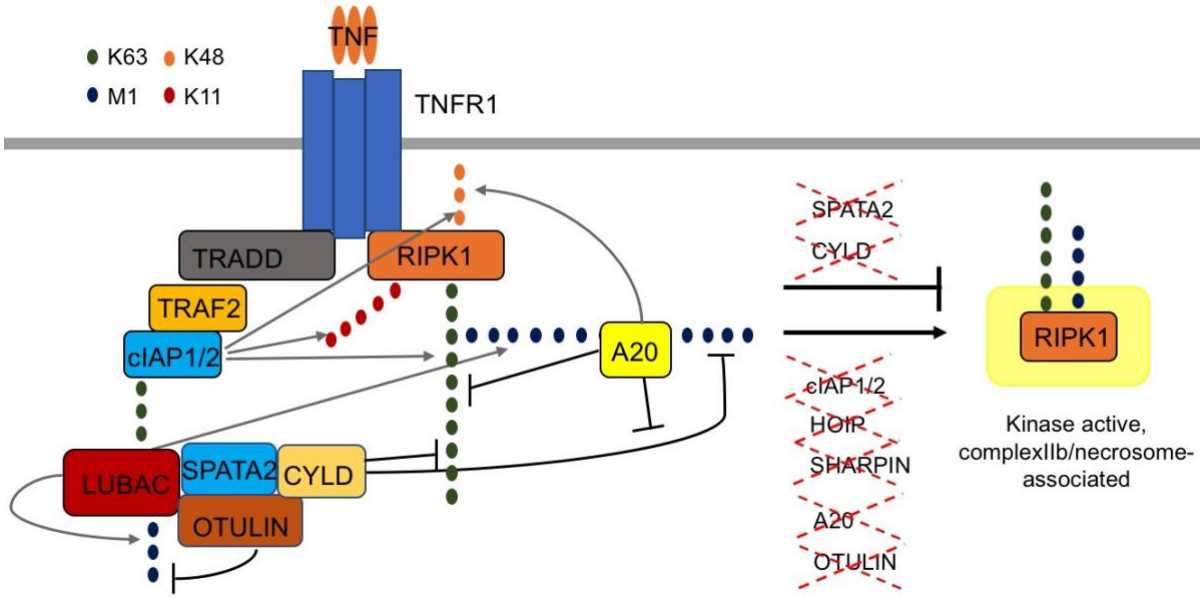

Figure 6: Scheme depicting RIPK1 regulation by ubiquitinating and deubiquitinating enzymes in response to TNFR1 ligation. The ubiquitin ligases cIAP1/2 and LUBAC attach K63-, K48- and K11- or M1-linked chains to RIPK1, respectively. The deubiquitinating enzymes CYLD, A20 and OTULIN hydrolyze chains on RIPK1 with different linkage specificity. A20 attaches K48-linked chains to RIPK1 which induces its degradation and binds to M1-linked chains to stabilize complex I. Ubiquitination and deubiquitination events constitute an important regulatory layer on RIPK1 that controls RIPK1 kinase activity-dependent integration into cell death-inducing complexes. Lack of cIAP1/2, HOIP, SHARPIN, A20 or OTULIN promotes the formation of complexes that mediate cell death, while deficiency in SPATA2 or CYLD inhibits their formation. Of note, RIPK1 was reported to be ubiquitinated with M1- and K63-linked chains in the necrosome.

1.5.2. Cleavage by caspase-8

Caspase-8 has for long been known to restrict necroptosis and caspase-8 inhibitors are routinely employed as sensitizers to necroptosis in cellular in vitro experiments. Supporting a negative regulatory function of caspase-8 on necroptosis, the embryonic lethality of caspase-8 or FADD-deficient mice (Varfolomeev et al., 1998; Yeh et al., 1998) can be prevented by deletion of RIPK1 (Dillon et al., 2014; Kaiser et al., 2014; Rickard et al., 2014b). Indeed, human

RIPK1 was reported to be cleaved by caspase-8 at aspartic acid (D)324 in its intermediate domain (Lin et al., 1999). Strikingly, mutation of the caspase-8 cleavage site in RIPK1 in mice (*Ripk1*$^{D325A/D325A}$) results in death of embryos during midgestation (Lalaoui et al., 2020; Newton et al., 2019; Zhang et al., 2019a) mimicking the embryonic lethality of mice expressing catalytically inactive caspase-8 between E10.5 and E 12.5 (*Caspase-8*$^{C362A/C362A}$) (Newton et al., 2019). Mutation of the caspase-8 cleavage site in other reported caspase-8 substrates such as itself, cFLIP or CYLD on the other hand did not affect embryonic development (Newton et al., 2019), supporting the idea that RIPK1 is the key target of the necroptosis-restricting function of caspase-8. Primary MEFs from *Ripk1*$^{D325A/D325A}$ mice show prominent RIPK1 auto-phosphorylation and undergo increased cell death in response to TNF (Newton et al., 2019; Zhang et al., 2019a). Interestingly, mice in which RIPK1 activity is blocked in addition to its cleavage by caspase-8 (*Ripk1*$^{D138N,D325A/D138N,D325A}$) are born, however succumb to serve inflammatory pathology before weaning in a RIPK3-dependent manner (Lalaoui et al., 2020; Newton et al., 2019). These data indicate that caspase-8 mediated RIPK1 cleavage represents a critical brake on RIPK1 kinase activity, however is later in life also required to restrict scaffolding function of RIPK1. Embryonic lethality of *Ripk1*$^{D325A/D325A}$ mice was furthermore prevented by ablation of TNFR1(Newton et al., 2019). Interestingly, ablation of MLKL alone rescues the embryonic lethality of mice expressing catalytically inactive caspase-8, while neither *Ripk1*$^{D325A/D325A}$ *Ripk3*$^{-/-,}$ nor *Ripk1*$^{D325A/D325A}$ *Mlkl*$^{-/-}$ mice are viable. *Ripk1*$^{D325A/D325A}$ mice with concurrent ablation of FADD and MLKL or Caspase-8 and RIPK3 on the other hand are born (Lalaoui et al., 2020; Newton et al., 2019; Zhang et al., 2019a). Therefore, caspase-8 mediated cleavage on RIPK1 stalls both excessive RIPK1-mediated apoptosis and -necroptosis downstream of TNFR1 during development.

Importantly, human patients with missense mutations in the caspase-8 cleavage site of RIPK1 develop a “cleavage-resistant RIPK1-induced autoinflammatory syndrome” characterized by periodic fever and lymphoadenopathy (Lalaoui et al., 2020; Tao et al., 2020). In keeping with Caspase-8 restricting RIPK1 kinase activity and cell death by cleavage of RIPK1, peripheral blood mononuclear cells from these patients display increased RIPK1 activity and sensitivity to TNF-induced apoptosis and necroptosis as well as increased RIPK1-mediated expression of inflammatory cytokines and chemokines (Tao et al., 2020). Fibroblasts from the same patients on the other hand were resistant to RIPK1-induced cell death, hinting to some degree of cell type-specificity (Tao et al., 2020).

In conclusion, these studies show that caspase-8-mediated cleavage constitutes a conserved brake on RIPK1 activation that protects from aberrant TNFR1-induced apoptosis and necroptosis.

1.5.3. Phosphorylation by other kinases

While RIPK1 ubiquitination has initially been considered the main mechanism that restrains RIPK1 kinase activity, more recently, RIPK1 phosphorylation by other kinases has been established as a crucial aspect of post-translational regulation on RIPK1.

As described under 1.4.3.1., the absence of the IKK complex subunit NEMO in IECs in mice leads to RIPK1 kinase activity-dependent IEC death and colitis development (Vlantis et al., 2016). Importantly, the pathology is not phenocopied by IEC-specific ablation of NF-κB subunits (Vlantis et al., 2016), therefore indicating an NF-κB-independent role of the IKK complex in regulating RIPK1 kinase activity. Indeed, it was found that IKK1/2 directly phosphorylate RIPK1 at S25, and possibly other residues, to repress complex IIb/necrosome formation and apoptosis or necroptosis (Figure 7,8) (Dondelinger et al., 2019; Dondelinger et al., 2015). A phosphorylation-mimicking serine to aspartic acid (D) mutation at residue 25 (S25D) decreases the enzymatic activity of recombinant RIPK1 and inhibits RIPK1-kinase activity-dependent cell death in conditions of IKK repression or inhibition of its upstream kinase TAK1 (Dondelinger et al., 2019). Supporting the physiological relevance of S25, RIPK1S25D mutation protects mice from TNF-injection-induced lethal shock and compromises the cell-death-dependent clearance of *Yersinia* bacteria, a physiological model of TAK1/IKK inhibition, that both depend on RIPK1 kinase activity (Dondelinger et al., 2019). Mechanistically, as S25 is located in the phosphate-binding, glycine rich loop of RIPK1, it has been proposed that phosphorylation at this site might result in an altered ability of RIPK1 to use ATP. An additional layer of regulation on RIPK1 is imposed by the p38 substrate MAP kinase-activated protein kinase 2 (MK2), a kinase that is activated downstream of TAK1 (Figure 7). Three groups independently showed that MK2 phosphorylates RIPK1 on S321 in the intermediate domain (Figure 8) to restrain RIPK1 kinase-activity-dependent cell death (Dondelinger et al., 2017; Jaco et al., 2017; Menon et al., 2017). In contrast to IKK1/2, that phosphorylate RIPK1 in complex I, MK2 targets RIPK1 in complex I as well as in the cytoplasm (Dondelinger et al., 2017; Jaco et al., 2017). Of note, also TAK1 has been suggested as the direct upstream kinase for S321 (Geng et al., 2017), which however contradicts the observation that phosphorylation at this site is abolished when MK2 is absent, a condition in which TAK1 remains functional (Jaco et al., 2017). Additionally, S336 (Figure 8) (Dondelinger et al., 2017; Menon et al., 2017) and S332/334 (Geng et al., 2017) have been reported to be targeted by MK2 or TAK1, respectively, and these sites may also be involved in regulation of RIPK1 kinase activity-dependent cell death. Mechanistically, phosphorylation at S321 was suggested to preclude RIPK1 autophosphorylation and its association with cell death-inducing complexes (Jaco et al., 2017). As opposed to IKK1/2, MK2 does not constitutes a main restricting factor on RIPK1, but rather acts as an additional layer of regulation limiting the amount of cell death, as ablation of MK2 is not enough to induce cell death by itself, but only further sensitizes to death in

situations in which a cell death-sensitizing mechanism is already in place (Dondelinger et al., 2017; Jaco et al., 2017; Menon et al., 2017). Nevertheless, this checkpoint was shown to be physiologically significant, as MK2 deficiency sensitizes mice to death in a model of TNF-induced sterile shock (Dondelinger et al., 2017). Other kinases recruited to complex I have furthermore been shown to directly regulate RIPK1 activity. Similar to IKK1/2, the kinases TBK1 and IKKε are recruited to TNFR1 complex I via Nemo, while they additionally require the adaptors NAP1 and TANK (Figure 7) (Lafont et al., 2018). TBK1-deficiency in mice is embryonically lethal and this phenotype is rescued by genetic inactivation of RIPK1's enzymatic activity of (Xu et al., 2018), revealing a negatively regulatory function of TBK1 acting on RIPK1 kinase activity. Indeed, TBK1 was reported to phosphorylate RIPK1 in TNFR1-induced complex I, which suppresses its kinase activity and cell death-inducing potential (Lafont et al., 2018; Xu et al., 2018). While also other sites may be targeted (Lafont et al., 2018), threonine (T)189 in human RIPK1 (T190 in murine RIPK1), that is located in the RIPK1 activation loop (Xie et al., 2013), has been proposed as the main TBK1 target site (Figure 8). Functional studies on the role of this residue however are not conclusive as both phospho-mimetic and non-phosphorylatable mutation at T189/T190 block RIPK1 catalytic activity and cell death (Xu et al., 2018). Interestingly, TBK1-deficiency in cells was reported to result in TAK1 overactivation (Xu et al., 2018), thereby demonstrating substantial crosstalk between different RIPK1-restraining mechanisms. IKKε additionally phosphorylates RIPK1 on sites that partially overlap with TBK1-, MK2- and IKK1/2-target residues (Lafont et al., 2018). Nevertheless, TBK1/IKKε are not completely functionally redundant with MK2 and IKK1/2 as their inhibition increases TNF-induced cell death in vitro and importantly sensitizes mice to a model of TNF-induced shock (Lafont et al., 2018). Thus, TBK1 and IKKε constitute another, physiologically important checkpoint safe-guarding RIPK1 kinase activity in TNFR1 signaling. Furthermore, most recently, the autophagy-initiating kinase ULK1 (Unc-51 Like Autophagy Activating Kinase 1) has been proposed to regulate RIPK1 via direct phosphorylation at human RIPK1 residue S357, (Wu et al., 2020), which is equivalent to mouse S356, thereby establishing a crosstalk between autophagy and TNFR1-induced signaling. ULK1 was proposed to directly interact with RIPK1 via its C-terminal domain and mediate inhibitory phosphorylation of a cytoplasmic pool of RIPK1 (Figure 7). While ULK1 was also reported to be recruited to TNFR1, RIPK1 phosphorylation in this context seems to be hampered by RIPK1 ubiquitination in the intermediate domain. Studies in overexpression systems showed that RIPK1S357A mutation decreased TNF-induced RIPK1 kinase activity-dependent apoptosis and necroptosis (Wu et al., 2020), but the relevance of this site still awaits confirmation in systems with physiological RIPK1 levels and in-vivo systems.

In summary, multiple kinases directly phosphorylate RIPK1 on different residues to keep its cell death-inducing potential in TNFR1-induced complex I in check and thereby provide yet another mechanism of regulation on RIPK1.

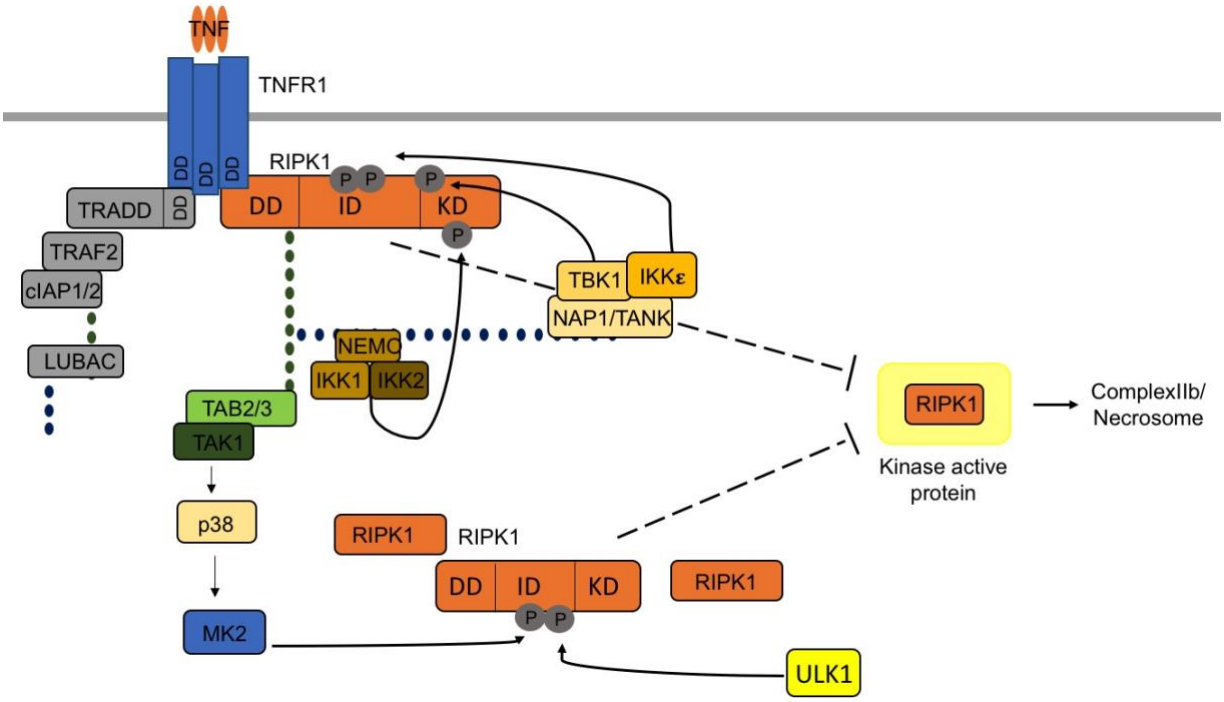

Figure 7: Scheme depicting the network of phosphorylation events regulating RIPK1 kinase activity downstream of TNFR1. TNFR1 complex I-associated RIPK1 is targeted by IKK1/2 as well as TBK1/IKKε by direct phosphorylation which restricts its kinase activity and association with cell death-inducing complexes. The p38-activated kinase MK2 directly targets RIPK1 in complex I and a cytoplasmic pool of RIPK1 by phosphorylation which restricts its catalytic activity. The autophagy-initiating kinase ULK1 furthermore has been proposed to phosphorylate RIPK1, thereby inhibiting the formation of the RIPK1 kinase activity-dependent complexIIb/necrosome.

1.5.4. RIPK1 auto-phosphorylation

In the search for targets of RIPK1 kinase activity, the mitochondrial fission-involved protein DRP-1 has been suggested to be a substrate of RIPK1 (Park et al., 2018), however convincing evidence for a direct phosphorylation event is missing. Also, although RIPK1 and RIPK3 interact in amyloid signaling complexes, RIPK3 is not a target of RIPK1 (Cho et al., 2009). On the other hand, RIPK1 was reported to auto-phosphorylate on multiple sites in the kinase domain including S14/15, S20, S161 and S166 in humans (Degterev et al., 2008) and S14/15, S161, S166 and T169 in mice (Figure 8) (Berger et al., 2014; Dondelinger et al., 2019; Ofengeim et al., 2015; Zhang et al., 2017b). The fact that RIPK1 remains the only known and validated target of its own kinase activity may suggest that RIPK1 auto-phosphorylation mechanistically transmits the cell death inducing signal by inducing conformational changes

within itself. It has been speculated that such conformational rearrangement might lead to exposure of structures which are required to induce cell death signaling, such as the RHIM domain (Newton, 2020). This might then license RIPK1 to interact with other RHIM-containing proteins, such as RIPK3, to activate the cell death machinery. Nevertheless, functional evidence for this is still missing.

Although RIPK1 kinase activity is implicated in RIPK1-induced cytotoxicity, auto-phosphorylation of RIPK1 is not restricted to situations when RIPK1 acts as an inducer of cell death. Instead, phosphorylation at S166 is detected in wt MEFs in RIPK1 immunoprecipitates within minutes of TNF stimulation (Newton et al., 2016b). On the other hand, RIPK1 in complex IIb/necrosome is heavily auto-phosphorylated at S166 (Lafont et al., 2018; Meng et al., 2018; Tang et al., 2019), and RIPK1 signals for cell death in this context. RIPK1 autophosphorylation was reported to be promoted via DD-mediated homodimerization which requires residue K599 in human RIPK1 or K584 in murine RIPK1 (Meng et al., 2018).The RIPK1RHIM on the other hand is dispensable for autophosphorylation at S166 (Newton et al., 2016b).

Several studies have used in-vitro cellular systems to address the importance of different sites for RIPK1-mediated cell death, their functional relevance however remains poorly understood. All known autophosphorylation sites are located in the kinase domain of RIPK1 and S161, S166 and T169 reside in the activation loop/T-loop. As described under 1.4.1., the activation loop is a crucial element controlling kinase activation and can switch between a closed conformation that occludes the catalytic cleft of the kinase and an open conformation which allows for catalytic activity. Phosphorylation of the T-loop is a common regulatory mechanism leading to kinase activation (Adams, 2003). Interestingly, the activation loop of RIPK1 was found to be very similar to that of B-RAF and homology modelling suggests that RIPK1 can assume a similar conformation to B-RAF in which S161 in RIPK1 corresponds to T598 in the activation loop of B-RAF (Degterev et al., 2008), which is auto-phosphorylated to activate the kinase. Mutation of serine at position 161 in RIPK1 to alanine was reported to reduce its kinase activity and lead to a partial reduction of necroptosis in Jurkat cells (Degterev et al., 2008), while necroptosis in HEK293T cells was unaffected by this mutation (McQuade et al., 2013). Alanine at this site was later proposed to lack capability for proper T-loop stabilization, promoting an open activation loop conformation (Zhang et al., 2017b). Phosphomimetic S161E mutation the other hand was able to overcome the kinase-inactivating K45A mutation to induce cell death in an L929 cellular overexpression system (Zhang et al., 2017b). These results imply that S161 is both necessary and sufficient to transduce the lethal signal by RIPK1, however to date lack functional validation in-vivo.

On the other hand, antibodies have been developed to detect auto-phosphorylation at S166 (Berger et al., 2014), which is used as a standard biomarker for RIPK1 activation in the field (Dondelinger et al., 2017; Newton et al., 2016b; Ofengeim et al., 2015; Patel et al., 2020). A

study reported that RIPK1 S20/S161/S166 mutation in HEK293T cells did not affect necroptosis induction (McQuade et al., 2013), however there are no data on the effect of single S166 mutation. Therefore, the functional role and in-vivo relevance of this site to date remain unknown.

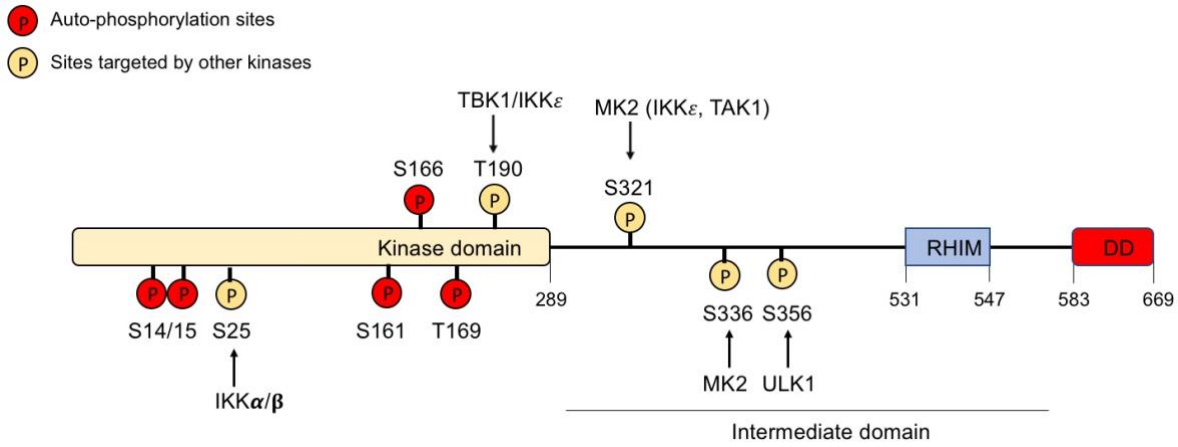

Figure 8: RIPK1 phosphorylation sites. Mouse RIPK1 and its reported auto-phosphorylation sites (red) as well as selected other phosphorylation sites for which the upstream kinase has been identified and mutational studies suggest a functional relevance (yellow) are shown.

1.6 Aim of the study

Despite robust evidence that RIPK1 kinase activity acts as a driver of cell death and inflammation (Berger et al., 2014; Kondylis et al., 2015b; Newton, 2020; Vlantis et al., 2016), the mechanistic role of the catalytic function of RIPK1 kinase activity for the induction of cell death remains unclear. Based on lack of validated downstream targets of RIPK1 and the fact that auto-phosphorylation has been proposed to be functionally important for RIPK1 kinase activity-dependent cell death (Degterev et al., 2019; Zhang et al., 2017b), to-date, auto-phosphorylation is believed to be the main and crucial function of RIPK1 kinase activity that is required for cell death induction. The function and role of specific sites in this context however remains poorly understood. Here, we aimed at shedding light on the mechanistic role of RIPK1 kinase activity by studying the function of auto-phosphorylation at S166 for RIPK1-mediated signaling using CRISPR-Cas9-assisted gene targeting in mice. We furthermore aimed to elucidate the *in-vivo* importance of RIPK1 auto-phosphorylation at S166 for the induction of RIPK1-mediated cell death and inflammation using relevant mouse models.

2. Material and Methods

2.1 Chemical and biological materials

Kits and chemicals used in this study were purchased from the indicated companies. All solutions were prepared with double-distilled water (ddH_2O).

Table 1: Reagents and Chemicals used in this study

Reagent/chemical	Supplier (catalogue number)
Acrylamid/Bis solution	Serva (10688.01)
Agarose ultra-pure	Biozym (840004)
Ammonium persulphate (APS)	Sigma (A3678-100G)
Birinapant	BioVision (2597)
Chloroform	VWR (22711290)
Collagenase Type II	Worthington (44N15307B)
cOmplete Tablets Mini (Protease EDTA-free Inhibitor Cocktail)	Roche (11836145001)
dimethyl sulfoxide (DMSO)	AppliChem (A3672,0050)
dNTPs	Invitrogen (10297-117)
Draq5	Cell Signaling Technology (#4084L)
Dulbecco's Modified Eagle Medium (DMEM)	Gibco (41965-062)
Dynabeads™ Protein G	Invitrogen (10009D)
ECL Western Blotting Detection Reagent	GE Healthcare
Entellan	Merck Millipore (107960)
Ethanol absolute	AnalR Normapur (20821-321)
Fetal Bovine Serum	PAN Biotech
Fetal Bovine Serum Superior	Biochrom
FLAG M2 affinity gel	Sigma-Aldrich (A4596)
Fluoromount-G	Southern Biotech 0100-01
Glutamine	Gibco
Glycerol	VWR (24386-298)
Glycine	VWR (101196X)
HEPES buffer	Gibco
Hydrochloride acid (HCl) 37%	AppliChem (A2427-2500)
Isopropanol (2-Propanol)	AppliChem (A3928)
LPS	Enzo (ALX-581- 010-L002)
LysC (Lysyl Endopeptidase, Mass Spectrometry Grade)	Wako Chemicals USA (121-05063)

Methanol (MetOH)	Sigma (494437)
$MgCl_2$	
N,N,N',N' Tetra methylenediamine (TEMED)	Serva (35925)
NaCl	VWR (7647-14-5)
Nec-1s	BioVision (2263)
nonfat dry milk	Serva (68514-61-4)
Paraformaldehyde (PFA)	AppliCHem (A3813)
Penicillin (10000U/ml)/Streptomycin (10000ug/ml)	Invitrogen (15140163)
Phospahte buffered saline (PBS)	Gibco (14190-094)
Phosphatase inhibitor cocktail tablets, PhosSTOP	Roche (04906837 001)
Pierce™ 660 nm Protein Assay	ThermoScientific (22660)
Poly(I:C)	EDM Millipore (42424-50-0)
Proteinase K	Roche (3115852)
Proteinmarker PeqGold	Peqlab (27-2210)
Random hexamer primers	Invitrogen (48190-011)
Recombinant Mouse Macrophage Colony Stimulating Factor (rm M-CSF)	Immunotools (12343112)
Recombinant Mouse Macrophage Colony Stimulating Factor (rm M-CSF)	Immunotools (12343118)
Recombinant mouse TNF	VIB Protein Service Facility, Ghent
Red-Taq DNA Polymerase 2X MasterMix	VWR (733-2131)
Restore Western Blot stripping buffer	Thermo Fisher Scientific (21059)
RNase OUT	Invitrogen (10777-019)
Sodium Azide (NaN_3)	Merck (S2002)
Sodium dodecyl sulfate (SDS)	Millipore (817034.1000)
Sodium pyruvate (100mM)	Gibco (11360-039)
SuperScript III Reverse Transcriptase	Invitrogen (18080-044)
SuperScript™ III First Strand Synthesis System	Thermo Fisher Scientific (18080-051)
SuperSignal™ West Femto	Thermo Fisher Scientific (34095)
SuperSignal™ West Pico Chemiluminescent substrate	Thermo Fisher Scientific (34080)
SuperSignal™ West Pico PLUS Chemiluminescent Substrate	Thermo Fisher Scientific (34580)

TaqMan Gene Expression Master Mix RTqPCR Mastermix	Thermo Fisher Scientific (4369542)
Tissue-Tek O.C.T™ Compound	Sakura (4583)
Tris(hydroxymethyl)aminomethan (TRIS)	VWR (103156X)
Tris(hydroxymethyl)aminomethan Hydrochlorid (TRIS HCl)	VWR (85.827.297)
Triton X-100	AppliChem (A4975-0500)
Trizol reagent	Invitrogen (15596-018)
Trypsin	Promega (V5111)
Trypsin EDTA	Gibco (12603-010)
Tween-20	Sigma (P1379-500)
Yoyo™-1 Iodide	Invitrogen (Y3601)
Z-VAD-FMK	Enzo (ALX-260-020-M005)
β-mercaptoethanol	Sigma (M7522)

Table 2: Kits used in this study

Kit	**Supplier (Catalogue Number)**
ABC Kit Vectastain Elite	Vector (PK 6100)
Avidin/Biotin Blocking Kit	Vector (SP-2001)
Liquid DAB Substrate Chromogen System	DakoCytomation (Code K3466)
NucleoSpin™ Gel- and PCR Cleanup Kit	Macherey-Nagel (11992462)
NucleoSpin™ RNA kit	Macherey-Nagel (740955.50)
RNA extraction RNeasy mini Kit	Qiagen (74106)
RNase-free DNase set	Qiagen (79254)
SuperScriptIII cDNA synthesis Kit	Invitrogen (18080-044)
TaqMan® Gene expression Master Mix	Applied Biosystems (4369542)

Table 3: Buffers, solutions and media used in this study

Buffer/solution/medium	
5x Laemmli loading buffer	250 mM Tris-HCL (pH 6.8), 10% (w/v) SDS, 50% Glycerol (v/v), 0.01% Bromphenolblue (w/v), 10% β-Mercaptoethanol (v/v)
Antigen retrieval buffer	10mM NaCitrate 0.05%Tween-20, pH 6
Blocking buffer	PBS, 5% nonfat dry milk, 0.1% Tween 20

BMDM medium	DMEM, 10% Fetal Bovine Serum Superior (Biochrom), Penicillin-Streptomycin, 1% glutamine, 1% sodium pyruvate , 1% HEPES buffer, 20 ng/ml rm M-CSF (freshly added)
Collagenase solution	30 mg of collagenase Type II in 10 ml of DMEM, sterile filtered before usage
Fibroblast medium	DMEM, 10% Fetal Bovine Serum (PAN Biotech) 1% Penicillin-Streptomycin, 1% glutamine, 1% sodium pyruvate, 1% HEPES buffer
Freezing medium	Fetal Bovine Serum (Superior), 10% DMSO
IHC blocking buffer	PBS, 1% BSA, 0.003% NaN3, 0.2 % fish skin gelatine, 0,05% Tween-20
Immunoprecipitation (IP) buffer	(20mM HEPES-KOH (pH 7.6), 150mM NaCl, 2mM EDTA, 1% Triton X-100, 10% Glycerol, cOmplete Tablets Mini and PhosSTOP
NP-40 lysis buffer	10% glycerol, 1% NP-40, 150mM NaCl and 10mM Tris-HCl pH 8, cOmplete Tablets Mini and PhosSTOP
PCR reaction mix (per reaction)	12.5 µl Taq 2x Mastermix, 2µl Primer mix (forward and reverse 1:1, 10µM), 10.5 µl H_20, 2 µl genomic DNA
Peroxidase blocking buffer	0.04 M NaCitrate, 0.121 M Na_2HPO_4 0.03 M NaN_3, 3% H_2O_2
Primary antibody dilution buffer	PBS, 0.1% Tween 20, (1% BSA), NaN_3
Secondary antibody dilution buffer	PBS, 0.1% Tween 20
Tail lysis buffer	100 mM Tris/HCl, 5 mM EDTA, 0.2%SDS, 200 mM NaCl
TBS	50 mM Tris-Cl, pH 7.5; 150 mM NaCl
TBS-T	TBS, 0.1% Tween-20
TE-buffer	10 mM Tris/HCl pH 8, 1 mM EDTA pH 8
Transfer buffer	25 mM Tris-base, 192 mM Glycine, 20% MetOH
Tris-glycine electrophoresis buffer	25 mM Tris-base, 192 mM Glycine, 0.1% SDS
Triton X lysis buffer	20 mM HEPES-KOH (pH 7.6), 150 mM NaCl, 2 mM EDTA, 1% Triton X-100, 10% Glycerol,

	supplemented with PhosStop and cOmplete Tablets

2.2 Animal experiments

2.2.1. Mouse care

Mice used in this study were maintained at the SPF animal facilities of the Institute for Genetics and the CECAD Research Center of the University of Cologne, under a 12 h light cycle, at a temperature of 22 ± 2 °C, 55 ± 5% relative humidity and given a regular chow diet (Harlan, diet number 2918 or Prolab Isopro RMH3000 5P76) ad libitum. All animal procedures were conducted in accordance with European, national and institutional guidelines and protocols were approved by the responsible local authorities (Landesamt für Natur, Umwelt und Verbraucherschutz Nordrhein-Westfalen, Germany; ethical committee of Ghent University, Belgium). In case that animals required medical attention, they were provided with appropriate care and sacrificed when they developed macroscopically visible skin lesions or to minimize suffering. *Ripk1*$^{D138N/D138N}$ (Polykratis et al., 2014) , *Nemo*^{FL} (Schmidt-Supprian et al., 2000), *Villin-Cre* (Madison et al., 2002), *Alfp-Cre* (Kellendonk et al., 2000) and *Sharpin*$^{cpdm/cpdm}$ (Seymour et al., 2007) mice were described previously.

2.2.2. Mouse generation using CRISPR/Cas9-mediated gene targeting

For the generation of *Ripk1*$^{S166A/S166A}$ mice, Cas9 mRNA (TriLink) together with the 120 bp ssDNA repair oligo (IDT) and the short guide RNA(s) (sgRNA) were microinjected into the pronucleus of fertilized oocytes obtained from C57BL/6 mice. A single sgRNA targeting a site adjacent to pos 166 was used (5'gacatggagcaaactgacta3'). On the next day, the injected embryos were transferred to foster mothers and allowed to develop to term. Mutations in the genome of progeny were determined by analysis of genomic DNA using the T7 endonuclease I assay (NEB) and sequencing. Sequenced DNA fragments were aligned using Benchling [Biology Software] (2020, https://benchling.com). The sequence of the ssDNA oligo used as repair templates was 5' CTC TTC TTT TCC AGA TAG CCG ATC TTG GTG TGG CTT CCT TTA AGA CAT GGG CCA AAC TGA CTA AAG AGA AAG ACA ACA AGC AGA AAG AAG TGA GCA GCA CCA CTA AGA AGA ACA ATG GTG 3'.

2.3 Cell culture

2.3.1. Primary cell isolation and culture

2.3.1.1. Bone marrow-derived macrophages (BMDMs)

For the differentiation of bone marrow-derived macrophages (BMDMs) from bone marrow, tibia and femura from mice were collected and kept in PBS on ice. Under the sterile hood, excess muscle and fibre was removed and bones were flushed with ice-cold PBS to isolate the bone-marrow using a 23G needle. Flushing medium was subsequently spun down at 1200 rpm for 5 min and bone marrow from one leg was resuspended and plated in 23 ml of BMDM medium (Table 3) on non-coated petri dishes or frozen in 500 µl of freezing medium (Table 3). After two and four days of culture, cells were topped up with 10 ml of BMDM medium and after six days of culture, differentiated macrophages were trypsinized and seeded for experiments on coated dishes.

2.3.1.2. Lung fibroblasts

For the isolation of lung fibroblasts, lungs were collected and kept in PBS on ice. Under the sterile hood, lungs were cut in small pieces in well of 6-well plate. Then tissue pieces were transferred to Eppendorf tube and covered in 1 ml of collagenase solution (Table 3) and placed at 37°C at 600 rpm shaking for 30 min or until tissue pieces had started dissolving. Cells from one lung were plated on two 15 cm tissue culture coated dishes in 23 ml of fibroblast medium (Table 3) each. After three days or when a substantial amount of cells had attached, medium was removed and cells were washed with PBS, then new medium was added to plate and cells were grown until confluency before plating for experiments.

2.3.1.3. Dermal fibroblasts

For the isolation of dermal fibroblasts, ears and tail tissue was collected from mice and placed in 70% Ethanol. Under the sterile hood, tissue was air dried for 5 min and then cut in very small pieces in well of a 6 well plate. Pieces were transferred to Eppendorf tube and covered in collagenase solution and placed at placed at 37°C at 600 rpm shaking for 1,5 h. Cells from one mouse were then plated on one 15 cm dish and cells were grown until confluency before plating with exchange of medium when necessary.

2.4 Molecular Biology

2.4.1. Preparation of genomic DNA from tail biopsies

To isolate genomic DNA from mouse tail biopsies, tissue was lysed using 1-3 µl of Proteinase K in 200 µl of tail lysis buffer overnight at 56 °C. The next day, lysate was centrifuged at 13

000 rpm for 1 min and supernatant was transferred to sterile tube containing 200 µl isopropanol followed by centrifugation at 13 000 rpm for 1 min. Pellet was washed in ethanol and air dried for 20 min before dissolving in TE buffer.

2.4.2. Genotyping PCRs

Routine mouse genotypings were performed by polymerase chain reaction (PCR) on genomic DNA isolated from tail/ear biopsies. Point mutations were screened for using mutation (mut)- and wildtype-allele specific primers which resulted in presence or absence of a PCR fragment as a readout. To detect floxed alleles and transgenes, allele-specific genomic region was amplified to determine genotypes via size of the resulting PCR product. PCR mixes were prepared using a general scheme (Table 3) using specific primers (Table 4). PCR programs consisted of a five step program comprising an initial denaturation (step 1), followed by denaturation (step 2), primer annealing (step 3), extension (step 4) and a final extension (step 5) (Table 4). PCR products were run in 2% agarose gels and visualized using UV light.

Table 4: Genotyping PCR protocols

Allele	Primer sequence (5'-3')	Expected band size	Program (step 1 -5)	Cycles (step 2-4)
Ripk1^{S166A}	Fw: TTC ACA CAC ACA TCT TGG CA	wt: 338 bp (fw+wt_rv) mut: 338 bp (fw+mut_rv)	94°C 3min 94°C 30 sec 60°C 45 sec 72°C 40 sec 72°C 3min	40
	Wt_rv: TCT TTC TCC TTA GTC AGT TTG CT			
	Mut_rv: TCT TTC TCC TTA GTC AGT TTG GC			
Villin-Cre	ACA GGC ACT AAG GGA GCC AAT G	wt: ~ 900 bp tg: ~ 350 bp	94°C 3 min 94°C 1 min 67°C 1 min 72°C 1 min 72°C 5 min	35
	AT TGCA GGT CAG AAA GAG GTC ACA G			
	GTT CTT GCG AAC CTC ATC ACT C			
Alfp-Cre	TCC AGA TGG CAA ACA TAC GC	wt:no band tg: 300 bp	94°C 3 min 94°C 30 sec 60°C 30 sec 72°C 3 min 72°C 10 min	35
	GTG TAC GGT CAG TAA ATT GGA C			

Sharpin^{cpdm}	wt_fw: TTA GGC ACC GAG CCT GGG G mut_fw TTA GGC ACC GAG CCT GGG C rv: TCG ACC AGG TGG CCC GGA CAT ATT	wt: 500 bp (wt_fw+vr) mut: 500 bp (mut_fw+rv)	96°C 4 min 96°C 30 sec 67°C 30 sec 72°C 1 :30 min 72°C 10 min	30
Nemo^{FL}	CGT GGA CCT GCT AAA TTG TCT ATC ACC TCT GCA AAT CAC CAG ATG TGC CCA AGA ACC ATC CAG	wt: 301 bp floxed: 446 bp deleted: 644 bp	94°C 3 min 94°C 30 sec 60°C 30 sec 72°C 30 sec 72°C 3 min	35
Ripk1^{D138N}	TAC CTT CTA AC AAA GCT TTC C AAT GGA ACC ACA GCA TTG GC CCC TCG AAG AGG TTC ACT AG	wt: 220bp mut: 180 bp	94°C 2 min 94°C 30 sec 60°C 30 sec 72°C 30 sec 72°C 5 min	40

2.4.3. Sanger sequencing of PCR products

For Sanger sequencing of PCR products in mice with point mutations at position 166 in *Ripk1*, the region surrounding the knock-in site was amplified by PCR using a standard PCR reaction mix (Table 3) and site-specific primers (Table 5). PCR products were purified using a NucleoSpin™ Gel- and PCR Cleanup Kit (Macherey-Nagel, Table 2). Concentration of PCR products was measured and purified PCR products were Sanger sequenced with forward and/or reverse primers using the SUPREMERUN Tube sequencing service (Eurofins Genomics).

Table 5: PCR protocol for Sanger Sequencing of region surrounding position 166 in Ripk1

Allele	Primer sequence (5'-3')	Expected band size	Program (step 1 -5)	Cycles (step 1-4)
Ripk1 (position 166)	fw: TGAGAATCTGTTGCAAGGTAGC rv: TGTCTTACTCTCATAGGGCTCC	408 bp	94°C 3min 94°C 30 sec 60°C 30 sec 72°C 30 sec 72°C 3min	34

2.4.4. Isolation of RNA from tissue

For RNA isolation from colon tissues for microarray analysis, frozen samples were disrupted using a Precellys 24 (Bertin technologies) and total RNA was extracted using a Nucleospin® RNA kit (Macherey-Nagel, Table 2) according to manufacturer's instruction.

For RNA isolation from whole skin tissues, tissue was similarly disrupted in a Precellys 24 but in 1 ml Trizol reagent. Samples were subsequently spun down for 10 min at 13 000 rpm. In order to extract RNA, supernatants were transferred to new tubes and 200 µl chloroform was added and samples were mixed and left for incubation for 5 min. To separate the organic and the aqueous phase, the samples were subsequently centrifuged for 15 min at 13 000 rpm. The aqueous phase supernatants were transferred to new tubes and an equal volume of 70 % (v/v) ethanol was added and samples were mixed. Samples were then further processed using the RNA extraction RNeasy mini Kit (Qiagen, Table 2) following manufacturer's instructions. Possible RNA contamination by DNA was subsequently checked by PCR using ß-Actin-specific primers (fw: TAA AAC GCA GCT CAG TAA CAG TCC G and rv: TGG AAT CCT GTG GCA TCC ATG AAA C) and a standard PCR reaction mix (Table 3). Concentration and purity of the extracted RNA were measured using a NanoDrop™ Spectrophotometer (Thermo Fisher Scientific).

2.4.5. cDNA synthesis and quantitative RT-qPCR

cDNA was synthesized using the SuperScriptIII cDNA synthesis Kit (Invitrogen, Table 2) according to manufacturer's instructions. 1 ug of RNA was used in reaction mixes with a final volume of 10 ul with 50 ng random hexamer primers and 100 mM dNTPs (Table 1). To allow for primer annealing, reaction mixes were heated for 5 min to 65°C for and subsequently placed on ice shortly. Afterwards, 10 ul of cDNA reaction mix (2x RT-reaction buffer, 10 mM $MgCl_2$, 20 mM DTT, 40 units RNase OUT and 200 units of SuperScript III polymerase (Table 1)) were added to each sample. Samples were incubated for 10 min at 25°C to allow for reverse transcription of RNA, followed by cDNA was synthesis for 50 min at 50°C and heat inactivation for 5 min at 85°C. Remaining RNA was digested using RnaseH (1ul per sample, Table 1) for 20 min at 37°C and cDNA reaction mixes were diluted 1:10. To test for efficiency of cDNA synthesis ß-Actin PCRs were performed.

Quantitative real time PCR (qRT-PCR) was performed using gene-specific Taqman probes (Table 6). Reactions contained 5 ul qRT-PCR Mastermix, 5 ul qRT-PCR primer-probe mix and 2.5 ul nuclease-free water and 2 ul cDNA. Samples were run in technical duplicates and TATA-box-binding protein (Tbp) served as reference gene. RT-qPCRs were run on a Quant Studio Real-Time PCR System (Thermo Fisher Scientific) in 384-well format. Programs consisted of an initial polymerase activation step at 95°C for 10 min, followed by 40 amplification cycles

consisting of 10 sec at 95 °C and 1 min at 60°C. The relative expression of gene transcripts was analyzed using the 2-ΔCt method.

Table 6: Taqman probes used for qRT-PCR

Gene	Taqman probe
Ccl3	Mm00441258_m1
Cxcl3	Mm01701838_m1
Il-1β	Mm00434228_m1
Il-6	Mm00446190_m1
Tnf	Mm02583406_s1
Tbp	Mm00446973_m1

2.4.6. Microarray analysis

Clariom-S mouse microarray analysis (Thermo Fisher Scientific) was performed using 100 ng of total RNA per sample. For target preparation, the Gene Chip™ WT PLUS Reagent Kit (Thermo Fisher Scientific) was using according to manufacturer's instructions followed by hybridization in a Gene Chip Hybridization Oven 645 for 16 h at 45 °C. The Gene Chip Scanner 7 G was used to scan Gene chips. The Clariom-S-mouse array was performed in a 169 format, using the Fluidics Protocol FS450-0007. Affymetrix Expression Console or Transcriptome Analysis Console (TAC) Software was employed for array-quality control. InstantClue (Nolte et al., 2018) was used for Z score transformation and to perform heat cluster data analysis.

2.5 Biochemistry

2.5.1. Preparation of protein extracts

For preparation of protein extracts from cells, cell culture plates were placed on ice and cells were washed with ice cold PBS twice. Cells were then incubated with Triton X lysis buffer (Table 3) for 20 min with occasional shaking, before collection of lysates using a scraper. When necessary, for example due to unequal seeding, protein concentrations were measured by Pierce™ 660 nm Protein Assay (Thermo Fisher Scientific, Table 1) and adjusted using lysis buffer (Table 3). Protein extracts were supplemented with 1x Laemmli buffer containing β-Mercaptoethanol (β-ME) in case of sample preparation for analysis under reducing conditions and without β-ME for nonreducing conditions, heated to 95°C for 10 min with 1000 rpm shaking to denature proteins and shear chromosomal DNA. Samples were left to cool down to room temperature before freezing at -80 °C or analysis via SDS gel-electrophoresis.

2.5.2. SDS-PAGE and Immunoblotting

Sodium dodecyl sulfate polyacrylamide gel electrophoresis (SDS-PAGE) consisted of a stacking step at 70 V for around 15 min in a 5% SDS stacking gel, followed by separation at 110 V in a 10% resolving gel (Table 7). Polyvinylidene difluoride (PVDF) membranes were used for immunoblotting and were activated in 100% methanol prior to transfer and soaked in transfer buffer. Wet transfers were performed at 4°C for 2h at 210-220 mA or overnight at 40V for 20h. To judge transfer efficiency, blotted membranes were shortly placed in 100% methanol, then stained with Ponceau solution. Ponceau staining was removed by washing in 0,1 % TBS-T. Membranes were subsequently blocked in 5% skim milk in 0,1 % TBS-T for at least one hour. Before overnight incubation with primary antibody at 4°C (Table 8), membranes were washed 2x for 5 min in TBS-T to remove blocking buffer. The next day, membranes were washed with TBS-T three times for 5-10 min and incubated with the secondary antibody in TBS-T for 1,5 hours (Table 9). Subsequently, membranes were washed 3x in TBS-T for 5 min. Depending of signal intensity, membranes were incubated with Amersham ECL Western Blotting Detection Reagent (Table 1, GE Healthcare), SuperSignal™ West Pico Chemiluminescent substrate, SuperSignal™ West Pico PLUS Chemiluminescent Substrate or SuperSignal™ West Femto (Table 1, all Thermo Fisher Scientific) for 5 min and exposed to X-ray films which were developed to detect protein bands. Blots were stripped using Restore™ Western Blot Stripping Buffer (Thermo Fisher Scientific) and re-probed. In order to lower pH to ease subsequent stripping, blots were washed in H_20 dest. twice. Stripping was performed for 1-1,5 hours in a volume of stripping buffer that enables the membranes to “swim”.

Table 7: Composition of 5% stacking and 10% resolving SDS gels

5% stacking gel	**Volume (ml) per 5ml gel volume**
H_2O	3.4
30% acrylamide mix	0.83
1.5 M Tris (pH 8.8)	0.63
10% SDS (w/v)	0.05
10% ammonium persulfate (w/v)	0.05
TEMED	0.005

10% resolving gel	**Volume (ml) per 10 ml gel volume**
H_2O	4.0
30% acrylamide mix	3.3
1.5 M Tris (pH 8.8)	2.5
10% SDS (w/v)	0.1
10% ammonium persulfate (w/v)	0.1
TEMED	0.004

2.5.3. Immunoprecipitation

For RIPK1 immunoprecipitations, custom-made anti-RIPK1 serum was used which was crosslinked to BS3-Dynabeads™ Protein G (Invitrogen). In brief, cells were placed on ice after treatment and lysed in immunoprecipitation (IP) buffer (Table 3). Beads crosslinked to anti-RIPK1 serum were added to lysates and rotated overnight at 4 °C. The following day, beads were washed twice in IP buffer before elution of proteins from beads by boiling in Laemmli buffer. To detect FADD and caspase-8 interacting proteins by immuprecipitation, the protocol was similar, however in this case Protein G beads were preincubated with anti-FADD antibody (sc-6036, Santa Cruz Biotechnology) or anti-caspase-8 custom-made serum without cross-linking and subsequently added to cell lysates and incubated overnight. For TNFR1 complex I IPs, 8 x 10^6 BMDMs were plated and treated with 1 µg ml^{-1} FLAG-hTNF the following day and lysed in NP-40 lysis buffer (Table 3). The cell lysates were spun down for 15min at 4 °C and the supernatants were left for overnight incubation with FLAG M2 affinity gel (Sigma-Aldrich). The following day, beads were washed three times in NP-40 lysis buffer, followed by elution of FLAG-tagged and co-immunoprecipitated proteins using 150 ng μl^{-1} 3X FLAG peptide for 30min. FLAG eluates were diluted in Laemmli buffer and used for SDS Page and immunoblotting.

Table 8: List of primary antibodies

Antibody	kDa	Dilution	source	company	Catalogue #
p-IκBα	39	1:1000	rabbit monoclonal	Cell Signaling Technolgy	2856
IκBα	39	1:1000	rabbit polyclonal	Santa Cruz Biotechnology	sc-371
p-p65 (S536)	65	1:1000	rabbit monoclonal	Cell Signaling Technolgy	3033
p65/Rel A	65	1:1000	rabbit polyclonal	Santa Cruz	sc-372
p-SAPK/JNK (Thr183/Tyr185)	46,54	1:1000	rabbit polyclonal	Cell Signaling Technolgy	4668
SAPK/JNK	46,54	1:1000	Rabbit polyclonal	Cell Signaling Technolgy	9252
p-p38 (Thr180/Tyr182)	38	1:1000	rabbit polyclonal	Cell signaling Technolgy	9211
p38	38	1:1000	rabbit polyclonal	Cell Signaling Technolgy	9212
p-ERK (Thr202/Tyr204)	42,44	1:1000	rabbit polyclonal	Cell Signaling Technolgy	9101
ERK	42,44	1:1000	rabbit polyclonal	Cell Signaling Technolgy	9102
p-RIPK1 (S166)	74	1:1000	Rabbit polyclonal	Cell Signaling Technology	31122

RIPK1	74	1:1000	rabbit monoclonal	BD biosciences	3493
RIPK1	74	1:000	Rabbit polyclonal	Custom-made serum	
p-RIPK3 (Thr321/S232)	57	1:1000	rabbit polyclonal	Cell Signaling Technology	57220
RIPK3	57	1:1000	rabbit polyclonal	Enzo Life Sciences	ADI-905-242-100
RIPK3	57	1:1000	rat polyclonal (clone 1G6.14)	Genentech Inc.	(Newton et al., 2014)
RIPK3	57	1:1000	rabbit polyclonal	Thermo Fisher Scientific	PA5-19956
p-MLKL (S345)	54	1:1000	rabbit monoclonal	Cell Signaling Technology	D6E3G
p-MLKL	54	1:1000	rabbit monoclonal	Abcam	Ab196436
MLKL	54	1:1000	rat monoclonal	Millipore	MABC604
Caspase-8	55/18	1:1000	rat monoclonal	Alexis	ALX-804-447
FADD	23	1:000	mouse monoclonal	upstate	05-486
FADD	23	1:1000	goat polyclonal	Santa Cruz Biotechnology	Sc-6036
FADD	23	1:000	mouse monoclonal	Enzo Life Sciences	ADI-AAM-212-E
TRADD	34	1:1000	mouse monoclonal	Bio-Rad Laboratories	AHP2533
GAPDH	36	1:5000	mouse monoclonal	Nocus Biologicals	NB300-221
Tubulin	55	1:5000	mouse monoclonal	Sigma-Aldrich	T6074
Tubulin	55	1:5000	rabbit polyclonal	Abcam	Ab21058

Table 9: List of secondary antibodies

Antibody	Dilution	source	company	Catalogue #
Anti-Goat Horseradish peroxidase (HRP)-linked	1:1000	donkey	Jackson Immuno Research	705-035-003
Anti-Mouse HRP-linked	1:10000	sheep	GE Healthcare	NA931
Anti-Rabbit HRP-linked	1:10000	sheep	GE Healthcare	NA934V
Anti-rat IgG HRP-linked	1:100000	goat	Jackson Immuno Research	112-035-003

2.6 Cell death assays

To monitor cell death, cells were seeded in 96 well plates at a density of 25.000 BMDMs or 10.000 dermal or lung fibroblasts per well in technical replicates. The next day, cells were for 30 min pre-treated with combinations of Z-VAD-FMK (20 μM, if not specified otherwise), Nec1s (20 μM) and Birinapant in medium containing the dead cell stain Yoyo™-1 Iodide (Yoyo-1; 0,5 μM for fibroblasts and 0,25 μM for BMDMs), before addition of recombinant mouse TNF, LPS (100 ng ml^{-1}) or Poly (I:C) (0.5 μg ml^{-1}). An IncuCyte® S3 Live-Cell Analysis System (Essen Bioscience) was used to image cell death in real-time for 24 h in intervals of 2 h. Two wells per genotype were treated with the cell- permeable fluorescent stain Draq5 (500 μM, Table 1) and imaged at a 0 h timepoint to quantification of the total number of cells present per field. Images were analyzed using the software package of the IncuCyte to quantify the number of Yoyo-1 or Draq5-positive cells. Percentages of cell death were calculated by dividing the number of Yoyo-1 positive cells by the number of total (Draq5 positive-) cells at a 0h timepoint.

2.7 Histological analysis

2.7.1. Tissue preparation

Mice were sacrificed using cervical dislocation. For the collection of skin tissue, backs of mice were shaven and skin tissue was collected and snap-frozen on dry ice for RNA extraction. For histological examination, pieces of ~ 1 cm length were stretched on paper and fixed in 4 % paraformaldehyde (PFA) in histological cassettes or snap frozen in Tissue-Tek in cryomolds on dry ice. For collection of colon samples, colon and small intestine were prepared and washed with PBS. For micoarray analysis, ~0,5cm long colon samples were taken from close to the anus, snap frozen on dry ice and stored at -80°C until further processing. For histological analysis, the remaining colon was collected, cut longitudinally, washed in PBS to remove feces and subsequently rolled up into “Swiss rolls” from proximal to distal and fixed in 4% PFA overnight at 4°C.

2.7.2. Haematoxylin and Eosin staining of paraffin-fixed tissues

Haematoxylin and Eosin (H&E) staining was done on paraffin-embedded tissue sections with a thickness of 3 μm in the case of skin and 5 μm in the case of colon and liver. For the staining, tissue sections were de-paraffinized for 20 min in xylol and re-hydrated using EtOH solutions (2min Isopropanol, 2min 96% EtOH, 2 min 75% EtOH) and placed in water. Afterwards, tissue sections were incubated in Heamatoxylin, followed by differentiation in tap water and incubation in Eosin for Finally, sections were dehydrated using increasing EtOH solutions, fixed in Xylol and mounted with Entellan.

2.7.3. Immunoshistochemistry

For immunohistochemical analysis of caspase-3 cleavage on paraffinized tissue sections using 3,3'-Diaminobenzidin (DAB), tissue sections were deparaffinized as described in section 2.7.2. and endogenous peroxidase activity was quenched for 15 min in peroxidase blocking buffer followed by heat induced epitope retrieval in antigen retrieval buffer (Table 3) for 20 min. After cooling down, sections were incubated with IHC blocking buffer supplemented with Avidin for 1h at RT. Subsequently, sections were incubated with primary antibodies diluted in IHC blocking buffer supplemented with Biotin at 4 °C overnight. The following day, the sections were washed three times in PBS with 0.05 % (v/v) Tween-20 and incubated with biotinylated secondary antibodies in IHC blocking buffer for 1 h at room temperature. After washing of sections with 0.05 % PBS-T and Subsequently, sections were incubated with DAB chromogen (DAKO and Vector Laboratories) until stainings became visible and the reaction was stopped by immersion in tap water. Sections were counterstained with Hematoxylin for a maximum of 1 min and subsequently dehydrated using EtOH solutions in increasing concentrations. Sections were kept in Xylol and mounted with Entellan (Merck).

For fluorescent stainings (Keratin 6, Keratin 10/14) on paraffin sections, depraffinization and antigen retrieval steps were similar. Blocking was done in IHC blocking buffer (Table 3). Afterwards, sections were incubated with primary antibodies in 0.2% fish skin gelatine for 2h or overnight, followed by incubation with secondary antibodies in 0.2 % fish skin gelatine in the dark for 2-3 h. Sections were subsequently washed in PBS and distilled water and mounted with Fluoromount-G.

Table 10: List of antibodies for Immunohistochemistry

antibody	Dilution	Source	Company	Catalogue number
Keratin14	1:400	mouse	Neo Markers	MS-115-P1
Keratin 10	1:300	rabbit	Covance	PRB-159P
Keratin 6	1:600	rabbit	Covance	PRB-169P
Anti cleaved caspase-3	1:500	Rabbit	R&D Systems	Clone AF835
Anti mouse-alexa 488	1:800	goat	Molecular probes	A11001
Anti-rabbit alexa 594	1:800	goat	Molecular probes	A11012
Anti-rabbit alexa 488	1:800	goat	Molecular probes	A11008

Anti-rabbit biotinylated	1:1000	goat	Perkin Elmer	NEF813

2.7.4. Histolopathological scoring

Colonic pathology was evaluated histologically on H&E stained intestinal tissue sections as described previously (Adolph et al., 2013). In brief, inflammation was assessed both by the presence and the location of immune cell infiltrates (0: absent, 1: mucosal, 2: submucosal, 3: transmural extending into muscularis and serosa, and 4: diffuse). Tissue damage was evaluated based on four scores assessing crypt hyperplasia, epithelial injury and death of epithelial cells (0: absent, 1: mild, 2: moderate and 3: severe). The sum of these scores describing inflammation or tissue damage was then multiplied by a factor which assesses the percentual extent of inflammation or tissue damage on the section: 1: < 25%; 2: 25–50%; 3: 50–70% and 4: >75%. The sum of inflammation and damage marks is represented by the total histological score.

Percentages of cleaved caspase-3 positive crypts were calculated by determining the number of crypts with cleaved caspase-3 positive cells in a representative area of the section and normalizing to the total number of crypts counted.

2.8 LC-MS/MS phosphorylation analysis

For Liquid chromatography/tandem mass-spectrometry (LC-MS/MS), for each condition, two 10 cm dishes were seeded with 8 x 10^6 BMDMs. The following day, cells were treated and lysed in Triton X lysis buffer (Table 3). Lysates from both plates were pooled and proteins were precipitated with acetone at -20°C overnight. Pellets were resuspended in 8M Urea and reduced with dithiothreitol (DTT), followed by carbamidomethylation with indole-3-acetic acid (IAA). Then proteins were digested overnight at RT, using the proteases LysC (Wako) and trypsin (Promega). Samples were desalted using SepPak C18 cartridges (Waters) and phosphorylated peptides were enriched with the High-Select TiO2 Phosphopeptide Enrichment Kit (Thermo Fisher Scientifc) according to manufacturer's instruction. Proteomic analysis was performed using an Easy nLC 1000 UHPLC coupled to a QExactive Plus mass spectrometer (Thermo Fisher Scientifc). In brief, peptides were resuspended in Solvent A (0.1% formic acid (FA)), picked up with an autosampler and loaded onto in-house made 50 cm fused silica columns (internal diameter (I.D.) 75 μm, C18 1.7 μm, Dr. Maisch beads) at a flow rate of 0.75 µl min^{-1}. A 90 min segmented gradient of 8-48% Solvent B (80% Acetonitrile (CAN) in 0.1% FA) over 61 min, 48-70% Solvent B over 6 min, and 70-95% Solvent B over 5 min at a flow rate of 250 nl min^{-1} was used to elute peptides. Eluted peptides were sprayed into the heated transfer capillary of the mass spectrometer using a nano-electrospray ion source (Thermo Fisher Scientifc). The mass spectrometer was operated in a data-dependent mode,

where the Orbitrap acquired full MS scans (300-1750 m/z) at a resolution (R) of 70,000 with an automated gain control (AGC) target of 3Å~10^6 ions collected within 20 ms. The dynamic exclusion time was set to 20 s. From the full MS scan, the 10 most intense peaks ($z \geq 2$) were fragmented in the high-energy collision-induced dissociation (HCD) cell. The HCD normalized collision energy was set to 25%. MS/MS scans with an ion target of 1Å~10^6 ions were acquired with R = 17,500, with a maximal injection time of 80 ms and an isolation width of 2.0 m/z. The raw filles were processed using MaxQuant software (Version 1.5.3.8.) and its implemented Andromeda search engine. Minimum score for modifed peptides was set to 0, remaining parameters were set to default values and Phospho (STY) was added as variable modification. Phosphosite intensities were logarithmized and gene ontology annotations assigned using Perseus software.

2.9 Software

Sequence alignments were performed using benchling.com; for translation of base codes to amino acids http://web.expasy.org/cgi-bin/translate/dna_aa was used.

2.10 Statistical analysis

In case that data fulfilled the criteria for Gaussian distribution, one-way Anova was chosen; otherwise the nonparametric one-sided Kruskal-Wallis test was performed. Statistical analysis was done using Prism, GraphPad. Histological analysis was performed independently on tissue samples from at least three animals per genotype.

2.11 Data accessability

The microarray data generated within this project have been deposited in the Gene Express Omnibus database (NCBI) (Edgar et al., 2002) and are accessible through GEO Series accession number GSE131855. The mass spectrometry data have been deposited to the ProteomeXchange Consortium via the PRIDE (Perez-Riverol et al., 2019) partner repository with the dataset identifier PXD014097.

3. Results

3.1 Generation of *Ripk1*$^{S166A/S166A}$ mice

Protein phosphorylation is reversible and can be subject to rapid turnover due to the action of de-phosphorylating enzymes, rendering the study of phosphorylation events challenging. To explore the role of RIPK1 auto-phosphorylation at S166 in vitro and in vivo we therefore aimed to generate mice that express RIPK1 with a non-phosphorylatable mutation at position 166 from the endogenous *Ripk1* locus. Serine to alanine mutation is the standard approach for phosphorylation site replacement as alanine can in many cases mimic a non-phosphorylated serine due to chemical similarities of both amino acids regarding size and charge. Therefore, we aimed to mutate serine at position 166 in RIPK1 to alanine, to abolish auto-phosphorylation at S166, while at the same time minimizing the risk of causing disturbances in protein structure. To generate *Ripk1*^{S166A} mice, we used Clustered Regularly Interspaced Short Palindromic Repeats/CRISPR-associated 9 (CRISPR/Cas9)-mediated gene targeting in mouse zygotes, which allows for the efficient and precise modification of genomic DNA in vivo. This bacteria-derived technique relies on the nuclease activity of the Cas9 enzyme, which causes DNA double strand breaks in a defined genomic location (Jinek et al., 2012). Together with a single guide (sg)RNA, Cas9 assembles into the so called CRISPR-Cas9-gRNA complex. The sgRNA contains a short stretch of RNA termed crRNA, which directs Cas9 to its DNA target site as it harbors a targeting sequence. The DNA target site is followed by a proto-spacer adjacent motif with the sequence (5'-NGG-3'), approximately three bases upstream of which Cas9 cleaves the DNA strand. Following the introduction of a double strand break, the insertion of knock-in mutations is facilitated by homology-directed repair, a cellular DNA damage repair process, which employs a DNA template (Figure 9). In order to introduce an S166A mutation in *Ripk1*, together with the CRISPR-Cas9-gRNA complex, we delivered a ssDNA repair template into the cell, containing a serine (AGC) to alanine (GCC) mutation at position 166 flanked by homologous DNA sequences, for homology-directed guidance to the Cas9 target site (Figure 9). This repair template furthermore contained a silent mutation of the PAM sequence, to prevent re-cutting of Cas9 after successful recombination with the ssDNA oligo (Figure 9).

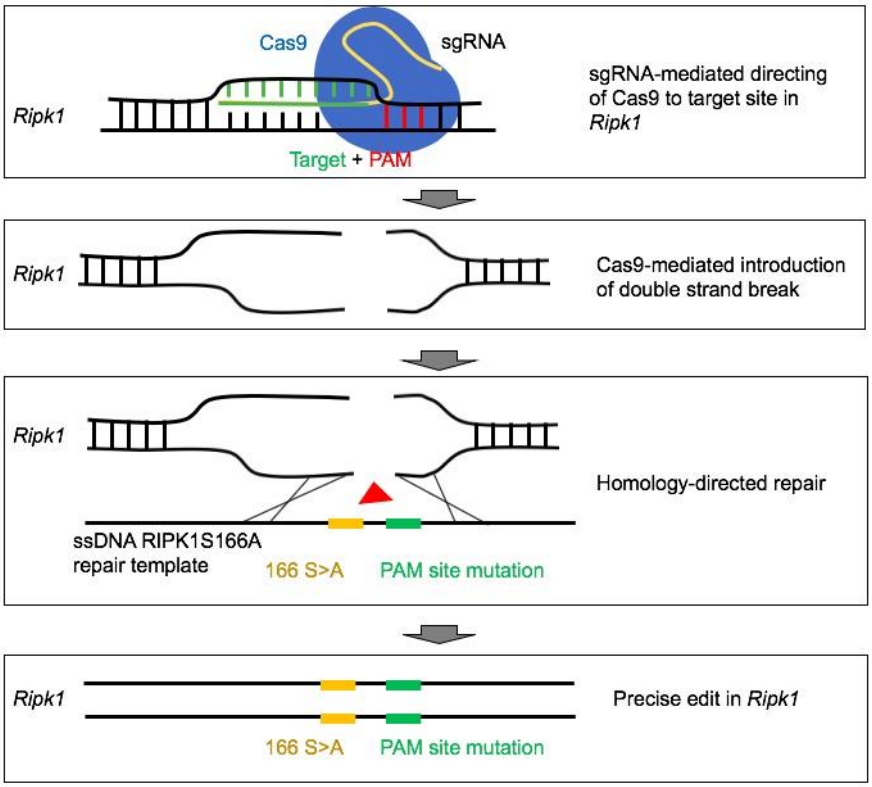

Figure 9: Scheme of CRISPR-Cas9 mediated gene targeting in Ripk1. A sgRNA directs Cas9 to its target location in *Ripk1* where it creates a double strand break. The introduction of an ssDNA repair template containing an AGC (serine) to GCC (alanine) mutation at the position corresponding to amino acid 166 in RIPK1 allows for the desired gene editing via homology directed repair.

Following CRISPR-Cas9-mediated gene targeting in mouse zygotes as described, we screened the F0 generation for the insertion of the *Ripk1*^{S166A} knock-in by using mutation-specific primers and sanger sequencing. We obtained a mouse containing serine (AGC) to alanine (GCC) mutation at position 166 as well as mutation of the PAM site (AGG to AAG) containing a silent mutation in lysine at position 170. This mouse was subsequently used as a founder to establish a colony of Ripk1$^{S166/S166A}$ mice (Figure 10).

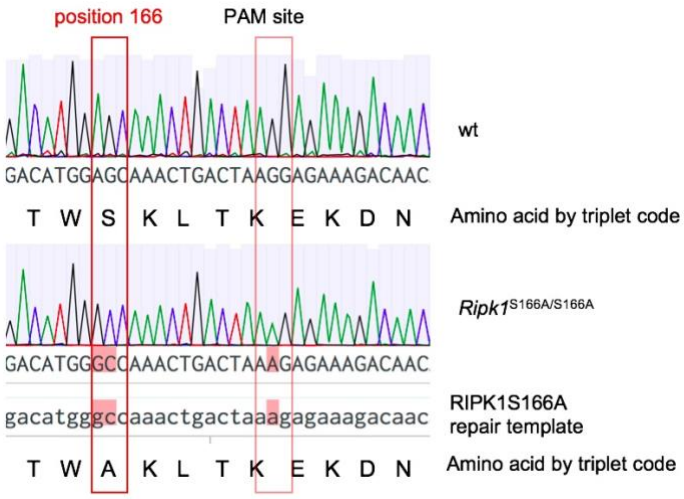

Figure 10: Serine to Alanine mutation at position S166 in *Ripk1*$^{S166A/S166A}$ mice. Sequences of the region surrounding position 166 of the endogenous *Ripk1* gene from *Ripk1*$^{S166A/S166A}$ mice as well as the RIPK1S166A repair template are aligned to the sequence of a wt mouse. Amino acids by base triplet code are indicated. Mismatched bases are highlighted in red. *Ripk1*$^{S166A/S166A}$ mouse generation was performed by Dr. Teresa Corona.

3.2 Auto-phosphorylation at S166 is not required for RIPK1 scaffolding function downstream of TNFR1, TLR 3 and TLR4

Downstream of TNFR1, TLR3 and TLR4 RIPK1 signals in a kinase activity-independent manner for the activation of NF-κB and MAPKs, while downstream of these receptors its kinase activity promotes cell death. In order to dissect the functional relevance of auto-phosphorylation at S166 for RIPK1-mediated signaling, we aimed to evaluate the effect of S166A mutation on RIPK1 kinase activity-dependent or -independent signaling downstream of these receptors.

3.2.1. RIPK1 S166A mutation does not affect TNFR1 complex I formation

In response to TNFR1 ligation, RIPK1 is recruited to the receptor via DD interaction leading to the assembly of complex I in which it is heavily ubiquitinated (Bertrand et al., 2008; Dynek et al., 2010; Gerlach et al., 2011). In order to determine whether auto-phosphorylation at S166 is required for RIPK1 recruitment to TNFR1 and its ubiquitination in complex I, we aimed to analyze TNFR1-bound RIPK1 in wt and *Ripk1*$^{S166A/S166A}$ cells upon receptor ligation. To this end, we treated BMDMs from wt and *Ripk1*$^{S166A/S166A}$ mice with FLAG-tagged human TNF, which is cross-reactive with mouse TNFR1, for 0 and 5 min, immunoprecipitated FLAG-TNF and detected associated proteins by immunoblotting. RIPK1 was co-immunoprecipitated with FLAG-TNF in wt cells after 5 min of treatment, showing its recruitment to TNFR1. Consistent with its ubiquitination in complex I, the RIPK1 antibody detected a high molecular weight smear

at this timepoint in wt cells, likely representing ubiquitin chains of different lengths attached to RIPK1 (Figure 11). In FLAG-TNF immunoprecipitates from *Ripk1*$^{S166A/S166A}$ cells, the amount of RIPK1 and ubiquitination levels of RIPK1 after 5 min of TNF treatment were similar as in wt cells indicating that RIPK1 recruitment to and ubiquitination in complex I was equally efficient as in wt cells. Of note, also TRADD recruitment to TNFR1 was not affected by RIPK1S166A mutation (Figure 11), consistent with its association with TNFR1 via RIPK1-independent DD interactions (Hsu et al., 1995). Conclusively, RIPK1 auto-phosphorylation at S166 is not required for RIPK1 recruitment to TNFR1 and its ubiquitination in complex I.

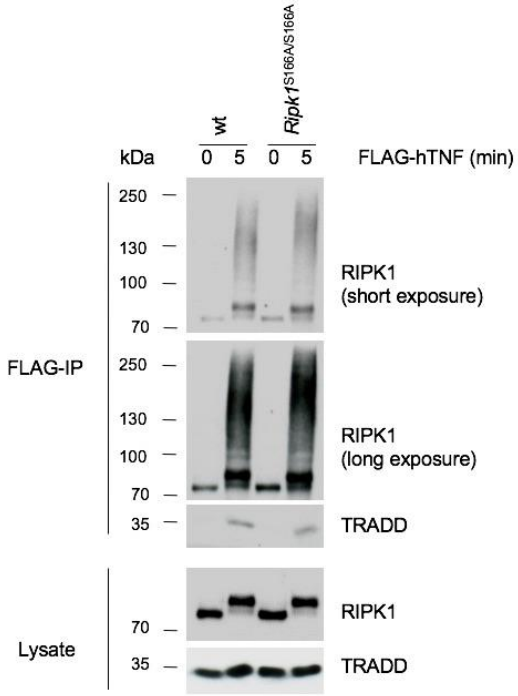

Figure 11: RIPK1S166A mutation does not affect the formation of TNFR1-induced complex I. BMDMs from mice of the indicated genotypes were treated with FLAG-tagged hTNF for 0 and 5 min and FLAG-tagged proteins were immunoprecipitated. FLAG-IPs and lysates were analyzed by immunoblot using the indicated antibodies. Experiments in this figure were performed by Tom Delanghe. Immunoblots shows are representative of two independent experiments.

3.2.2. RIPK1 S166A mutation does not affect TNF-induced NF-κB and MAPK activation

TNFR1-induced complex I signals for the activation of NF-κB and MAPKs, inducing the expression of inflammatory and pro-survival proteins, in a manner independently of RIPK1 kinase activity (Polykratis et al., 2014). To determine whether RIPK1 auto-phosphorylation at S166 is required for the activation of NF-κB and MAPK signaling downstream of TNFR1, we treated BMDMs from wt and *Ripk1*$^{S166A/S166A}$ mice over a timecourse of 0, 5, 15, 30 and 60 min with TNF and analyzed levels of indicatory proteins for the activation of NF-κB and MAPK signaling by immunoblotting. Phosphorylation of the NF-κB-sequestering protein IκBα, which leads to its ubiquitination and proteasomal degradation (Scheidereit, 2006), was observed after 5 min of TNF treatment in wt and *Ripk1*$^{S166A/S166A}$ cells (Figure 12). Consistently, IκBα was

completely degraded after 15 min of treatment and reappeared after 30 min, both in wt and *Ripk1*$^{S166A/S166A}$ cells (Figure 12). Phosphorylation of the NF-κB subunit p65, which is indicative for its nuclear translocation, was detected after 5 min in wt cells. Activation of p65 seemed slightly prolonged in *Ripk1*$^{S166A/S166A}$ cells. This difference however might be owed to overall reduced p65 levels at 15 min in wt cells, pointing to a slightly reduced protein loading at this timepoint (Figure 12). In line with this, we did not observe prolonged phosphorylation of p65 in *Ripk1*$^{S166A/S166A}$ cells in replicates of this experiment. Complex I-induced MAPK activation was assessed by phosphorylation of the MAPKs JNK, p38 and ERK, which is indicative for their activation. Phosphorylation of JNK peaked at 15 min in wt cells, similar as in *Ripk1*$^{S166A/S166A}$ cells. Phosphorylation and activation of p38 and ERK were observed after 5 and 15 min both in wt and *Ripk1*$^{S166A/S166A}$ cells (Figure 12). Conclusively, the activation of NF-κB and MAPK signaling downstream of TNFR1 were both in strength and kinetics very similar in wt and *Ripk1*$^{S166A/S166A}$ cells, indicating that RIPK1 auto-phosphorylation at S166 is not required for the kinase activity-independent role of RIPK1 to induce these signaling pathways.

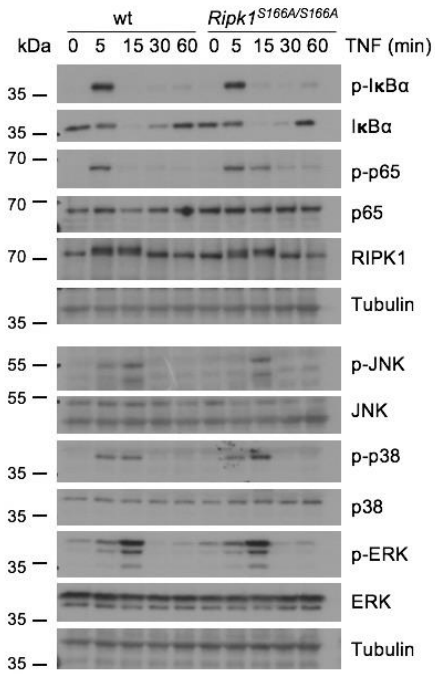

Figure 12: RIPK1S166A mutation does not affect TNF-induced NF-κB and MAPK activation. BMDMs from mice of the indicated genotypes were treated with TNF for a timecourse of 0, 5, 15, 30 and 60 min and lysates were analyzed by immunoblot using the indicated antibodies. Immunoblot shown is representative of three independent experiments.

3.2.3. RIPK1S166A mutation does not affect LPS-or Poly(I:C)-induced NF-κB and MAPK activation

Ligation of TLR3 or TLR4 in a cell under steady state conditions induces the activation of NF-κB and MAPKs signaling, which in case of both TLR3 and 4 occurs via TRIF and RIPK1 requires RIPK1 as a scaffold, while TLR4 can also signal via MyD88 independently of RIPK1.

In order to explore whether RIPK1S166A mutation has an impact on the induction of pro-inflammatory and pro-survival signaling downstream of these receptors, we treated BMDMS from wt and *Ripk1*$^{S166A/S166A}$ mice for a timecourse of 0, 15, 30, 60 or 120 min with Poly(I:C) or LPS to induce TLR3- or TLR4-mediated signaling, respectively. The TLR3 ligand Poly(I:C) induced phosphorylation and degradation of IκBα after 15 min in wt and *Ripk1*$^{S166A/S166A}$ BMDMs, similarly (Figure 13A). Phosphorylation of p65 was most prominent after 15 min and decreased towards 120 min in both genotypes. Furthermore, phosphorylation and activation of the MAPKs JNK, p38 and ERK was detected at 15 and 30 min both in wt and *Ripk1*$^{S166A/S166A}$ BMDMs (Figure 13A). TLR4 ligation by LPS induced phosphorylation of IκBα after 15 min as well as 60 and 120 min of treatment in wt and *Ripk1*$^{S166A/S166A}$ cells similarly (Figure 13B). In line with this, phosphorylation of p65 was detected after 15, 60 and 120 min in both genotypes (Figure 13B). Phosphorylation and activation of JNK and p38 was detected at 15 and 60 min and phosphorylation of ERK was most prominent after 15 min in wt and *Ripk1*$^{S166A/S166A}$ BMDMs.

Taken together, RIPK1S166A mutation did not affect TLR3- or TLR4-induced NF-κB and MAPK signaling in response to receptor ligation, indicating that auto-phosphorylation at S166 is not required for the scaffolding function of RIPK1 downstream of these receptors.

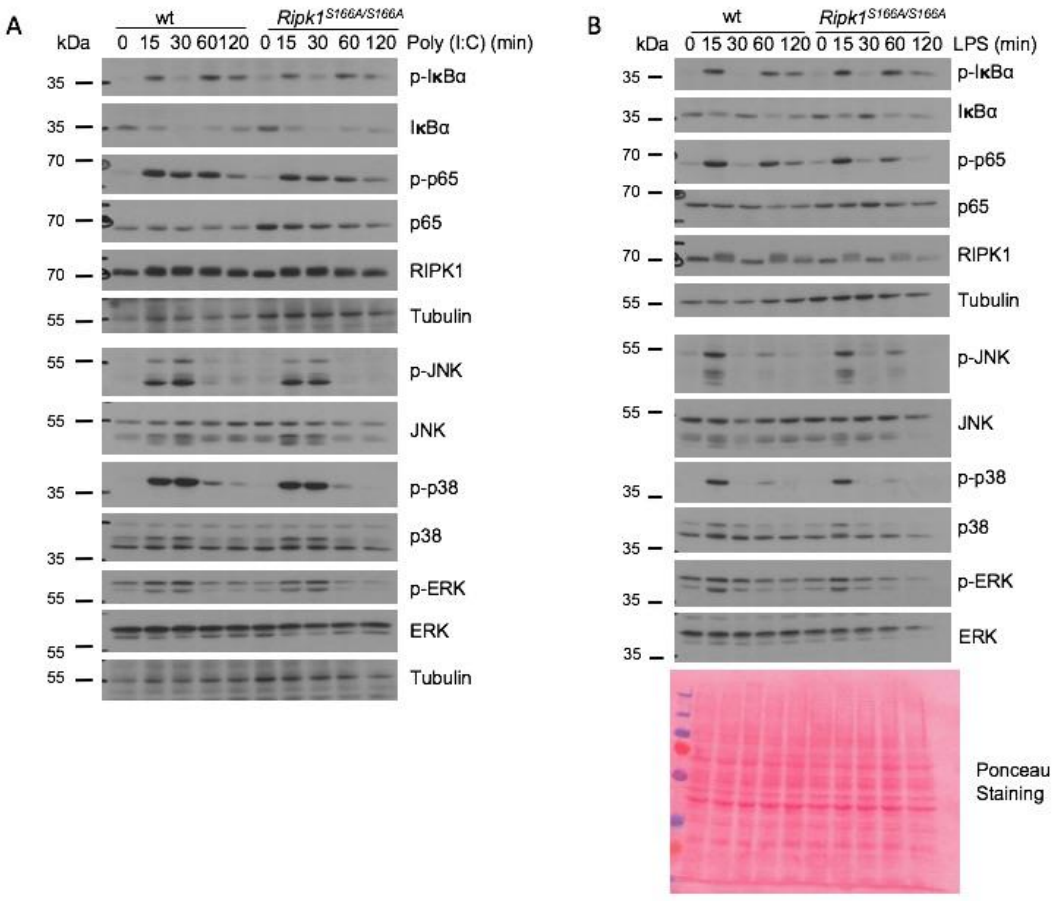

Figure 13: RIPK1S166A mutation does not affect TLR3- or TLR4-induced NF-κB and MAPK activation. (A) BMDMs from mice of the indicated genotypes were treated with Poly(I:C) for 0,15, 30,

60 or 120 min and lysates were analyzed by immunoblot with the indicated antibodies. (B) BMDMs from mice of the indicated genotypes were treated with LPS for 0, 15, 30, 60 or 120 min and lysates were analyzed by immunoblot with the indicated antibodies. (A),(B) Data shown represent one experiment.

3.3 RIPK1 auto-phosphorylation at S166 drives RIPK1 kinase activity-dependent death complex formation and cell death downstream of TNFR1, TLR3 and TLR4

Our results thus far indicate that RIPK1 auto-phosphorylation at S166 is not required for the kinase activity-independent function of RIPK1 to induce NF-κB and MAPK signaling downstream of TNFR1, TLR3 and TLR4. Previously, RIPK1 auto-phosphorylation has been implicated in mediating the cytotoxic potential of RIPK1 (Degterev et al., 2008; Zhang et al., 2017b), which relies on its catalytic activity. We thus wondered whether auto-phosphorylation at S166 plays a role for the function of RIPK1 to induce RIPK1 kinase activity-dependent TNFR1-, TLR3- and TLR4-induced cell death.

3.3.1. RIPK1 auto-phosphorylation at S166 drives TNF-induced RIPK1 kinase activity-dependent cell death

To test whether RIPK1 auto-phosphorylation at S166 is involved in TNF-induced RIPK1 kinase activity-dependent cell death, we checked the effect of S166A mutation both in RIPK1 catalytic activity-dependent apoptosis and necroptosis downstream of TNFR1.

To induce RIPK1 kinase activity-dependent apoptosis downstream of TNFR1, we treated cells from wt, *Ripk1*$^{S166A/S166A}$ and *Ripk1*$^{D138N/D138N}$ mice with TNF in combination with the SMAC mimetic birinapant (TS), which induces the degradation of cIAPs and shifts the TNF response to apoptosis (Varfolomeev et al., 2007; Wang et al., 2008). Indeed, TS treatment induced cell death in wt lung fibroblasts, which was prevented by pre-incubation of cells with the RIPK1-specific inhibitor Nec1s (Takahashi et al., 2012) or ablation of RIPK1 kinase activity in *Ripk1*$^{D138N/D138N}$ cells (Figure 14A), showing that cell death was dependent on enzymatic function of RIPK1. Importantly, RIPK1S166A mutation partly protected cells from TS-induced death, although to a lesser extent than RIPK1D138N mutation or Nec-1s treatment (Figure 14A). Similarly, TS treatment induced cell death in wt dermal fibroblasts, which was largely blocked by RIPK1D138N mutation (Figure 14B). *Ripk1*$^{S166A/S166A}$ cells were partially protected from this cell death (Figure 14B). Of note, we could not induce a substantial amount of cell death using TS treatment in BMDMs (not shown), therefore it was not possible to investigate the role of S166A mutation in TS-induced apoptosis in this cell type.

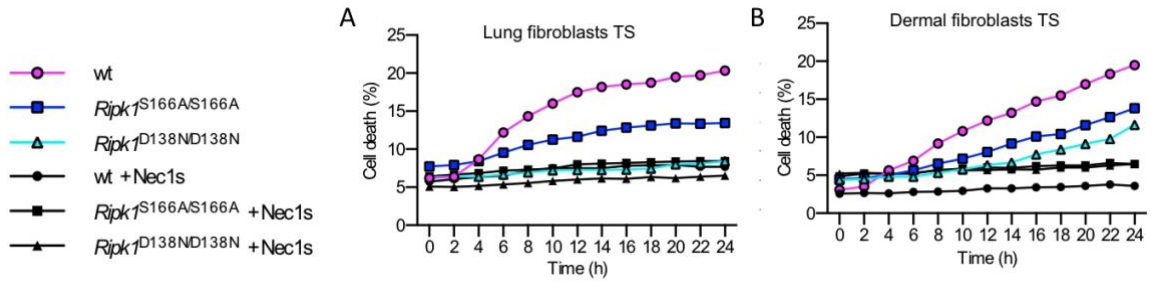

Figure 14: RIPK1S166A mutation protects from TNF-induced RIPK1 kinase activity-dependent apoptosis. (A) Lung fibroblasts from mice of the indicated genotypes were treated with a combination of TNF(T) and Smac mimetic (S) with or without Nec1s, (B) Dermal fibroblasts from mice of the indicated genotypes were treated with a combination of TNF(T) and Smac mimetic (S) with or without Nec1s. Cell death was measured using an IncuCyte as described. (A) Data shown is representative of four independent experiments. (B) Data shown is representative of three independent experiments.

In order to investigate the effect of RIPK1 S166A mutation in RIPK1-kinase activity-dependent necroptosis downstream of TNFR1, we induced this cell death by blocking of caspases using the pan-caspase-inhibitor Z-VAD-FMK in conditions of TS treatment (TSZ) (Pasparakis and Vandenabeele, 2015). TSZ treatment resulted in high levels of death in wt BMDMs, which was strongly prevented by pharmacological or genetic ablation of RIPK1 kinase activity (Fig 15A). Ablation of auto-phosphorylation at S166 in *Ripk1*$^{S166A/S166A}$ cells also inhibited cell death induced by TSZ in BMDMs (Figure 15A), although not as strong as inhibition of RIPK1 kinase activity. In the same line, we observed partial inhibition of TSZ-induced necroptosis in lung- and dermal fibroblasts from *Ripk1*$^{S166A/S166A}$ mice (Figure 15B,C), which was completely dependent on RIPK1 kinase activity in both cell types.

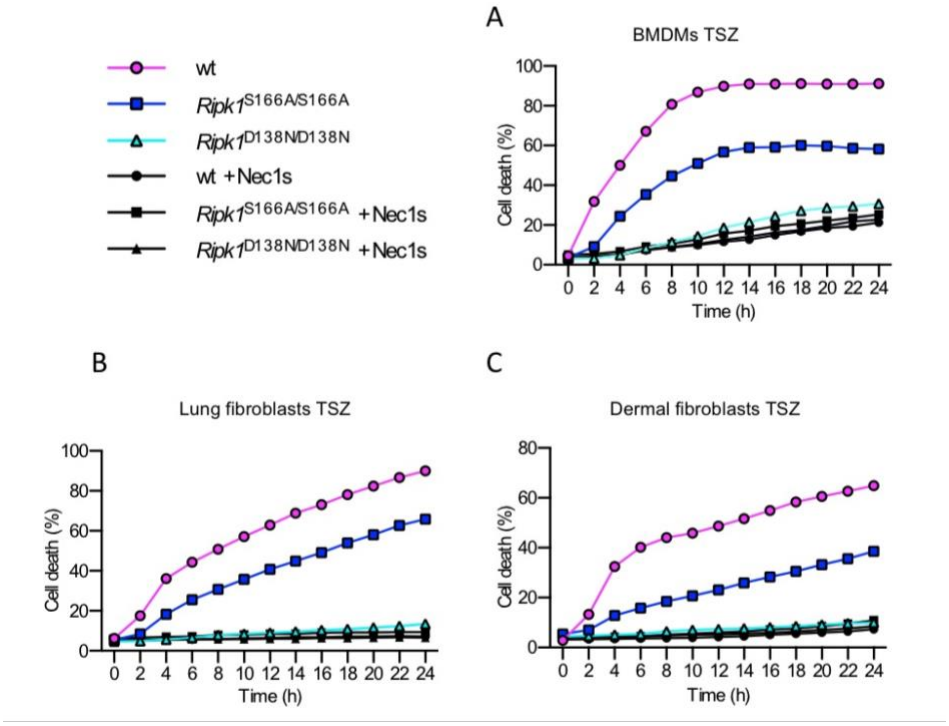

Figure 15: RIPK1S166A mutation protects from TNF-induced RIPK1 kinase activity-dependent necroptosis. (A) BMDMs from mice of the indicated genotypes were treated with a combination of TNF(T), Smac mimetic (S) and Z-VAD-FMK (Z) with or without Nec1s, (B) Lung fibroblasts from mice of the indicated genotypes were treated with a combination of TNF(T), Smac mimetic (S) and Z-VAD-FMK (Z) with or without Nec1s, (C) Dermal fibroblasts from mice of the indicated genotypes were treated with a combination of TNF(T), Smac mimetic (S) and Z-VAD-FMK (Z) with or without Nec1s. Cell death was measured using an IncuCyte as described. (A),(B) Data shown is representative of four independent experiments. (C) Data shown is representative of three independent experiments.

On the other hand, RIPK1S166A mutation did not affect cell death induced by TNF in combination with cycloheximide, which was also not blocked by genetic or pharmacological inhibition of RIPK1 kinase activity (Figure 16), as previously described (Wang et al., 2008), showing that RIPK1 auto-phosphorylation at S166 is dispensable for RIPK1 kinase activity-independent cell death downstream of TNFR1.

Taken together, RIPK1S166A mutation partially protects from RIPK1 kinase-activity-dependent apoptosis and necroptosis downstream of TNFR1 in vitro, indicating that auto-phosphorylation at S166 is involved in mediating both types of cell death downstream of this receptor.

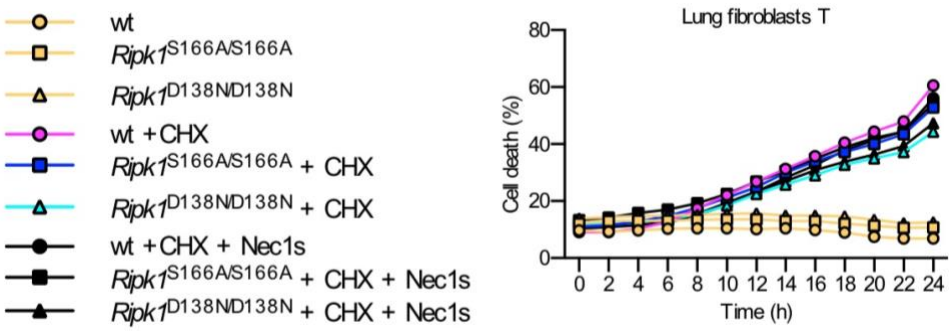

Figure 16: RIPK1S166A mutation does not protect from TNF-induced RIPK1 kinase activity-independent apoptosis. BMDMS from mice of the indicated genotypes were treated with TNF(T) with or without Cycloheximide (CHX) and Nec1s. Cell death was measured using an IncuCyte as described. Data shown is representative of two independent experiments.

3.3.2. RIPK1 auto-phosphorylation at S166 drives Poly(I:C)- and LPS-induced RIPK1 kinase activity-dependent cell death

Next, we asked whether auto-phosphorylation at S166 was also required for necroptosis downstream of TLR3 or TLR4, which proceeds in response to receptor ligation in conditions of caspase-8 inhibition and relies on RIPK1 kinase activity (Dillon et al., 2014; He et al., 2011; Kaiser et al., 2013; Polykratis et al., 2014). To this end, we treated wt, *Ripk1*$^{S166A/S166A}$ and *Ripk1*$^{D138N/D138N}$ BMDMs with Poly(I:C) in combination with the pan-caspase inhibitor Z-VAD-FMK (PZ) or LPS in combination with Z-VAD-FMK (LZ) to induce TLR3 and TLR4-mediated necroptosis, respectively. PZ treatment in wt BMDMs lead to almost 50% of cell death, which was completely RIPK1 kinase activity-dependent as shown by genetic or pharmacological inhibition of RIPK1 catalytic activity (Figure 17A). *Ripk1*$^{S166A/S166A}$ BMDMs on the other hand were partially, but not completely protected from cell death under these conditions (Figure 17A). LZ treatment induced robust cell death in wt BMDMs which was strongly inhibited by ablation of RIPK1 kinase activity (Figure 17B). RIPK1 S166A mutation provided a partial protection under these conditions (Figure 17B).

Conclusively, RIPK1S166A mutation partially, but not completely inhibited TLR3- and TLR4-induced necroptosis, indicating that in addition to TNFR1-induced cell death, auto-phosphorylation at S166 is involved in RIPK1 kinase-activity dependent necroptosis downstream of these receptors.

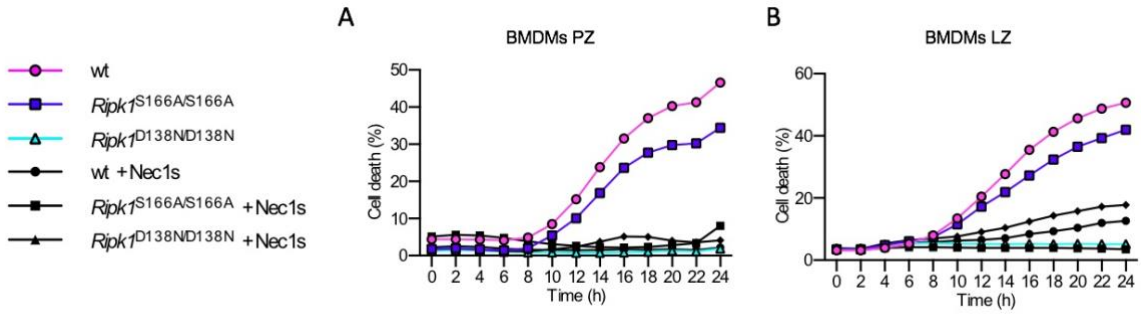

Figure 17: RIPK1S166A mutation partially protects from necroptosis downstream of TLR3 and TLR4. (A) BMDMs from mice of the indicated genotypes were treated with Poly(I:C) in combination with Z-VAD-FMK (PZ) with or without Nec1s. (B) BMDMs from mice of the indicated genotypes were treated with LPS in combination with Z-VAD-FMK (LZ) with or without Nec1s. (A),(B) Cell death was measured using an IncuCyte as described. Data shown is representative of three independent experiments in (A) and three independent experiments in (B).

3.3.3. RIPK1 auto-phosphorylation at S166 drives complex II formation and MLKL oligomerization downstream of TNFR1

Our results indicate that RIPK1 auto-phosphorylation at S166 is required for RIPK1 kinase activity-dependent apoptosis and necroptosis downstream of TNFR1, which lead us to investigate the mechanistic requirement of this site for cell death induction in response to TNF. In order to study the role of RIPK1 auto-phosphorylation at S166 in the molecular events leading to TNF-induced RIPK1 kinase activity dependent apoptosis, we examined the effect of the S166A mutation on formation of complex II as the driver of this cell death. Apoptosis activation by complex II relies on RIPK1 interaction with the caspase-8 adaptor FADD, allowing for recruitment and auto-proteolytic activation of caspase-8 (Chang et al., 2003; Hughes et al., 2009; Pasparakis and Vandenabeele, 2015; Salvesen and Dixit, 1999). To induce the formation of complex II in cells, we used TNF in combination with the SMAC mimetic Birinapant and additionally added the pan-caspase inhibitor Z-VAD-FMK (TSZ treatment) to increase the stability of complex II and facilitate biochemical analysis. Z-VAD-FMK permits initial caspase-8 cleavage events (p43 fragment) within procaspase-8 but blocks the generation of active caspase-8 fragments (p10 and p18). We thus treated wt and *Ripk1*$^{S166A/S166A}$ BMDMs for 0, 2 and 4h with TSZ, immunoprecipitated RIPK1 from cell lysates and then checked for RIPK1-interacting proteins by immunoblot. Indeed, after 2 and 4 h of TSZ treatment, in wt BMDMs, RIPK1 was in complex with full length procaspase-8 as well as with a shorter form of caspase-8, likely resulting from an initial auto-cleavage event (Fig 18A). Furthermore, we detected FADD in this complex after 2 and 4h which was concurrent with RIPK1 auto-phosphorylation at S166 at these timepoints (Figure 18A). Strikingly, ablation of auto-phosphorylation at S166 in *Ripk1*$^{S166A/S166A}$ cells completely abolished RIPK1 interaction with caspase-8 and FADD both 2 and 4h after TSZ treatment, indicating that RIPK1 auto-phosphorylation at S166 is essential for RIPK1 interaction with FADD and Capase-8 recruitment to Complex II.

Furthermore, in order to dissect the mechanistic role of RIPK1 auto-phosphorylation at S166 in TNF-induced necroptosis, we aimed to investigate the effect of RIPK1S166A mutation on the assembly of MLKL oligomers, which constitute an essential step in necroptosis induction (Cai et al., 2014; Dondelinger et al., 2014; Petrie et al., 2018). To this end, we treated wt, *Ripk1*$^{S166A/S166A}$ and *Ripk1*$^{D138N/D138N}$ BMDMs with TSZ to induce necroptosis. We subsequently analyzed lysates by immunoblot under non-reducing conditions in order to retain integrity of disulfide bonds, which were shown to be present in MLKL oligomeric structures (Huang et al., 2017). Indeed, in wt cells we observed a shift of the MLKL band to a high molecular weight species, indicative of oligomer formation (Figure 18B). This shift was absent in Ripk1$^{D138N/D138N}$ cells, showing that MLKL oligomerization was dependent on RIPK1 kinase activity. Importantly, we did not observe a high molecular weight band in Ripk1$^{S166A/S166A}$ cells either (Figure 18B), indicating that RIPK1 auto-phosphorylation at S166 is essential for the formation of MLKL oligomers to mediate TNF-induced necroptosis.

Taken together, our results show that downstream of TNFR1, auto-phosphorylation at S166 is crucial for the formation of RIPK1 kinase activity-dependent apoptosis and necroptosis-inducing complexes.

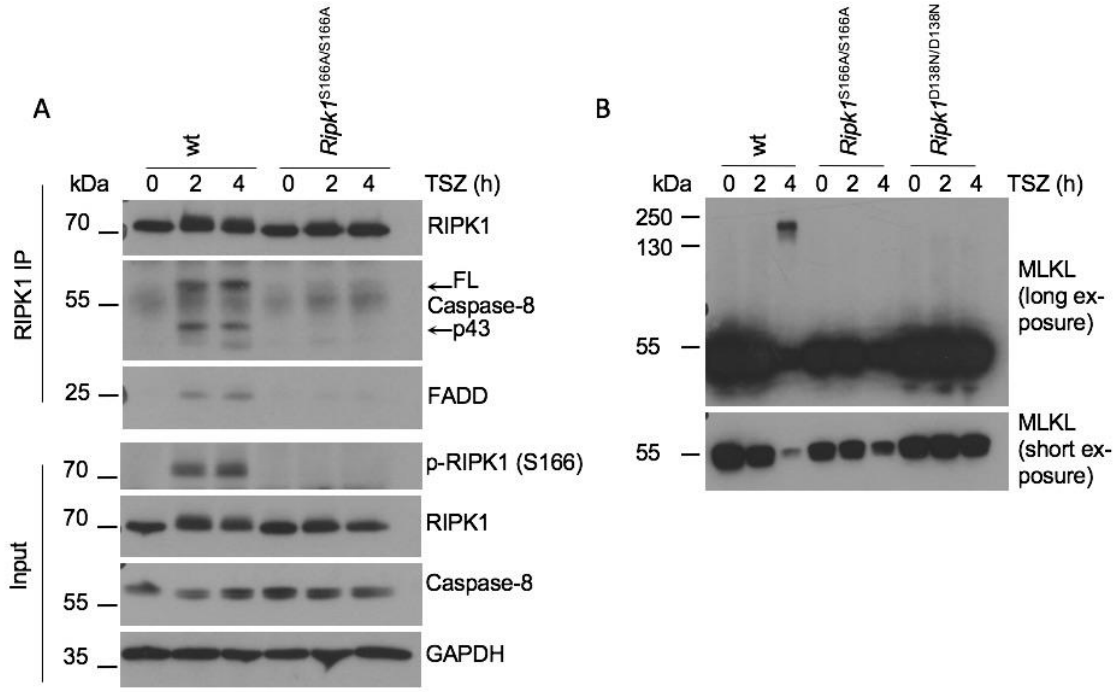

Figure 18: RIPK1S166A mutation inhibits the formation of cell death-inducing complexes downstream of TNFR1. (A) BMDMs from mice of the indicated genotypes were treated with a combination of TNF(T), Smac mimetic (S) and Z-VAD-FMK (Z) for 0, 2 and 4 h. RIPK1 immunoprecipitates and input were analysed by immunoblot using the indicated antibodies. Data shown are representative of three independent experiments. (B) BMDMs from mice of the indicated genotypes were treated with a combination of TNF(T), Smac mimetic (S) and Z-VAD-FMK (Z) for 0, 2 and 4 h. Lysates were analyzed under non-reducing conditions for the presence of MLKL. Data shown are representative of two independent experiments.

3.3.4. RIPK1 auto-phosphorylation at S166 drives formation of MLKL oligomers downstream of TNFR1, TLR3 and TLR4

Our results furthermore show that RIPK1 auto-phosphorylation is required for RIPK1 kinase activity-dependent necroptosis downstream of TLR3 and TLR4. To investigate how RIPK1S166A mutation inhibits TLR3 and TLR4-induced necroptosis mechanistically, we aimed to analyze the formation of MLKL oligomers and phosphorylation of MLKL as markers of necroptotic pathway activation. Therefore, we treated wt, *Ripk1*$^{S166A/S166A}$ and *Ripk1*$^{D138N/D138N}$ BMDMs with a combination of Poly(I:C) (P) or LPS (L) and Z-VAD-FMK (Z) to trigger TLR3- and TLR4-induced necroptosis respectively and analyzed cell lysates under non-reducing or reducing conditions. Thereby, the absence of reducing agents allowed us to maintain disulfide bond integrity in MLKL protein complexes, while their addition enabled analysis of protein phosphorylation.

PZ treatment induced MLKL oligomerization after 13 and 15h in wt cells (Figure 19A), which co-occurred with MLKL phosphorylation and RIPK1 phosphorylation at S166. On the other hand, MLKL oligomerization and phosphorylation of RIPK1 and MLKL were absent in *Ripk1*$^{D138N/D138N}$ cells, showing that these events are dependent on RIPK1 kinase activity. MLKL was phosphorylated 13 and 15 h after PZ treatment in *Ripk1*$^{S166A/S166A}$ BMDMs, however to a lesser extent as in wt cells and importantly this lower level of MLKL phosphorylation did not induce its oligomerization (Figure 19A).

LZ treatment in wt BMDMs similarly induced phosphorylation of RIPK1 at S166, phosphorylation of MLKL and an MLKL band shift after 13 and 15h of treatment, indicative of its oligomerization (Figure 19B). These events were RIPK1 kinase activity-dependent as ablation of RIPK1 kinase activity strongly prevented MLKL phosphorylation and completely blocked RIPK1 phosphorylation and MLKL oligomerization. On the other hand, ablation of RIPK1 auto-phosphorylation at S166 inhibited but did not prevent MLKL phosphorylation in *Ripk1*$^{S166A/S166A}$ cells, while MLKL oligomerization was strongly inhibited (Figure 19B).

Conclusively, these results show that RIPK1 auto-phosphorylation at S166 is critical for MLKL oligomerization in TLR3- and TLR4-induced necroptosis.

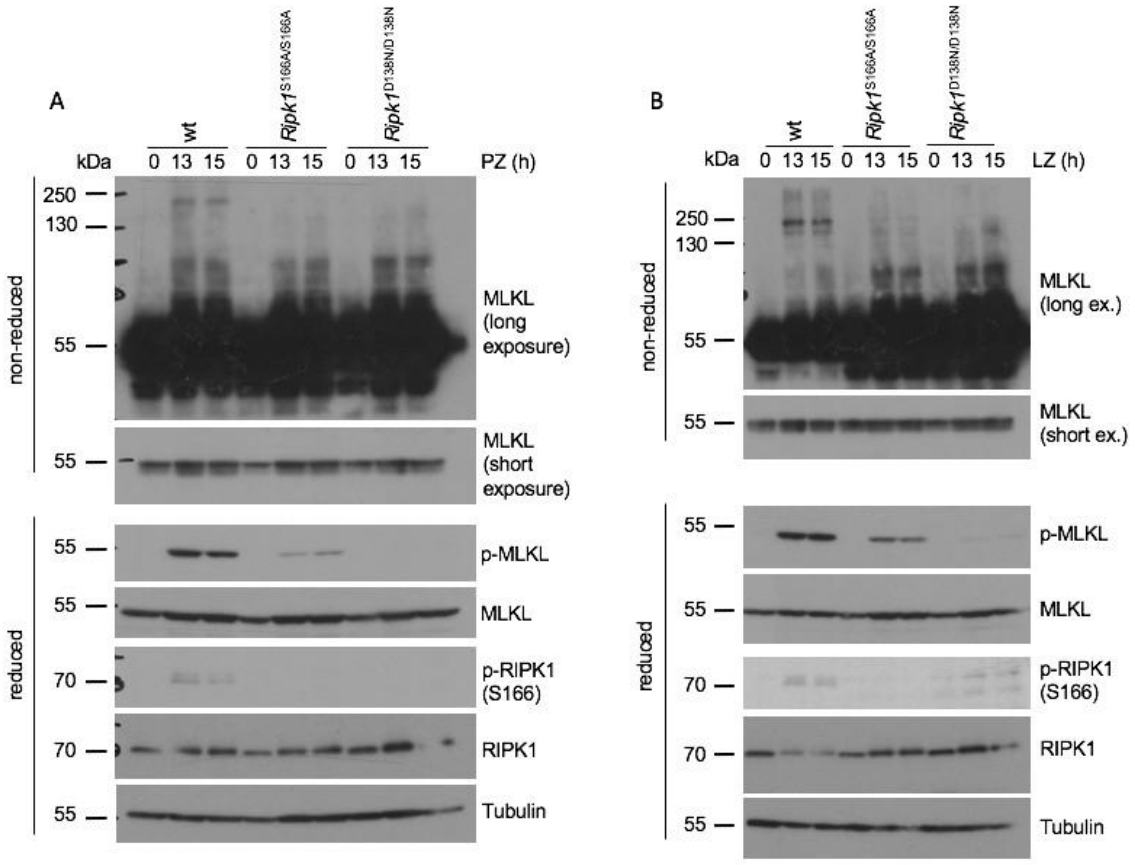

Figure 19: RIPK1S166A mutation inhibits the formation of MLKL oligomers downstream of TLR3 and TLR4. (A) BMDMs from mice of the indicated genotypes were treated with Poly(I:C) (P) in combination with Z-VAD-FMK (Z) for 0, 13 and 15 h and lysates were analyzed under reducing or non-reducing conditions by immunoblot using the indicated antibodies. Data shown is representative of three independent experiments. (B) BMDMs from mice of the indicated genotypes were treated with LPS (L) in combination with Z-VAD-FMK (Z) for 0, 13 and 15 h and lysates were analyzed under reducing or non-reducing conditions by immunoblot using the indicated antibodies. Data shown is representative of two independent experiments.

3.4 RIPK1 auto-phosphorylation at S166 drives inflammation and cell death *in-vivo* in mouse models of RIPK1 kinase-activity-dependent pathology

Thus far, our data suggest that in vitro RIPK1 auto-phosphorylation at S166 is required for the formation of cell death-inducing complexes and drives RIPK1 kinase activity-dependent cell death downstream of TNFR1, TLR3 and TLR4. Nevertheless, the protective effect of RIPK1S166A mutation on cell death in vitro was only partial and not as strong as provided by ablation of RIPK1 kinase activity. However, as cell death induction modelled in vitro might not properly reflect the physiological importance of this phosphorylation event, we aimed to investigate the role of this site in-vivo. To this end, we examined the effect of RIPK1S166A mutation on pathologies in mouse models in different tissues that are driven by RIPK1 kinase activity-dependent cell death.

3.4.1. RIPK1 auto-phosphorylation at S166 drives cell death and colitis in NEMO^{IEC-KO} mice

As mentioned under 1.4.3.1., mice with IEC-specific ablation of the IKK complex subunit NEMO (NEMO^{IEC-KO}) spontaneously develop colitis (Vlantis et al., 2016). Macroscopically, colitis in NEMO^{IEC-KO} mice manifest with diarrhea and weight loss and analysis of colonic tissue from these mice revealed thickening of the colonic wall and erosion of the epithelium with open sores, termed ulcers. Furthermore, these mice showed increased infiltration of immune cells into the mucosa and submucosa. Importantly, colitis in NEMO^{IEC-KO} mice has been shown to be driven by RIPK1 kinase activity-dependent IEC apoptosis (Vlantis et al., 2016). We wondered whether RIPK1 auto-phosphorylation at S166 is required for IEC-death and colitis development in vivo in the absence of NEMO. To investigate the effect of the S166A mutation on IEC-death and colon inflammation in NEMO^{IEC-KO} mice we crossed the RIPK1S166A mutation into the *Nemo*^{FL} *VillinCre*^{tg} background, in which IEC-specific deletion of the floxed NEMO gene is achieved by expression of Cre recombinase under the control of the IEC-specific Villin promoter (Madison et al., 2002). As described previously, at the age of 11 weeks, while *Nemo*^{FL} mice showed a healthy colonic architecture, NEMO^{IEC-KO} mice presented with colonic inflammation characterized by thickening of the colonic wall, epithelial erosion, immune cell infiltration into the mucosa and submucosa and ulcer formation (Figure 20A) as revealed by histological analysis of H&E stained tissue sections. Strikingly, NEMO^{IEC-KO} *Ripk1*$^{S166A/S166A}$ mice on the other hand displayed a normal intestinal epithelial architecture in the colon similar to *Nemo*^{FL} littermates (Figure 20A). Specifically, RIPK1S166A mutation prevented ulcer formation, tissue inflammation and epithelial damage (Figure 20B,C). Overall, histopathological scores were highly significantly reduced in comparison to NEMO^{IEC-KO} mice and were comparable to Nemo^{FL} controls (Figure 20B,C).

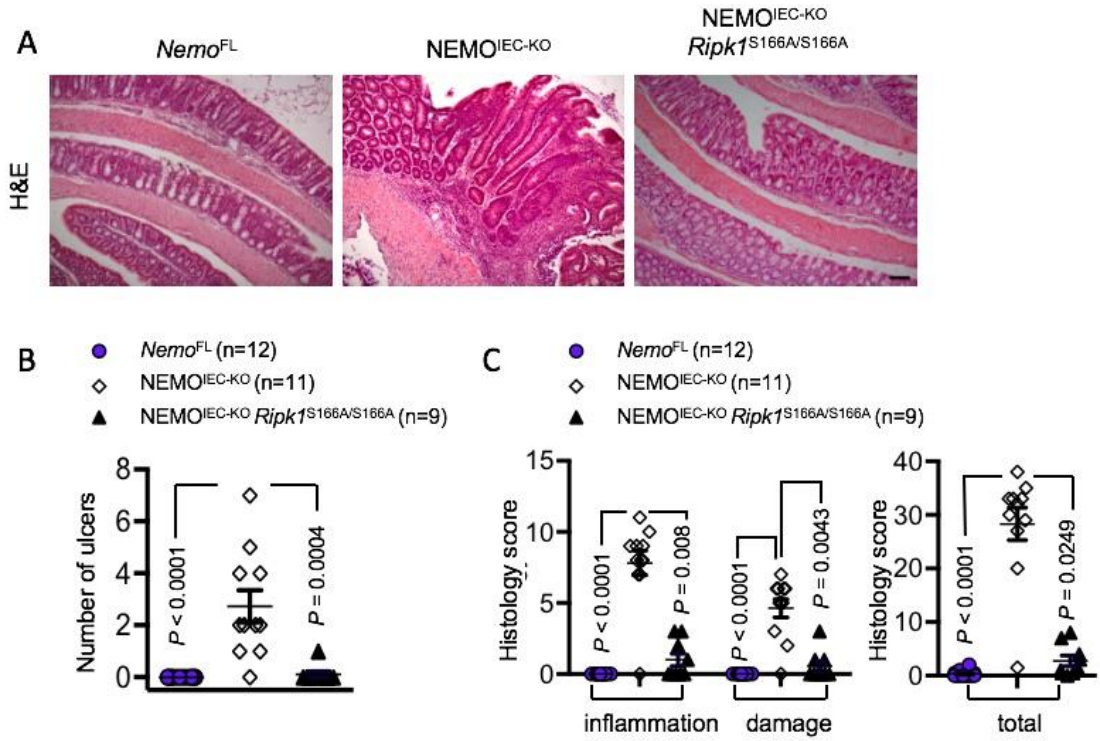

Figure 20: RIPK1 auto-phosphorylation at S166 drives colitis in NEMO^{IEC-KO} mice. (A) Representative images of colon sections from mice of the indicated genotypes stained with Hematoxylin and Eosin (H&E) at the age of 11 weeks are shown. (B) Graph depicting numbers of ulcers on colonic tissue sections from mice of the indicated genotypes. (C) Graphs depicting histological scores for inflammation, damage and overall histopathology (total) on colon sections from mice of the indicated genotypes. B, C One out of two independent blinded scorings is shown. The dots in the graphs represent individual mice. Horizontal lines indicate mean values ± s.e.m. Statistical significance was determined using a Kruskal-Wallis test (one-sided).

Previously, colitis development in NEMO^{IEC-KO} mice has been shown to be driven by apoptosis of IECs (Vlantis et al., 2016). Indeed, immunostaining for cleaved caspase-3 (CC3) on tissue sections from 11 week old NEMO^{IEC-KO} mice revealed the presence of increased numbers of apoptotic cells in the intestinal epithelium as compared to *Nemo*^{FL} mice which showed only very few numbers of CC3-positive cells (Figure 21A,B). Importantly, ablation of RIPK1 auto-phosphorylation at S166 strongly inhibited the apoptotic IEC death as NEMO^{IEC-KO} *Ripk1*$^{S166A/S166A}$ mice presented with only few scattered CC3-positive cells similar to control littermates (Figure 21A,B). These results show that RIPK1 auto-phosphorylation at S166 is essential to drive apoptotic IEC death and colonic inflammation in the absence in NEMO in vivo.

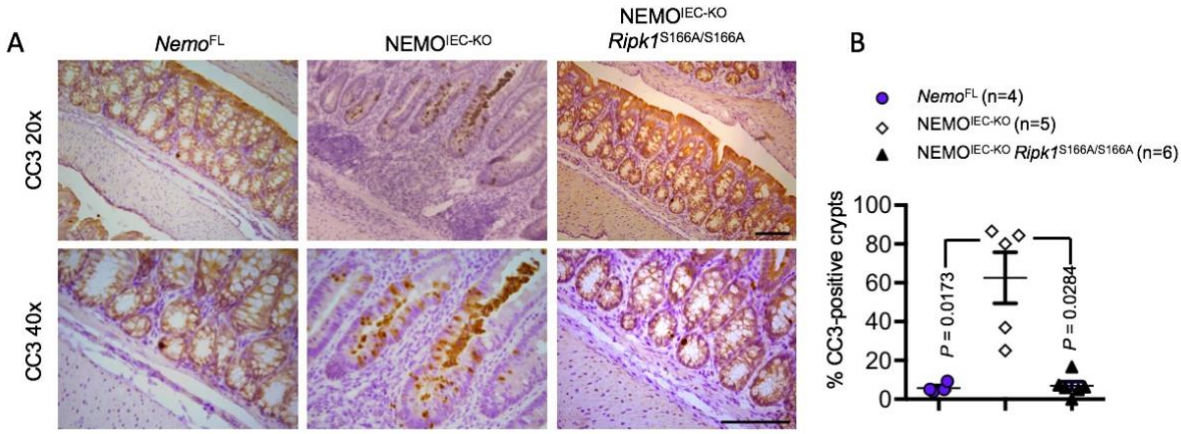

Figure 21: RIPK1 auto-phosphorylation at S166 drives caspase 3 cleavage in NEMO-deficient IECs. (A) Representative images of colon sections from mice of the indicated genotypes immunostained for cleaved caspase-3 (CC3) at the age of 11 weeks. Sections are shown in 20x and 40x magnification. (B) Graphs showing percentage of cleaved caspase-3 (CC3) positive crypts on colon sections from mice of the indicated genotypes. The dots in the graphs represent individual mice. Horizontal lines indicate mean values ± s.e.m. Statistical significance was determined using a Kruskal-Wallis test (one-sided). Cleaved caspase-3 stainings were performed by Jennifer Kuth.

Colitis development in NEMO^{IEC-KO} mice is furthermore accompanied by increased expression of inflammatory cytokines and chemokines, such as *Tnf*, *Il1b*, *Cxcl1*, *Ccl2* and *Ccl5* (Vlantis et al., 2016). We aimed to study the effect of RIPK1S166A mutation on gene expression in NEMO^{IEC-KO} mice using an unbiased approach. Therefore, we decided to perform a whole genome microarray analysis on RNA isolated from colonic tissue samples from 11 week-old *Nemo*^{FL}, NEMO^{IEC-KO} and NEMO^{IEC-KO} *Ripk1*$^{S166A/S166A}$ mice, which allowed us to analyze the gene expression profile of over > 20 000 well-annotated mouse genes simultaneously. We found 3088 genes significantly differentially regulated between *Nemo*^{FL} and NEMO^{IEC-KO} mice, indicating a globally altered gene expression profile in the colon in response to NEMO ablation. Strikingly, in a heat map clustering of genes with significantly differential expression between *Nemo*^{FL} and NEMO^{IEC-KO} mice, NEMO^{IEC-KO} *Ripk1*$^{S166A/S166A}$ formed a group with *Nemo*^{FL} mice (Figure 22A), showing that ablation of auto-phosphorylation at S166 normalized the altered gene expression in NEMO^{IEC-KO} mice. Specifically, ablation of auto-phosphorylation at S166 of RIPK1 in NEMO^{IEC-KO} *Ripk1*$^{S166A/S166A}$ mice reverted the altered expression of 30 cytokines and chemokines such as *Tnf*, *Ccl3*, *Cxcl1* and *Il1b* as compared to NEMO^{IEC-KO} mice to *Nemo*^{FL} levels (Fig 22B).

In conclusion, Ripk1 auto-phosphorylation at S166 drives colonic inflammation and IEC apoptosis as well as deregulated cytokine and chemokine expression in response to NEMO ablation.

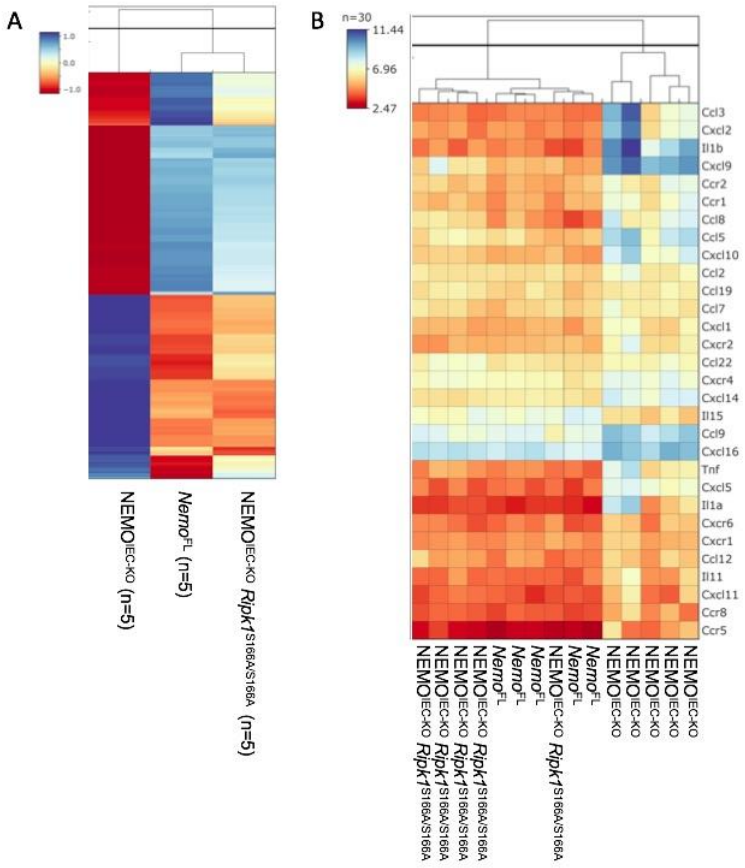

Figure 22: RIPK1 S166A mutation reverts inflammatory gene signature in NEMO^{IEC-KO} mice. (A) Clustered heatmaps showing whole genome microarray analysis of gene expression from colons from mice of the indicated genotypes. only genes that were differentially regulated (Fold change > 1.4999 or < - 1.4999, P < 0.05) between *Nemo*^{FL} and NEMO^{IEC-KO} mice were included. The values were normalized using Z score transformation. (B) Clustered heat maps showing 30 cytokines that were significantly differentially regulated (Fold change > 1.4999 or < - 1.4999, P < 0.05) between *Nemo*^{FL} and NEMO^{IEC-KO} mice. Values of individual mice are plotted, n=5 per group.

3.4.2. RIPK1 auto-phosphorylation at S166 drives cell death and skin inflammation in *Sharpin*$^{cpdm/cpdm}$ mice

Given the complete protection from TNFR1-induced IEC apoptosis in vivo by RIPK1S166A mutation, we wondered about the involvement of RIPK1 auto-phosphorylation at S166 in cell death and inflammation in other tissues. Mice with homozygous cpdm mutation in *Sharpin*, develop severe inflammation predominantly in the skin but also in other organs such as the liver, spleen and lung (Gijbels et al., 1996; Seymour et al., 2007)(described under 1.4.3.1.). Previously, skin inflammation in *Sharpin*$^{cpdm/cpdm}$ mice was shown to be driven by TNFR1-induced keratinocyte apoptosis (Kumari et al., 2014; Rickard et al., 2014a) and importantly *cpdm* pathology was completely prevented by ablation of RIPK1 kinase activity (Berger et al., 2014). To understand the involvement of RIPK1 autophosphorylation at S166 in driving the *cpdm* inflammatory phenotypes we crossed the cpdm strain to *Ripk1*$^{S166A/S166A}$ mice.

As previously reported, *Sharpin*$^{cpdm/cpdm}$ mice developed a severe dermatitis characterized by inflammatory skin lesions on their backs at the age of 15-17 weeks. In line with a driving role of RIPK1 kinase activity in this phenotype (Berger et al., 2014), abrogation of RIPK1 catalytic activity in Sharpin$^{cpdm/cpdm}$ *Ripk1*$^{D138N/D138N}$ mice completely prevented skin lesion development (Figure 23A,B). Remarkably, cross of the cpdm mutation to a *Ripk1*$^{S166A/S166A}$ background similarly resulted in a complete protection from the dermatitis phenotype at least until 40 weeks of age (Figure 23A,B), showing that auto-phosphorylation at S166 drives skin lesion development in *Sharpin*$^{cpdm/cpdm}$ mice.

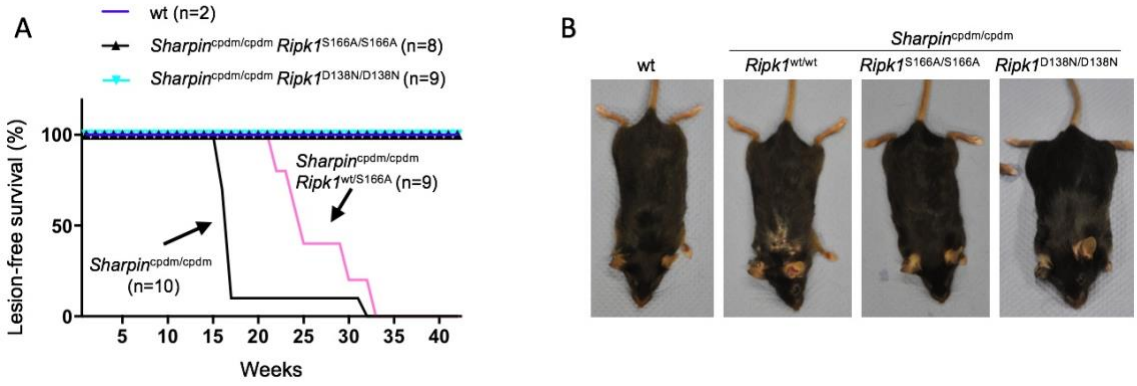

Figure 23: RIPK1 auto-phosphorylation at S166 drives skin lesion development in *Sharpin*$^{cpdm/cpdm}$ mice. (A) Kaplan Meyer Curve depicting lesion-free survival of mice with the indicated genotypes. (B) Macroscopic pictures of mice with the indicated genotypes at 15-17 weeks of age

We were intrigued to investigate how RIPK1S166A mutation affects the dermatitis-underlying histopathological changes, such as cell death, epidermal homeostasis and inflammation in *Sharpin*$^{cpdm/cpdm}$ mice (Kumari et al., 2014). Firstly, to assess the role of RIPK1 auto-phosphorylation at S166 on keratinocyte apoptosis as the driver of *cpdm*-mediated dermatitis (Kumari et al., 2014), we immunostained skin sections from wt, *Sharpin*$^{cpdm/cpdm}$ *Ripk1*$^{wt/wt}$, *Sharpin*$^{cpdm/cpdm}$ *Ripk1*$^{S166A/S166A}$ and *Sharpin*$^{cpdm/cpdm}$ *Ripk1*$^{D138N/D138N}$ using antibodies against Cleaved caspase-3 (CC3). As previously reported (Kumari et al., 2014; Rickard et al., 2014a), *Sharpin*$^{cpdm/cpdm}$ mice showed increased numbers of CC3-positive keratinocytes compared to wt mice (Figure 24). This aberrant cell death was blocked in *Sharpin*$^{cpdm/cpdm}$ *Ripk1*$^{D138N/D138N}$ mice and therefore dependent on RIPK1 kinase activity. Importantly, similar to RIPK1D138N mutation, S166A mutation in *Sharpin*$^{cpdm/cpdm}$ *Ripk1*$^{S166A/S166A}$ mice resulted in a strong reduction of CC3 positive cells compared to *Sharpin*$^{cpdm/cpdm}$ mice (Figure 24), indicating that RIPK1 auto-phosphorylation at S166 is required to drive RIPK1 kinase activity-dependent keratinocyte death in response to Sharpin cpdm mutation.

The dermatitis in *Sharpin*$^{cpdm/cpdm}$ mice is closely linked to a loss of epidermal homeostasis, which is essential to maintain skin composition and function. The mammalian epidermis is a constantly renewing tissue with a horizontally stratified structure made up of distinct cellular

layers, which are, listed from inner to outermost layer, the basal layer, the spinous, granual and cornified layer (Allen and Potten, 1974). Stem cells in the basal layer give rise to transit-amplifying, suprabasally moving cells that, following a few division events, initiate a process of terminal differentiation which transforms them into cornified dead cells that are eventually shed. Epidermal homeostasis is maintained by a tight balance between proliferation and differentiation of keratinocytes, that can be assessed by expression of different keratin markers. We aimed to analyze the role of RIPK1 auto-phosphorylation at S166 in the reported epidermal hyperplasia phenotype in *Sharpin*$^{cpdm/cpdm}$ mice (Kumari et al., 2014) by immunostaining skin sections from 15-17 week-old wt, *Sharpin*$^{cpdm/cpdm}$ *Ripk1*$^{wt/wt}$, *Sharpin*$^{cpdm/cpdm}$ *Ripk1*$^{S166A/S166A}$ and *Sharpin*$^{cpdm/cpdm}$ *Ripk1*$^{D138N/D138N}$ mice using antibodies against Keratin 6, that functions as a marker for epidermal hyperproliferation (Zhang et al., 2019b). In contrast to wt mice, where Keratin 6 expression was confined to a thin layer of cells, Keratin 6 expression in the epidermis of Sharpin$^{cpdm/cpdm}$ was widely spread, showing excessive proliferation of keratinocytes and epidermal hyperplasia (Figure 24). Strikingly, Keratin 6 expression in *Sharpin*$^{cpdm/cpdm}$ *Ripk1*$^{S166A/S166A}$ and *Sharpin*$^{cpdm/cpdm}$ *Ripk1*$^{D138N/D138N}$ mice on the other hand was similar as in wt mice. Furthermore, we investigated the role of RIPK1 auto-phosphorylation at S166 in the disturbed epidermal differentiation in *Sharpin*$^{cpdm/cpdm}$ mice (Kumari et al., 2014). Transit amplifying cells express Keratin 14, which is downregulated when cells exit cell cycle and embark on a program of terminal differentiation and coincides with upregulation of keratin 10 expression (Liu et al., 2013). While in the epidermis of wt mice expression of keratin 10 and 14 was clearly restricted to distinct epidermal layers, this strcutre was lost in *Sharpin*$^{cpdm/cpdm}$ mice (Figure 24), indicating loss of epidermal differentiation. In contrast, in *Sharpin*$^{cpdm/cpdm}$ *Ripk1*$^{S166A/S166A}$ and *Sharpin*$^{cpdm/cpdm}$ *Ripk1*$^{D138N/D138N}$ mice the staining pattern of keratin 10 and 14 was similar as in wt mice. Therefore, both hyperplasia and loss of differentiation in the epidermis of *Sharpin*$^{cpdm/cpdm}$ mice were dependent on RIPK1 kinase activity and required RIPK1 auto-phosphorylation at S166. We additionally assessed the role of RIPK1 auto-phosphorylation at S166 in the epidermal inflammation in *Sharpin*$^{cpdm/cpdm}$ mice, by immunostaining skin tissue for infiltrating macrophages using antibodies against the F4/80 macrophage marker. As reported the skin of *Sharpin*$^{cpdm/cpdm}$ mice showed prominent F4/80-positive macrophage infiltration, revealing massive inflammation (Figure 24). Importantly, tissue inflammation was strongly inhibited by RIPK1S166A mutation, similar to D138N mutation (Figure 24).

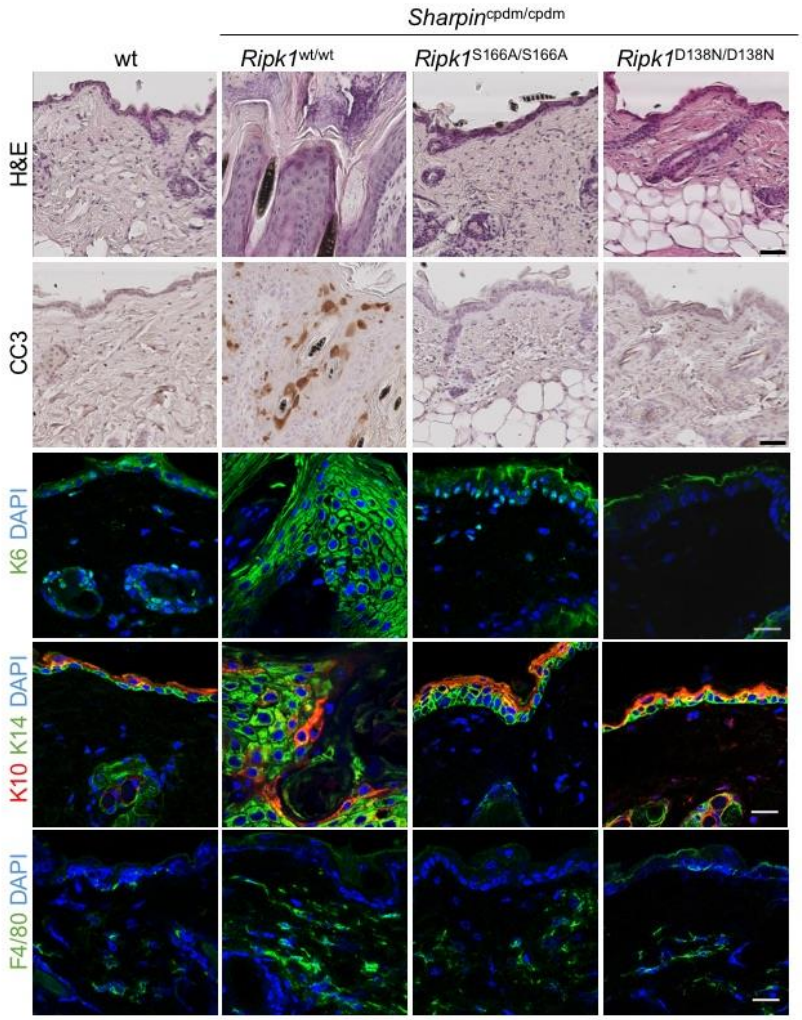

Figure 24: RIPK1 auto-phosphorylation at S166 drives hyperproliferation, loss of epidermal differentiation and inflammation in the skin of *Sharpin*$^{cpdm/cpdm}$ mice. Skin sections from mice with the indicated genotypes at the age of 15-17 weeks stained with Hematoxylin und Eosin (H&E) or immunostained with antibodies against Cleaved caspase-3 (CC3), Keratin 6 (K6), Keratin 10 and Keratin 14 (K10/14), and F4/80. Experiments in this figure were performed by Hannah Schünke.

We furthermore assessed the effect of RIPK1 auto-phosphorylation at S166 in the cytokine expression in the skin of Sharpin$^{cpdm/cpdm}$ mice by performing reverse transcription quantitative PCR (RTq-PCR) on skin lysates from wt, *Sharpin*$^{cpdm/cpdm}$ *Ripk1*$^{wt/wt}$, *Sharpin*$^{cpdm/cpdm}$ *Ripk1*$^{S166A/S166A}$ and *Sharpin*$^{cpdm/cpdm}$ *Ripk1*$^{D138N/D138N}$ mice at the age of 15-17 weeks. *Sharpin*$^{cpdm/cpdm}$ mice showed increased levels of the inflammatory cytokines *Tnf*, *IL-6*, *IL-1β*, *Ccl3* and *Cxcl*3 in their skin compared to wt mice, which was reduced by S166A mutation, similar to D138N mutation (Figure 25).

In conclusion, RIPK1 auto-phosphorylation at S166 is required for dermatitis development in mice with *cpdm* mutation and drives keratinocyte death, epidermal hyperplasia and loss of differentiation and as well as increased expression of inflammatory cytokines in the skin of these mice.

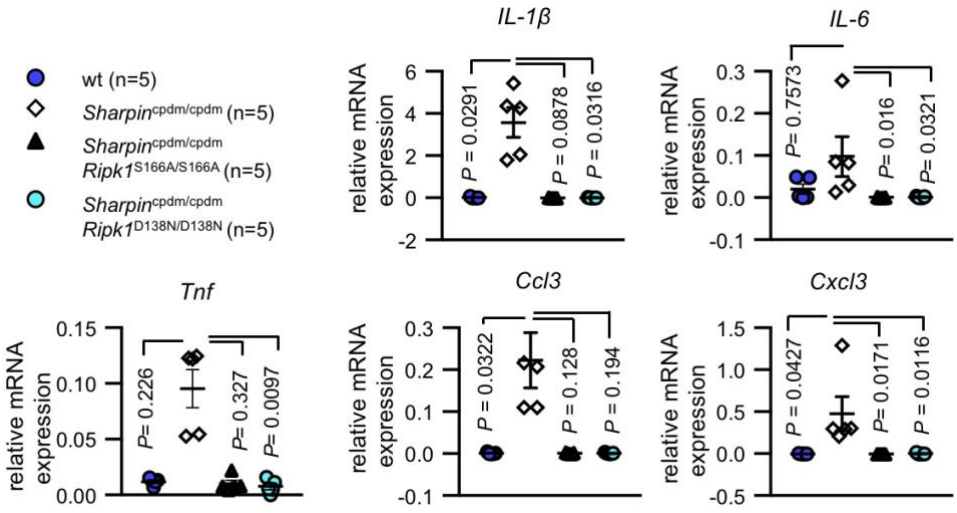

Figure 25: RIPK1 auto-phosphorylation at S166 drives inflammatory cytokine expression in *Sharpin*$^{cpdm/cpdm}$ mice. Graphs depicting relative mRNA expression in skin tissue from mice with the indicated genotypes at the age of 15-17 weeks measured by RT-qPCR. Dots indicate individual mice. Mean ± s.e.m. is shown. Statistical significance was determined using a Kruskal-Wallis test (one-sided). Experiments in this figure were performed by Hannah Schünke.

In addition to the skin, *Sharpin*$^{cpdm/cpdm}$ mice develop inflammation in multiple other organs including liver and lung (Seymour et al., 2007). We were intrigued the investigate whether auto-phosphorylation at S166, in addition to the dermatitis phenotype also mediates inflammation in these other tissues and therefore analyzed liver and lung sections from wt, *Sharpin*$^{cpdm/cpdm}$ *Ripk1*$^{wt/wt}$, *Sharpin*$^{cpdm/cpdm}$ *Ripk1*$^{S166A/S166A}$ and *Sharpin*$^{cpdm/cpdm}$ *Ripk1*$^{D138N/D138N}$ histologically. Indeed, livers and lungs from *Sharpin*$^{cpdm/cpdm}$ mice at the age of 15-17 weeks showed tissue inflammation, while tissue sections from these organs from *Sharpin*$^{cpdm/cpdm}$ *Ripk1*$^{S166A/S166A}$ as well as *Sharpin*$^{cpdm/cpdm}$ *Ripk1*$^{D138N/D138N}$ mice on the other hand looked grossly normal (Figure 26). Therefore, in addition to driving dermatitis in Sharpin$^{cpdm/cpdm}$ mice, RIPK1 auto-phosphorylation at S166 is required for RIPK1 kinase activity-dependent liver and lung inflammation in Sharpin-deficient mice.

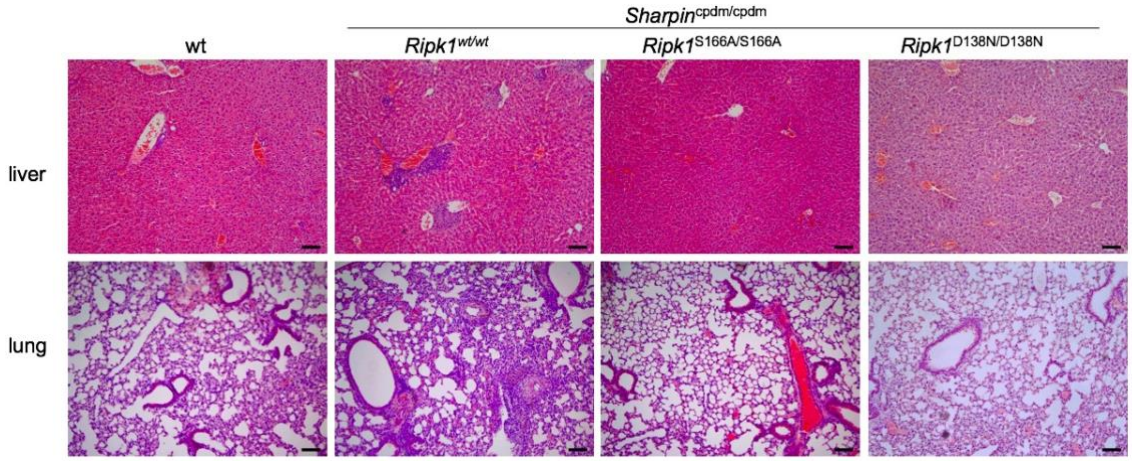

Figure 26: RIPK1 auto-phosphorylation at S166 drives multi-organ inflammation in *Sharpin*$^{cpdm/cpdm}$ mice. Representative images of tissue sections from liver and lung from mice with the indicated genotypes at the age of 15-17 weeks stained with Hematoxylin und Eosin (H&E).

3.4.3. RIPK1 auto-phosphorylation at S166 drives lethality in TNF-induced SIRS model

To strengthen our findings on the in-vivo role of RIPK1 auto-phosphorylation at S166 for RIPK1 kinase activity-driven cell death and inflammation, we aimed to evaluate the effect of RIPK1S166A mutation in other relevant disease settings.

Recently, studies using genetic and pharmacological inhibition of RIPK1 have established a driving role of RIPK1 kinase activity in TNF-induced systemic inflammatory response syndrome (SIRS) in mice (Berger et al., 2014; Duprez et al., 2011). TNF-induced SIRS in the literature is considered a mouse model of sterile sepsis, which is a clinical condition in which an exaggerated inflammatory response causes severe damage to the body's tissue and organs and thereby makes it a critical, life threatening condition. While the term sepsis defines an infection-triggered pathology, SIRS describes the underlying inflammatory state, but by definition is not necessarily induced by pathogens (Bone et al., 1992). SIRS pathology is characterized by symptoms such as abnormal body temperature, heart rate or respiratory rate as well as blood gas or an abnormal leukocyte count (Bone et al., 1992). While deregulation of various cytokines is associated with SIRS and sepsis, TNF has been established as a key mediator of these pathologies. Consistently, mice deficient for TNFR1 are protected from LPS-induced septic shock (Pfeffer et al., 1993). Therefore, to study the mechanisms underlying sepsis and SIRS pathology, the intravenous injection of high dose TNF to mice is a commonly employed model. Systemic TNF in this model induces a response characterized by temperature loss, inflammatory cytokine production and death (Duprez et al., 2011). IECs were found to be the critical target for TNF which mediates its effects through the action of TNFR1 (Van Hauwermeiren et al., 2013) by causing caspase-8-driven apoptosis as well as RIPK3/MLKL-driven necroptosis of IECs (Newton et al., 2016a). Furthermore, ablation of

RIPK1 kinase activity completely protected from SIRS-induced pathology (Berger et al., 2014; Duprez et al., 2011).

We were interested in the role of RIPK1 auto-phosphorylation at S166 in the RIPK1 kinase activity-driven shock response to TNF. To this end, we dosed wt and *Ripk1*$^{S166A/S166A}$ mice with 500 μg per kg body weight TNF and subsequently monitored body temperature and survival. As expected, TNF injection to wt mice induced hypothermia and resulted in death of 70% of wt mice (Figure 27A,B). Strikingly, the mean body temperature of *Ripk1*$^{S166A/S166A}$ mice was significantly higher in response to TNF than in wt mice after 13 and 24h of TNF dosing and consistent with a decreased responsiveness to systemic TNF, only 27% of *Ripk1*$^{S166A/S166A}$ mice succumbed (Figure 27A,B). These results show that RIPK1 auto-phosphorylation at S166 is critically involved in mediating hypothermia and lethality in a mouse model of TNF-induced SIRS.

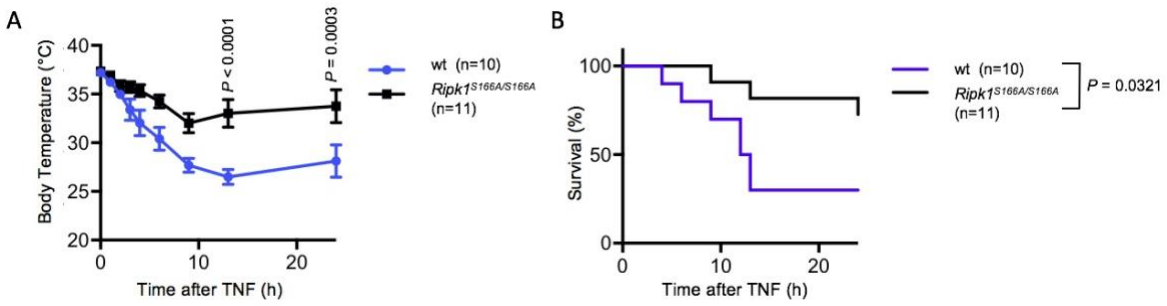

Figure 27: RIPK1 auto-phosphorylation at S166 is required for TNF-induced SIRS. (A) Graph shows body temperature curves of mice of the indicated genotypes that were injected with 500 μg kg^{-1} body wheight. Mean ± s.e.m. is shown. Statistical significance was determined using a two-way ANOVA. (B) Graph shows survival of mice of the indicated genotypes. Statistical significance was determined using a Log-rank (Mantel-Cox) test (two-sided). Experiments in this figure were performed by Tom Delanghe.

3.4.4. RIPK1 auto-phosphorylation at S166 drives hepatocyte apoptosis and hepatocellular carcinoma in Nemo^{LPC-KO} mice

Our results thus far indicate that in three TNFR1-driven disease models in different tissues, RIPK1 auto-phosphorylation at S166 mediates cell death and inflammation in-vivo, highlighting the crucial role of this site for RIPK1 kinase-dependent functions downstream of TNF sensing. Given the important role of RIPK1 kinase activity in other signaling pathways, we asked whether RIPK1 auto-phosphorylation at S166 is also required for TNFR1-independent cell death and inflammation in-vivo.

Mice that lack NEMO specifically in liver parenchymal cells (NEMO^{LPC-KO}) spontaneously develop features of chronic liver disease such as hepatocellular damage, chronic hepatitis, fibrosis and eventually hepatocellular carcinoma (HCC) (Ehlken et al., 2014; Kondylis et al., 2015b; Luedde et al., 2007). Steatohepatitis and hepatocarcinogenesis in these mice is driven

by hepatocyte apoptosis as it can be prevented by ablation of FADD (Ehlken et al., 2014; Luedde et al., 2007) or caspase-8, although NEMO^{LPC-KO} Caspase-8^{LPC-KO} mice develop a separate, spontaneous phenotype that involves massive liver necrosis (Liedtke et al., 2011). Furthermore liver pathology in NEMO^{LPC-KO} mice is dependent on RIPK1 kinase activity (Kondylis et al., 2015b), but, importantly, independent of TNFR1, TRAIL and Fas/CD95 signaling (Ehlken et al., 2014). We aimed to investigate the role of RIPK1 auto-phosphorylation in liver pathology in NEMO^{LPC-KO} mice and to this end, crossed the RIPK1S166A mutation into the NEMO^{LPC-KO} background.

Liver pathology in NEMO^{LPC-KO} mice is characterized by elevated serum levels of alanine aminotransferase (ALT) (Ehlken et al., 2014; Kondylis et al., 2015b; Luedde et al., 2007), an enzyme which predominantly occurs in the liver while its increase in the blood serves as a biomarker for liver damage. Indeed, at the age of 8 weeks, NEMO^{LPC-KO} mice presented with increased ALT levels in their sera as compared to their wt littermates or *Ripk1*$^{S166A/S166A}$ mice (Fig 28A). RIPK1S166A mutatiom in NEMO^{LPC-KO} mice on the other hand strongly prevented the increase in ALT levels (Figure 28A), showing that RIPK1 auto-phosphorylation at S166 promotes liver damage in NEMO^{LPC-KO} mice. To evaluate the role of RIPK1 auto-phosphorylation at S166 in apoptotic cell death in livers, we performed immunostaining for cleaved and activated caspase-3 on liver tissue sections from 8 week-old NEMO^{LPC-KO}, *Ripk1*$^{S166A/S166A}$ and NEMO^{LPC-KO} *Ripk1*$^{S166A/S166A}$ mice. In compliance with previous reports, we observed increased incidence of CC3-positive cells in NEMO^{LPC-KO} livers in comparison to livers from wt and *Ripk1*$^{S166A/S166A}$ mice (Figure 28B). Importantly, this apoptotic phenotype was strongly inhibited in NEMO^{LPC-KO} *Ripk1*$^{S166A/S166A}$ mice.

In response to chronic spontaneous hepatocyte death regenerative responses are known to be activated which include compensatory hepatocyte proliferation and activation of hepatic stellate cells to release extracellular matrix components, such as collagen (Kondylis and Pasparakis, 2019; Luedde et al., 2014). While in the short term, these mechanisms can preserve liver function, on the long term, they may lead to severe liver pathology and liver failure (Kondylis and Pasparakis, 2019). In line with this, NEMO^{LPC-KO} livers are described to present with a state of excessive accumulation of extracellular matrix proteins, known as fibrosis. Indeed, immunostaining for α-smooth muscle actin, a biomarker for liver fibrosis that detects the activation of hepatic stellate cells, revealed a pronounced fibrotic response in livers of NEMO^{LPC-KO} mice, which was not evident in wt mice (Figure 28B). Hepatic stellate cell activation in NEMO^{LPC-KO} *Ripk1*$^{S166A/S166A}$ mice on the other hand was very weak and similar as is wt mice. Furthermore, by staining for the Ki67 antigen, a nuclear protein associated with cellular proliferation, we detected increased amounts of proliferating hepatocytes in NEMO^{LPC-KO} mice indicative of a compensatory proliferative response in these mice (Figure 28B). Increased Ki67 cell positivity on the other hand was strongly inhibited by RIPK1S166A

mutation. In line with an inflammatory response in NEMO^{LPC-KO} mice, we observed increased infiltration of macrophages as detected by immunostaining for F4/80, which was strongly inhibited by RIPK1S166A mutation (Fig 28B).

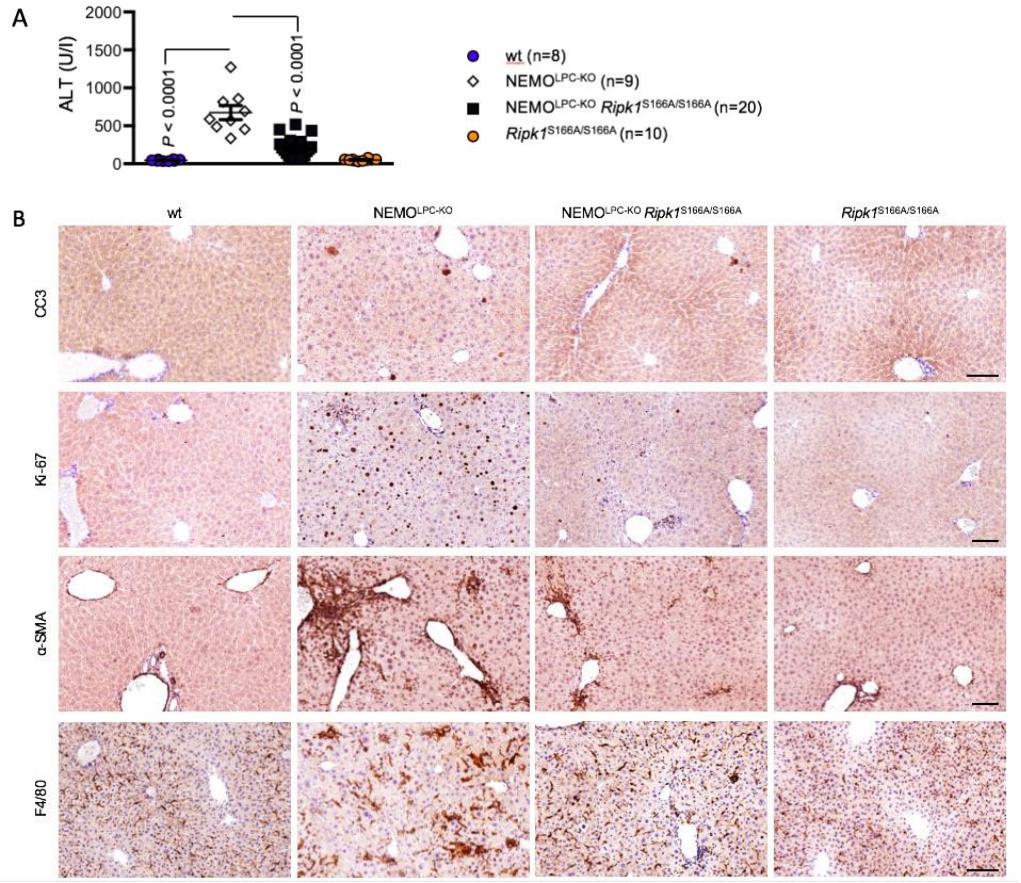

Figure 28: RIPK1 auto-phosphorylation at S166 drives steatohepatitis in NEMO^{LPC-KO} mice. (A) Graph depicting ALT levels in the serum of mice with the indicated genotypes at 8 weeks of age. Dots in the graph represent individual mice. Horizontal lines indicate mean values ± s.e.m. are indicated. Statistical significance was determined using one-way ANOVA. (B) Representative pictures of liver sections from mice with the indicated genotypes at 8 weeks of age stained with Hematoxylin and Eosin (H&E) or immunostained using antibodies against Cleaved caspase-3 (CC3), Ki-67, alpha smooth muscle actin (αSMA) or F4/80. Scale bars, 200 μm. Experiments in this figure were performed by Vangelis Kondylis.

Chronic spontaneous hepatocyte death and resulting liver damage stimulates compensatory proliferation as exemplified in livers of NEMO^{LPC-KO} mice. In the context of a fibrotic and inflammatory microenvironment, this increased proliferation promotes malignant transformation of hepatocytes and may subsequently lead to the initiation of liver tumors (Kondylis and Pasparakis, 2019). In line with this, NEMO^{LPC-KO} mice spontaneously develop large liver tumors by the age of 12 months (Ehlken et al., 2014; Kondylis et al., 2015b; Luedde et al., 2007). To investigate whether RIPK1 auto-phosphorylation at S166 is required for development of hepatocellular carcinoma (HCC) in NEMO^{LPC-KO} mice, we aged wt, NEMO^{LPC-KO}, NEMO^{LPC-KO} *Ripk1*$^{S166A/S166A}$ and *Ripk1*$^{S166A/S166A}$ mice until the age of 50 weeks and

evaluated the formation of liver tumors macroscopically. While livers from 50 week-old NEMO^{LPC-KO} showed multiple large HCC, NEMO^{LPC-KO} *Ripk1*$^{S166A/S166A}$ mice were tumor-free similar to wt and *Ripk1*$^{S166A/S166A}$ mice (Figure 29A-D). Histological analysis of liver sections from 50 week-old NEMO^{LPC-KO} confirmed morphological abnormalities in liver tissue such as increased cellularity and higher nuclear to cytoplasmic ratios in HCC areas as compared to nontumor areas in NEMO^{LPC-KO} mice (Figure 29B). NEMO^{LPC-KO} *Ripk1*$^{S166A/S166A}$ livers on the other hand looked normal apart from some small steatotic lesions characterized by increased lipid deposition and hepatocyte ballooning (Figure 29B). Furthermore, NEMO^{LPC-KO} mice had increased liver weight to body weight ratios (Figure 29C), illustrating liver tumor burden in these mice. Importantly, Increased LW/BW ratios and tumor incidence were both strongly inhibited by *Ripk1*$^{S166A/S166A}$ mutation.

Taken together, ablation of RIPK1 auto-phosphorylation at S166 significantly ameliorated the liver pathology observed in NEMO^{LPC-KO} mice by preventing hepatocyte apoptosis. As a result, compensatory proliferation, fibrosis and inflammation were decreased and HCC development was prevented.

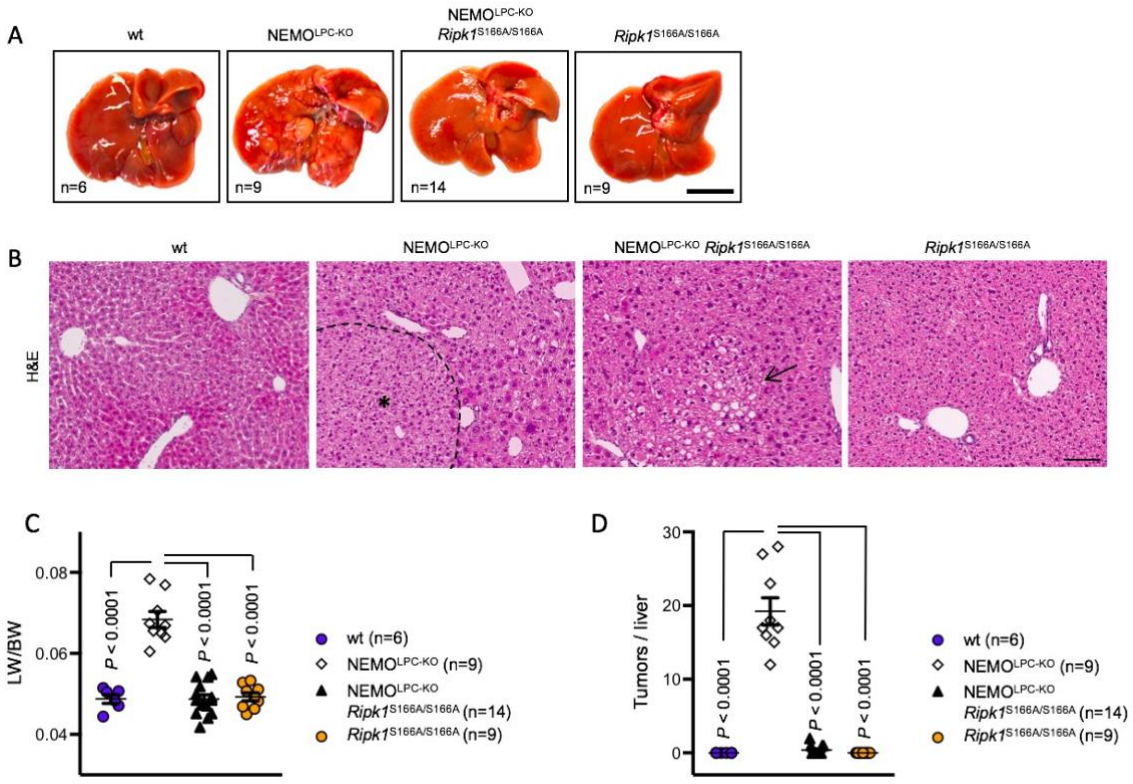

Figure 29: RIPK1 auto-phosphorylation at S166 is essential for hepatocellular carcinoma development in NEMO^{LPC-KO} mice. (A) Representative images of livers from mice with the indicated genotypes at 50 weeks. Scale bar, 1cm. (B) Representative pictures from liver sections from 50 week-old mice with the indicated genotypes. Hepatocellular carcinoma (HCC) areas are outlined and marked with an astersk. Arrows point at a small steatotic area observed in some NEMO^{LPC-KO} Ripk1$^{S166A/S166A}$ mice. (C) Graph depicting tumor load quantification in 50 week-old mice with the indicated genotypes

as liver wheight/ body wheight (LW/BW) ratios.(D)Graph depicting tumor numbers per liver in 50 week-old mice with the indicated genotypes. (C,D) Dots in the graph represent individual mice. Horizontal lines indicate mean values ± s.e.m. are indicated. Statistical significance was determined using one-way ANOVA. Experiments in this figure were performed by Vangelis Kondylis.

3.5 RIPK1 auto-phosphorylation at S166 drives RIPK1 kinase activity and auto-phosphorylation on other sites

3.5.1. RIPK1 auto-phosphorylates in-trans at S166 to promote RIPK1 kinase activity

Given our findings that RIPK1 auto-phosphorylation at S166 is essential for induction of RIPK1 kinase activity-dependent cell death in-vivo and the assembly of cell death-inducing complexes in vitro, we wondered how phosphorylation at this site transmits the cell death-inducing stimulus mechanistically. It is generally believed that the main purpose of the kinase activity of RIPK1 is to auto-phosphorylate, thereby promoting conformational changes in RIPK1 that allow for the interaction with downstream cell death inducing partners, such as FADD and RIPK3. Based on this model, the role of RIPK1 auto-phosphorylation at S166 in cell death induction might be to prompt this conformational remodeling by-itself and thereby directly allow the formation of cell death signaling platforms. Alternatively, RIPK1 auto-phosphorylation at 166 might act as an enhancer of kinase activity which could subsequently allow for auto-phosphorylation at other sites, such as S161 and T169 or other downstream events, to transmit the lethal stimulus.

We aimed to evaluate both possibilities for the role of RIPK1 S166 auto-phosphorylation. Previously, death domain-mediated dimerization of RIPK1 has been shown to be required for its activation (Meng et al., 2018). Furthermore, in RIPK1 dimers that were chemically induced in cell culture, auto-phosphorylation at S166 was reported to occur in trans (Xu et al., 2018).

In order to gain insight into the effect of the S166A mutation on RIPK1 kinase activity, we tested whether a RIPK1S166A molecule can auto-phosphorylate a D138N molecule at residue 166 in trans in a dimer. To exclude possible artefacts resulting from protein overexpression in this context, we designed an experiment in a physiological setting using *Ripk1*$^{D138N/S166A}$ mice, which we generated by crossing *Ripk1*$^{S166A/S166A}$ to *Ripk1*$^{D138N/D138N}$ mice. In cells from *Ripk1*$^{D138N/S166A}$ mice, three different combinations of RIPK1 dimers can form, which are S166A/S166A or D138N/D138N homodimers or D138N/S166A heterodimers (Figure 30A). Of these, D138N/D138N dimers lack kinase activity (Polykratis et al., 2014) and in S166A/S166A dimers residue S166 is unavailable for phosphorylation. Therefore, in this setup RIPK1 auto-phosphorylation at residue S166 can exclusively occur in D138N/S166A heterodimers by phosphorylation of a D138N molecule by an S166A molecule (Figure 30A), which we assessed by using p-S166-specific antibodies. To this end, we treated BMDMs and lung fibroblasts from wt, *Ripk1*$^{S166A/S166}$, *Ripk1*$^{D138N/D138N}$ and *Ripk1*$^{D138N/S166A}$ mice with TNF (T) in combination with

Smac mimetic (S) and Z-VAD-FMK (Z) to induce RIPK1 auto-phosphorylation under necroptotic conditions. TSZ treatment induced a strong p-S166 signal in wt cells, which coincided with phosphorylation of MLKL and phosphorylation of RIPK3 (Fig 30 B,C), indicative for activation of necroptotic signaling. As expected, phosphorylation at S166 was completely abolished in *Ripk1*$^{S166A/S166A}$ cells and *Ripk1*$^{D138N/D138N}$ cells, whereas importantly, we observed robust phosphorylation at S166 in *Ripk1*$^{D138N/S166A}$ cells. In comparison to wt cells, however, the p-S166 signal in these cells was strongly reduced. Our interpretation of these data is that RIPK1S166A exhibits kinase activity, which however is reduced compared to the wt protein. These data furthermore support previous studies (Xu et al., 2018) showing that RIPK1 can auto-phosphorylate in trans within a dimer.

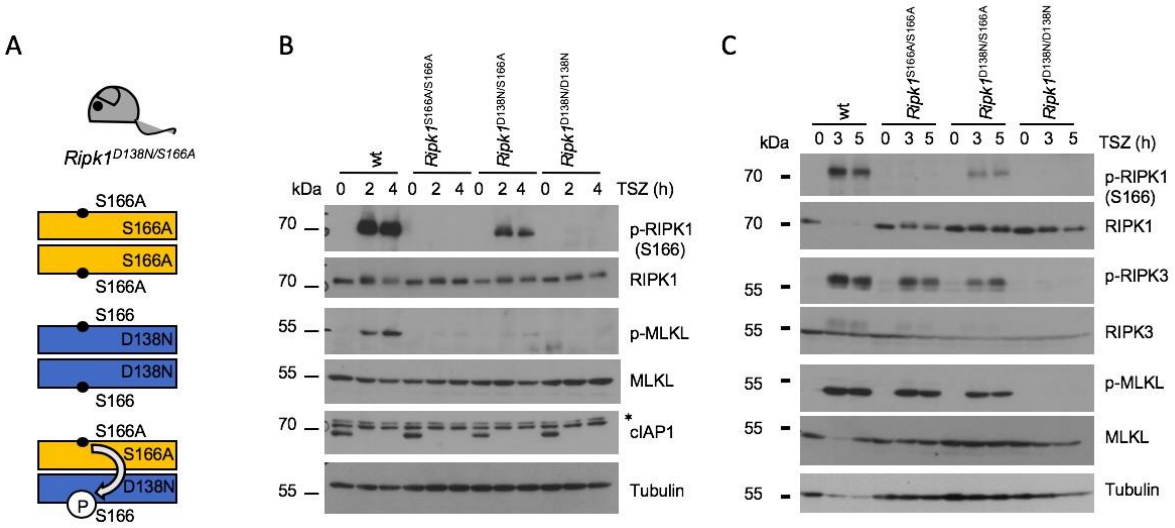

Figure 30: Auto-phosphorylation at S166 drives RIPK1 kinase activity. (A) Scheme depicting RIPK1 dimer combinations in Ripk1$^{D138N/S166A}$ mice. Residue S166 is indicated. (B) BMDMs from mice of the indicated genotypes were treated with TNF(T) in combination Smac mimetic (S) and Z-VAD-FMK (Z) for 0, 2 and 4 h. Lysates were analyzed using the indicated antibodies. *, non-specific band. (C) Lung fibroblasts from mice with the indicated genotypes were treated with TNF(T) in combination Smac mimetic (S) and Z-VAD-FMK (Z) for 0, 3 and 5 h. Lysates were analyzed using the indicated antibodies. (B), (C) Blots shown are representative of three independent experiments. Experiments in (B) were performed together with Masahiro Nagata.

3.5.2. RIPK1 auto-phosphorylation at S166 is not sufficient for cell death induction

Our data show that in vivo, autophosphorylation at S166 is necessary for induction of RIPK1 kinase activity-dependent cell death and hence constitutes an essential function of RIPK1 catalytic activity. Consequently, we asked whether auto-phosphorylation at S166 by itself was not only necessary, but also sufficient for cell death induction and therefore whether it represents the main and crucial role of RIPK1 kinase function. If indeed auto-phosphorylation at S166 was the crucial downstream event of RIPK1 kinase activity, we would expect that phosphorylation at S166 could overcome the inhibition on cell death induction imposed by

ablation of RIPK1 kinase activity. Given that in our previous experiments we observed prominent p-S166 phosphorylation on a D138N molecule, we were able to test whether P-S166 on a D138N RIPK1 molecule can provide the critical trigger for RIPK1 to transmit the cell death inducing stimulus by evaluating the potential of *Ripk1*$^{D138N/S166A}$ cells to undergo cell death. To this end, we treated BMDMs from wt, *Ripk1*$^{S166A/S166}$, *Ripk1*$^{D138N/D138N}$ and *Ripk1*$^{D138N/S166A}$ mice with TNF (T) in combination with Smac mimetic (S) and Z-VAD-FMK (Z). TSZ treatment induced high amounts of cell death in wt cells, which was largely RIPK1 kinase activity-dependent (Figure 31A). *Ripk1*$^{D138N/S166A}$ BMDMs on the other hand, similar to *Ripk1*$^{S166A/S166A}$ cells were partly protected from TSZ-induced cell death. Importantly, strength and kinetics of cell death in *Ripk1*$^{D138N/S166A}$ and *Ripk1*$^{S166A/S166A}$ cells were very similar (Figure 31A), showing that p-D138N molecules did not enhance cell death induction.

Furthermore, based on our data, RIPK1 auto-phosphorylation at S166 is required to enable the kinase activity-dependent engagement of RIPK1 in cell death activating complexes. To understand if mechanistically, auto-phosphorylation at 166 is sufficient for the assembly of cell death inducing complexes independently of RIPK1 kinase activity, we analyzed complex II/necrososme formation in Ripk1$^{S166A/D138N}$ cells. To this end, we treated cells with TSZ stimulus and assessed the formation of RIPK1, caspase-8, FADD and RIPK3-containing complexes by performing immunoprecipitations using antibodies against FADD (Figure 31B) or capase-8 (Figure 31C). While in wt cells, we observed strong recruitment of RIPK1 and RIPK3 to a FADD-containing complex, the interaction of FADD and RIPK1 was strongly reduced in *Ripk1*$^{D138N/S166}$ cells, similar to Ripk1$^{S166A/S166A}$ cells (Figure 31B). Consistently, the interaction of caspase-8 with RIPK1, RIPK3 and FADD was prominent in wt BMDMs but strongly inhibited in Ripk1$^{D138N/S166A}$ cells, similar to Ripk1$^{S166A/S166A}$ cells (Figure 31C). Therefore, RIPK1 auto-phosphorylation at S166 does not increase the potential of p-RIPK1D138N to engage in complex II, which is in line with similar levels of cell death that we observed in cells from *Ripk1*$^{S166A/S166A}$ and *Ripk1*$^{D138N/S166A}$ mice. Our interpretation of these results is that RIPK1 auto-phosphorylation at S166 by itself is not sufficient for cell death induction.

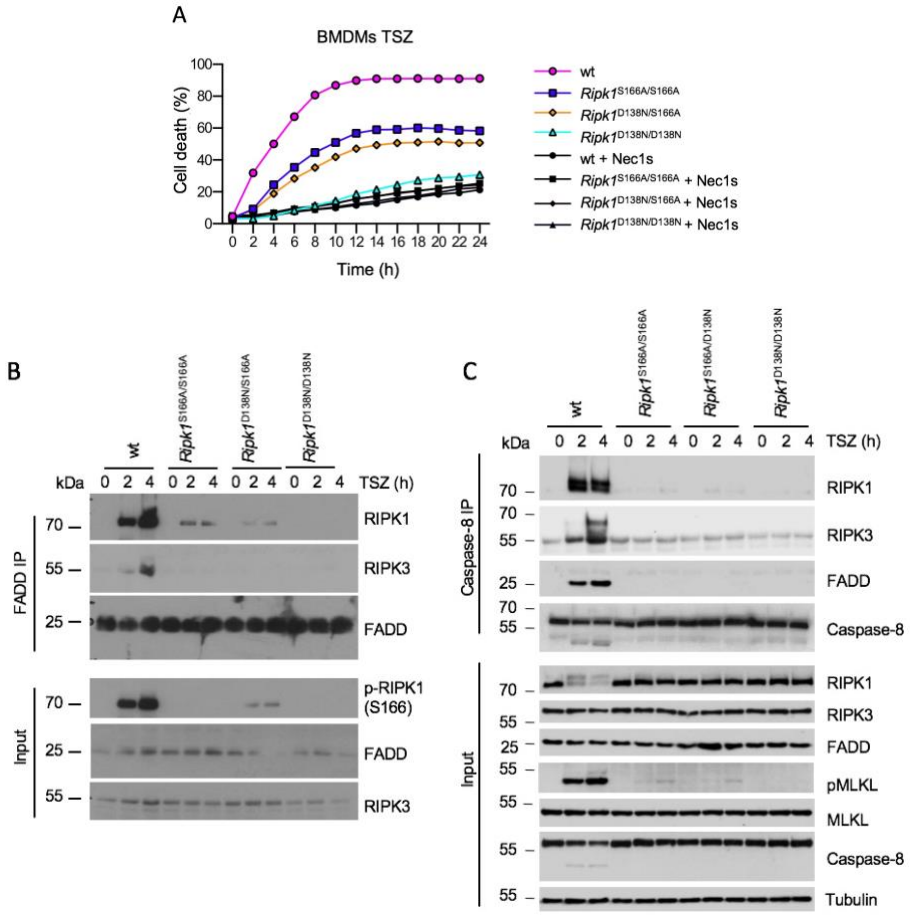

Figure 31: RIPK1 Auto-phosphorylation at S166 by itself is not sufficient for cell death induction. (A) BMDMs from mice with the indicated genoytpes were treated with TNF(T) in combination with Smac mimetic (S) and Z-VAD-FMK (Z). Cell death was analyzed using an IncuCycte as described. The data for the wt, *Ripk1*$^{S166A/S166A}$ and *Ripk1*$^{D138N/D138N}$ genotypes here are identical to those shown in Figure 15A for purpose of comparability. Data shown are representative of three independent experiments (B) BMDMs were treated with TNF(T) in combination with Smac mimetic (S) and Z-VAD-FMK (Z) for 0, 2 or 4 h. FADD-Immunoprecipitates and Input were analyzed by immunoblot using the indicated antibodies. (C) BMDMs were treated with TNF(T) in combination with Smac mimetic (S) and Z-VAD-FMK (Z) for 0, 2 or 4 h. Caspase-8-Immunoprecipitates and input were analyzed by immunoblot using the indicated antibodies. Experiment was performed by Tom Delanghe. (B), (C) Data shown represent one experiment.

3.5.3. p-RIPK1(S166) facilitates auto-phosphorylation on other sites

Besides S166, mouse RIPK1 has been shown to auto-phosphorylate at S14, S15 and S161, as well as T169, while human RIPK1 additionally self-targets S20, but T169 is not conserved (Degterev et al., 2008; Dondelinger et al., 2019). The presence of multiple autophosphorylation events indicates that modification of multiple sites, possibly in a sequential and hierarchical manner might be required to unfold the full cytotoxic potential of RIPK1. If so, p-S166 might be an upstream event in a potential signaling cascade of different auto-phosphorylation events. To evaluate whether this is the case, we aimed to explore the impact of RIPK1S166A mutation on RIPK1 autophosphorylation on other sites. To this end, we analyzed RIPK1 phosphorylation in TSZ-treated BMDMs from wt, *Ripk1*$^{S166A/S166A}$ and *Ripk1*$^{D138N/D138N}$ mice by mass

spectrometry (MS), due to the lack of specific antibodies recognizing phosphorylation at S161 and T169. We employed phospho-peptide enrichment with titanium dioxide (TiO_2) beads in order to improve the detection of phosphorylated peptides. Indeed, we found 13,547 phosphorylation sites in total cell lysates from TSZ-treated BMDMs, including 5 events on RIPK1. Phosphorylation at S313, which was previously suggested to be targeted by p38 (Menon et al., 2017), was detected in in wt, *Ripk1*$^{S166A/S166A}$ as well as *Ripk1*$^{D138N/D138N}$ cells in TSZ-treated as well as nontreated conditions (Figure 32A). Therefore, indeed this site seems to be phosphorylated by another kinase than RIPK1 independently of a necroptotic stimulus. Equal levels of RIPK1 phosphorylation at this site as well as equal levels of total RIPK1 protein under all conditions furthermore indicate that phospho-peptide enrichment was consistently efficient between the different samples (Figure 32A,C).

Interestingly, we measured a RIPK1 peptide containing double phosphorylation at S166 and T169 (p-S166/p-T169) in wt cells after two hours of TSZ treatment (Figure 32 A,B). On the other hand, we did not find phosphorylation at T169 in *Ripk1*$^{D138N/D138N}$ cells, therefore this site likely represents an autophosphorylation site. Importantly, in *Ripk1*$^{S166A/S166A}$ cells, we did not detect p-T169 either (Figure 32A), suggesting that phosphorylation at T169 might be dependent on auto-phosphorylation at S166. Previous studies have shown that S25 is an IKK target site (Dondelinger et al., 2019). We found RIPK1 to be phosphorylated at S25 in response to TSZ treatment independent of the genotype (Figure 32 D), confirming that this RIPK1 site is phosphorylated independently of its own catalytic activity. Interestingly, S25 phosphorylation was increased in TSZ-treated conditions. S14 of RIPK1 was previously suggested to be an autophosphorylation site (Degterev et al., 2008). We detected S14 phosphorylation also in Ripk1$^{S166A/S166A}$ cells, although at slightly reduced levels compared to wt cells. (Figure 32 E). Surprisingly, low levels of S14 phosphorylation were measured in kinase activity-deficient *Ripk1*$^{D138N/D138N}$ cells (Figure 32 E), suggesting that S14 is not exclusively a RIPK1 autophosphorylation site. Earlier studies reported RIPK1 autophosphorylation at S161 in response to necroptotic stimuli (Degterev et al., 2008; Zhang et al., 2017b). However, within two independent experiments we did not detect phosphorylation of S161 in TSZ-treated BMDMs, although in these replicates as well as in a broader context of MS experiments targeted to RIPK1, we reproducibly measured the non-phosphorylated peptide.

Collectively, these results suggest that autophosphorylation at S166 promotes auto-phosphorylation at T169 and potentially S14 on RIPK1.

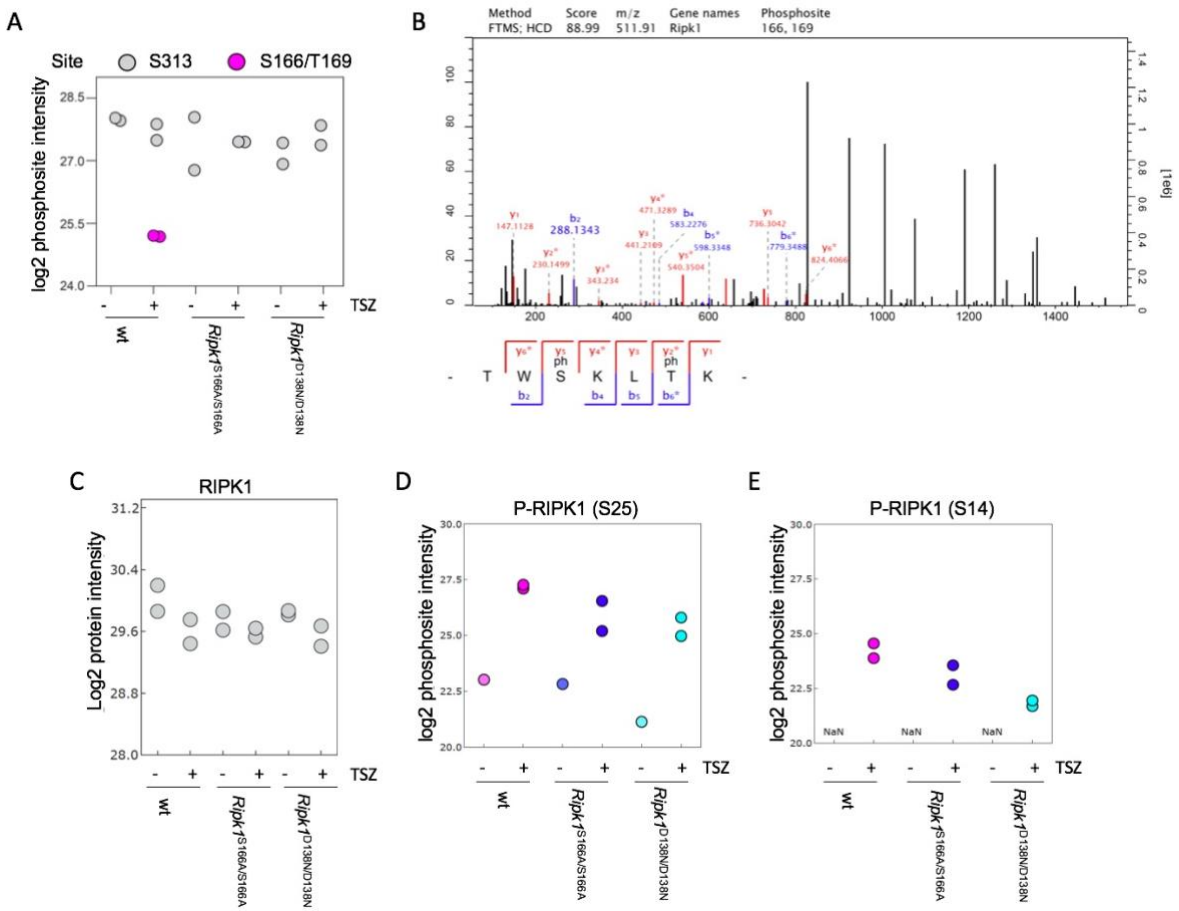

Figure 32: S166 phosphorylation promotes RIPK1 autophosphorylation at additional sites. (A) LC–MS/MS measured log2 intensities of the p-S166 p-T169- and p-S313 sites after indicated treatment with or without a combination of TNF, SMAC mimetic and Z-VAD-FMK (TSZ) for 2 h. (B) Selected LC–MS/MS scan of the p-S166/p-T169 RIPK1 peptide with annotated b-and y-ions. Fragment ions marked with asterisk (*) result from loss of the phospho-group. (C) LC–MS/MS measured log2 intensities of RIPK1 peptides after indicated treatment with or without a combination of TNF, SMAC mimetic and Z-VAD-FMK (TSZ) for 2 h. (D) LC–MS/MS measured log2 intensities of the RIPK1 p-S25 site after indicated treatment with or without a combination of TNF (10 ng ml−1), SMAC mimetic and Z-VAD-FMK (TSZ) for 2 h. (E) LC–MS/MS measured log2 intensities of the RIPK1 p-S14 site after indicated treatment with or without a combination of TNF, SMAC mimetic and Z-VAD-FMK (TSZ) for 2 h. (A), (C)-(E) Values from two independent experiments are shown. Experiments in this figure were performed together with Janica L. Wiederstein.

4. Discussion

RIPK1 kinase activity has previously been established as a driver of cell death and inflammation in vivo (Berger et al., 2014; Kondylis et al., 2015b; Newton, 2020; Vlantis et al., 2016). While to date, the mechanisms by which RIPK1 kinase activity transduces the cell death-inducing stimulus remain poorly understood, the main function of RIPK1's enzymatic activity is believed to be auto-phosphorylation (Degterev et al., 2008; Zhang et al., 2017b). Facilitated by the development of specific antibodies (Berger et al., 2014), autophosphorylation at S166 is used as a marker for catalytic activation of RIPK1 in the field, the mechanistic role and physiological importance of this site however remain unclear. Here, we investigated the role and mechanistic importance of auto-phosphorylation at S166 for function of RIPK1 in cell death and inflammation in vitro and in vivo.

4.1 Auto-phosphorylation at S166 is essential for RIPK1 kinase activity-dependent cell death

RIPK1 auto-phosphorylation at S166 is routinely used as a marker for RIPK1 activation in the field (Berger et al., 2014; Dondelinger et al., 2019; Jaco et al., 2017; Patel et al., 2020) and is considered indicative of a RIPK1 pool that can function as an inducer of cell death (Mifflin et al., 2020; Ofengeim et al., 2015). The mechanistic function and physiological relevance of this site however had not been studied. In cell death-inducing complexes that require RIPK1 kinase activity, RIPK1 is heavily auto-phosphorylated at S166 (Dondelinger et al., 2019; Lafont et al., 2018; Meng et al., 2018). On the other hand, S166 auto-phosphorylation has also been reported in response to TNF treatment alone (Newton et al., 2016b), which induces complex I formation, inflammatory and pro-survival signaling independently of RIPK1 kinase activity. Our data show that auto-phosphorylation at S166 was dispensable for the scaffolding function of RIPK1 in TNFR1-induced complex I to activate NF-κB and MAPK signaling. In the same line, autophosphorylation at S166 was not required for activation of NF-κB and MAPKs downstream of TLR3 and TLR4. On the other hand, we found that RIPK1 auto-phosphorylation at S166 is an essential event for the induction of RIPK1 kinase activity-dependent apoptosis and necroptosis. In vivo, ablation of auto-phosphorylation at S166 completely protected from RIPK1 kinase activity-driven apoptosis and inflammation in the colon of $NEMO^{IEC\text{-}KO}$ mice, liver of $NEMO^{LPC\text{-}KO}$ mice as well as skin of *Sharpin*$^{cpdm/cpdm}$ mice. Loss of auto-phosphorylation at S166 furthermore protected from systemic pathology in a model of TNF-induced SIRS, in which hypothermia and lethality are driven by both RIPK1 activity-dependent apoptotic and necroptotic cell death (Duprez et al., 2011; Newton et al., 2016a). Therefore, in vivo, RIPK1 auto-phosphorylation at S166 is cruical for RIPK1 kinase activity-dependent apoptosis and

possibly also necroptosis. Strikingly, while the protection from cell death and inflammation observed in these models in-vivo was as strong as, or similar, to that provided by ablation of RIPK1 kinase activity, the cell death-protective effect of the S166A mutation in-vitro, downstream of TNFR1, TLR3 and 4, was only partial. Our in vivo data therefore challenge the relevance of in-vitro experiments in which high concentrations of stimuli are used over long periods of time which likely do not occur in a comparable manner under physiological conditions in an organism.

Ablation of auto-phosphorylation at S166 not only protected from TNFR1-mediated pathologies in the NEMO$^{IEC\text{-}KO}$, *Sharpin*$^{cpdm/cpdm}$ and SIRS models, but also from hepatitis and hepatocellular carcinoma development in NEMO$^{LPC\text{-}KO}$ mice, that is independent on TNFR1, TRAIL or CD95 signaling (Ehlken et al., 2014). Therefore, auto-phosphorylation at S166 is driving TNFR1-dependent and -independent cell death and inflammation. Furthermore, we observed a cell death-protective effect in different tissues such as skin, liver and colon and different cell types such as BMDMs, lung-and dermal-fibroblasts. Overall, these results suggest a universal role of auto-phosphorylation at S166 as a regulator of cell death, independent of the cell type or tissue.

Its cell death-driving function is in line with the presence of auto-phosphorylation at S166 in cell death-inducing complexes (Dondelinger et al., 2019; Lafont et al., 2018; Meng et al., 2018), while leaving its presence in complex I (Newton et al., 2016b) unclear. According to our findings, phosphorylation at S166 is not functionally relevant in this complex, while it seems conceivable that complex I contains a pool of RIPK1 which is kinase active and might serve the assembly of cell death-inducing complexes upon sensing of a cell death stimulus.

4.2 Auto-phosphorylation at S166 acts as a driver of RIPK1 kinase activity

Based on lack of evidence for the existence of downstream targets of RIPK1's enzymatic activity, the prevailing model on how RIPK1 kinase activity promotes killing of a cell hypothesizes that auto-phosphorylation of RIPK1 leads to intra-protein conformational changes that facilitate its engagement in cell death-inducing complexes (Newton, 2020). Our findings support that auto-phosphorylation is crucial for cell death and cell death-induced complex formation and that it is mechanistically involved in transmission of the cell death-inducing stimulus.

By providing evidence that RIPK1S166A can auto-phosphorylate a RIPK1D138N protein in trans, we show that RIPK1S166A retains catalytic activity. Importantly, this demonstrates that RIPK1S166A is structurally and functionally intact and we can therefore exclude the possibility that RIPK1S166A-mediated inhibition on cell death stems from a general structural disturbance of the mutant protein. On the other hand, results from the same experimental setup imply that RIPK1S166A likely auto-phosphorylates with lower efficiency than a wt protein, pointing to a

reduced enzymatic activity of the molecule. These observations suggest that auto-phosphorylation at S166 is required for full activation of RIPK1's catalytic activity, indicating that RIPK1 auto-phoshorylation at S166 acts a as mechanism promoting RIPK1 kinase activity. Interestingly, activation-loop phosphorylation in many protein kinases is known to be crucially involved in stabilizing the enzymatically active conformation (Adams, 2003). Specifically, auto-phosphorylation in trans has been described as a common kinase-activating mechanism observed in eukaryotic protein kinases. What appears to be a "Catch 22 Situation", in which a kinase paradoxically catalyzes auto-phosphorylation in an inactive state, is often achieved by allosteric alignment of catalytic motifs, such as during dimerization, which results in a "prone-to-auto-phosphorylate conformation" (Beenstock et al., 2016). Our results confirm that in a system with physiological protein concentrations, RIPK1 forms homodimers as has previously been suggested (Meng et al., 2018; Xu et al., 2018). Importantly, our data shows that RIPK1 trans-auto-phosphorylates in these dimers. Therefore, based on our observations and the fact that S166 is located in the activation loop of RIPK1 (Xie et al., 2013), we propose that RIPK1 forms dimers and trans auto-phosphorylates at S166 in the activation loop in an auto-activating mechanism (Figure 33).

In the context of cell death induced in response to TNFR1, complexes that are dependent or independent on catalytic activity of RIPK1 may form in a dynamic fashion, raising the question on the spatial and temporal manner in which RIPK1 auto-phosphorylation and activation occur in the cell. Previously, DD-mediated dimerization was shown to be dispensable for RIPK1 recruitment to complex I, but required for the activation of a cytosolic pool of RIPK1 as well as for assembly of complex II (Meng et al., 2018). These results suggest that RIPK1 activation, driven by its dimerization, might mainly proceed during a transition from complex I to complex II. Nevertheless, also RIPK1 that lacks the DD can contribute to complex II formation (Jaco et al., 2017), whether the portion of RIPK1 DD-deficient proteins in complex II in this context lack catalytic activity however is not clear.

Conclusively, our data suggest that auto-phosphorylation at S166 acts as a kinase-activating mechanism, which may be driven by DD-dependent homodimerization of RIPK1. In which spatial and temporal manner RIPK1 activation and S166 auto-phosphorylation proceeds in a cell remains to be seen.

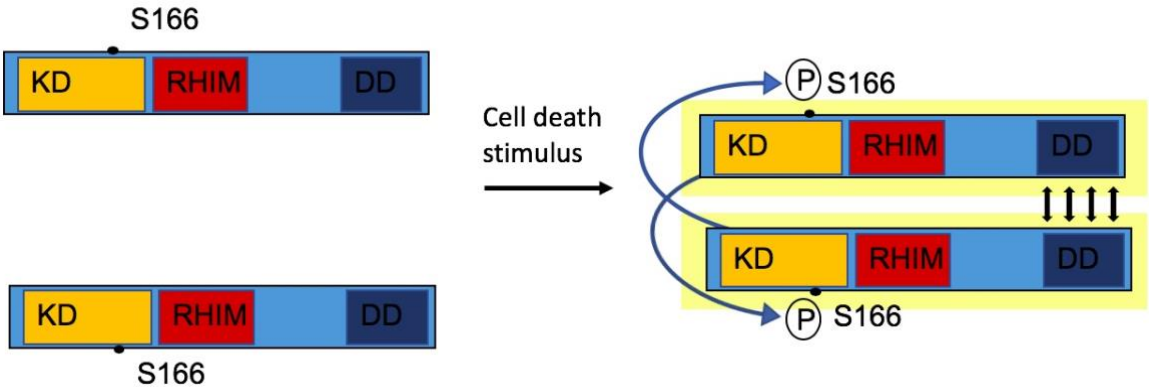

Figure 33: Model of RIPK1 kinase activation. RIPK1 proteins and their domain structure (KD = kinase domain, RHIM = RIP homotypic interaction motif; DD = death domain) are shown. In response to a cell death stimulus, RIPK1 homodimerizes through DD-interactions and trans-auto-phosphorylates at residue S166 in the kinase domain and thereby becomes kinase active (represented by glowing box).

4.3 RIPK1 auto-phosphorylation at S166 facilitates auto-phosphorylation at other sites

Whereas our study reveals a role for RIPK1 auto-phosphorylation at S166, our results also show that phosphorylation at S166 cannot overcome the cell death-inhibition imposed by ablation of RIPK1 kinase activity in a D138N molecule. Therefore, S166 by itself is not sufficient to provide the critical trigger which allows RIPK1 to transmit the cell death-inducing stimulus. This data argues that RIPK1 kinase activity has another mechanistic role, which may be additional auto-phosphorylation events or phosphorylation of a yet unknown downstream target. Furthermore, pointing to the existence of additional mechanisms regulating RIPK1 kinase activity and its cell death-inducing potential, in vitro, RIPK1S166A mutation only offers incomplete protection from cell death. This finding suggests that in the absence of auto-phosphorylation at S166, compensating mechanisms are in place. Besides S166, mouse RIPK1 has been shown to auto-phosphorylate at S14/15, S161 and T169 (Degterev et al., 2008; Dondelinger et al., 2019; Ofengeim et al., 2015). Hence, it is conceivable that other auto-phosphorylation events are involved in full activation of RIPK1's kinase activity and transmission of the cell-death inducing signal. Similar to S166, T169 is located in the activation loop of RIPK1(Xie et al., 2013). Whereas the role of phosphorylation at T169 has not been reported, our data confirm that it is an auto-phosphorylation site. Importantly, our results suggest that T169 is auto-phosphorylated in dependence of phosphorylation at S166. Previously, S14 has also been described as an auto-phosphorylation site (Degterev et al., 2008; Ofengeim et al., 2015). Surprisingly, in our experiments we measured phosphorylation at this site in cells lacking RIPK1 kinase activity. Nevertheless, S14 was more efficiently phosphorylated in wt cells than in *Ripk1*$^{D138N/D138N}$ cells. This indicates that this site is likely not

exclusively an auto-phosphorylation site but also targeted by other kinases, whereas RIPK1 kinase activity might be partially required for its phosphorylation. In line with impaired enzymatic activity of RIPK1S166A, phosphorylation at this site in *Ripk1*$^{S166A/S166A}$ cells was decreased compared to wt cells. Taken together, our data suggest that auto-phosphorylation at S166 facilitates auto-phosphorylation at T169 and potentially at S14.

Previously, based on studies in in vitro systems, auto-phosphorylation at S161 was reported to be required and sufficient for binding of RIPK1 to FADD and RIPK3 and triggering of TNF-induced necroptosis (Zhang et al., 2017b). To our surprise, we were unable to detect auto-phosphorylation at S161 in wt BMDMs in response to a necroptotic stimulus by mass-spectrometric analysis. At the same time, we reliably measured the non-phosphorylated peptide harboring S161, suggesting that there was no technical problem with peptide detection. Furthermore, under the same experimental conditions, wt cells displayed robust phosphorylation at S166 and T169, showing that RIPK1 was catalytically active. Considering the generally rapid turnover rates of phosphorylation events, it seems unlikely that S161 would be phosphorylated at a significantly different timepoint than S166 and T169, arguing that likely failure to detect auto-phosphorylation at S161 was not owed to the timepoint. While in this study, auto-phosphorylation events were analyzed in BMDMs, Zhang et al used L929 cells. Therefore, a cell-type-specific function of S161 might explain our inability to detect S161 phosphorylation. On the other hand, this would be in contrast to the broad relevance observed for S166 over a range of different cell types and tissues in this study. Conclusively, our findings question the importance of auto-phosphorylation at S161 and studies addressing the function of this site by using phosphomimetic and non-phosphorylatable amino acid replacement in systems with endogenous RIPK1 levels will be needed to clarify whether auto-phosphorylation at S161 is physiologically relevant.

Taken together, according to our data, RIPK1 acts as a driver of kinase activity and is required for additional auto-phosphorylation at T169 and partially required for phosphorylation at S14. These results suggest a model in which in response to a cell death-inducing stimulus, initially low RIPK1 kinase activity leads to auto-phosphorylation at S166 (possibly driven by DD-induced homodimerization), which boosts RIPK1 kinase activity. RIPK1 then auto-phosphorylates at T169 and possibly S14. These phosphorylation events might finally impose the critical conformational changes in RIPK1 that allow for engagement of RIPK1 in cell death-inducing complexes and induction of cell death (Figure 34).

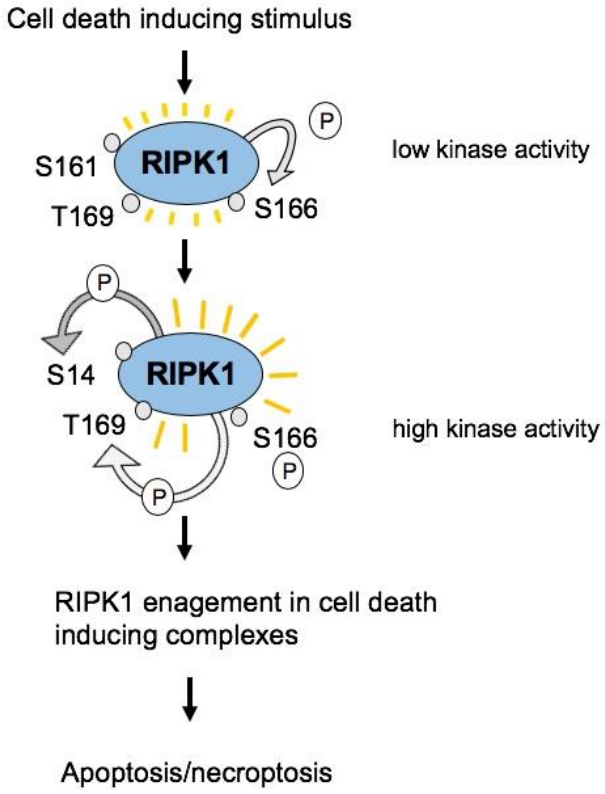

Figure 34: Model of RIPK1 kinase activation and cell death induction. In response to a cell death inducing stimulus, RIPK1 kinase activity reaches a critical threshold of activity (likely mediated by proximity-induced activation through DD-induced homodimerization; not shown) which allows for auto-phosphorylation at S166. Autophosphorylation at S166 then amplifies kinase activity and induces the auto-phosphorylation at other sites such as T169 and possibly also S14. These phosphorylation events might subsequently allow for the engagement of RIPK1 in cell death inducing complexes and the induction of apoptotic or necroptotic cell death. For matters of simplicity only single RIPK1 molecules are shown, however RIPK1 likely auto-phosphorylates in trans in a homodimer.

4.4 Autophosphorylation at S166 as a marker for RIPK1 kinase activation and possible clinical implications

A wide range of animal models of human pathologies have brought out RIPK1 as a promising therapeutic target. Whereas in mouse models of human disease the role of RIPK1 kinase activity in vivo can be relatively easily assessed by genetic or pharmacological inhibition of RIPK1 kinase activity, testing the pathological involvement in the human system is far more challenging. Assessment of benefits from RIPK1 inhibition in humans requires the evaluation of pharmaceutical targeting of RIPK1 in clinical studies, which are not only expensive, but may also be extremely lengthy. In order to obtain insight into the possible involvement of RIPK1 kinase activity in specific human pathologies, patient samples can be evaluated for the activity of RIPK1. The development of meaningful biomarkers in this context is especially important (Mifflin et al., 2020). RIPK1 auto-phosphorylation at S166 has been routinely used as a marker for RIPK1 activation in mice (Berger et al., 2014; Jaco et al., 2017; Ofengeim et al., 2015; Ofengeim et al., 2017; Patel et al., 2020) and has furthermore been applied to show RIPK1

activation in pathological human material from patients with diseases such as myocardial infarction (Oerlemans et al., 2012) or multiple sclerosis (Ofengeim et al., 2015). Importantly, auto-phosphorylation at S166 has previously been used a readout for testing of RIPK1 inhibitors in human PBMCs (Grievink et al., 2020), suggesting that human blood samples could be checked for presence of kinase-active RIPK1. Nevertheless, the physiological importance of auto-phosphorylation at S166 had previously remained unknown, hence also limiting its application as a marker in terms of interpretability regarding RIPK1's functional state. In light of our results, RIPK1 auto-phosphorylation at S166 should be interpreted as indicative of RIPK1 in a catalytically activated state, modified in a manner that we found essential for cell death-induction in-vivo and therefore "prone" to induce cell death. On the other hand, auto-phosphorylation at S166 per-se cannot be used as indicative of RIPK1 that acts as an inducer of cell death, as by itself this modification is not sufficient for cell death-induction.

Therefore, our results advance the knowledge on the functional context of p-S166 RIPK1 biomarker usage. Furthermore, our study supports the use of RIPK1 auto-phosphorylation at S166 as a marker of RIPK1 activation in general, which can help to identify patients in which RIPK1 inhibitors might be beneficial.

4.5 Outlook

In this study, we provide important insight into the role of RIPK1 auto-phosphorylation at S166 as a driver for its kinase activation that is essential for cell death and inflammation.

The mechanism of how RIPK1 kinase activity transmits the cell death-inducing stimulus on the other hand remain unknown. Our findings show that S166 auto-phosphorylation is important for auto-phosphorylation at other sites, indicating that these might be of mechanistic importance. It has been speculated that auto-phosphorylation induces conformational changes in RIPK1 that expose domains which are masked under catalytically inactive conditions (Newton, 2020). The RHIM domain is crucial for RIPK1 kinase activity-dependent RIPK1-RIPK3 amyloid formation for necroptosis induction (Cho et al., 2009; Li et al., 2012) and also an apoptosis-inducing complex II may involve a RIPK1-RIPK3 platform (Dondelinger et al., 2013). Therefore, it seems likely that RIPK1 kinase activity is required to sequentially auto-phosphorylate different sites on RIPK1 to induce conformational changes which exposes the RHIM domain for interaction with RIPK3. Alternatively, auto-phosphorylation might create other high-affinity docking sites that would be required for RIPK1 to interact in cell death-inducing complexes. In both these cases, auto-phosphorylation at specific residues by itself would provide the key trigger for cell death-induction. On the other hand, the possibility remains that RIPK1 phosphorylates a downstream target that is yet to be discovered, which might act as a cell death effector upon phosphorylation. In order to shed further light on the mechanism

of RIPK1 kinase activation and its cell death-inducing function, it will be important to determine the role of other auto-phosphorylation events. In this context, our finding that auto-phosphorylation at T169 relies on phosphorylation at S166 suggests that hierarchies between auto-phosphorylation events exist in which certain sites are more upstream or downstream than others in the process of cell death-induction. Additionally, autophosphorylation events in RIPK1 might function in a redundant manner, in line with the compensation for ablation of auto-phosphorylation at S166 in cell death induction that we observed in this study. Importantly, regarding the design of future studies, this study revealed discrepancies between in-vitro and in-vivo experiments. Considering the complex interplay between phosphorylation events that might underlay the role of RIPK1 kinase activity, these findings highlight the importance of the use of physiological models. The generation of mice containing different mutations of RIPK1 auto-phosphorylation sites, alone and in combination, therefore will be key to completely unravel the mechanism of RIPK1 kinase activation and cell death induction.

5. References

Adams, J.A. (2003). Activation loop phosphorylation and catalysis in protein kinases: is there functional evidence for the autoinhibitor model? Biochemistry *42*, 601-607.
Adolph, T.E., Tomczak, M.F., Niederreiter, L., Ko, H.J., Bock, J., Martinez-Naves, E., Glickman, J.N., Tschurtschenthaler, M., Hartwig, J., Hosomi, S.*, et al.* (2013). Paneth cells as a site of origin for intestinal inflammation. Nature *503*, 272-276.
Akira, S., and Takeda, K. (2004). Toll-like receptor signalling. Nat Rev Immunol *4*, 499-511.
Allen, T.D., and Potten, C.S. (1974). Fine-structural identification and organization of the epidermal proliferative unit. J Cell Sci *15*, 291-319.
Anderton, H., Bandala-Sanchez, E., Simpson, D.S., Rickard, J.A., Ng, A.P., Di Rago, L., Hall, C., Vince, J.E., Silke, J., Liccardi, G.*, et al.* (2019). RIPK1 prevents TRADD-driven, but TNFR1 independent, apoptosis during development. Cell Death Differ *26*, 877-889.
Annibaldi, A., Wicky John, S., Vanden Berghe, T., Swatek, K.N., Ruan, J., Liccardi, G., Bianchi, K., Elliott, P.R., Choi, S.M., Van Coillie, S.*, et al.* (2018). Ubiquitin-Mediated Regulation of RIPK1 Kinase Activity Independent of IKK and MK2. Mol Cell *69*, 566-580 e565.
Beenstock, J., Mooshayef, N., and Engelberg, D. (2016). How Do Protein Kinases Take a Selfie (Autophosphorylate)? Trends Biochem Sci *41*, 938-953.
Berger, S.B., Kasparcova, V., Hoffman, S., Swift, B., Dare, L., Schaeffer, M., Capriotti, C., Cook, M., Finger, J., Hughes-Earle, A.*, et al.* (2014). Cutting Edge: RIP1 kinase activity is dispensable for normal development but is a key regulator of inflammation in SHARPIN-deficient mice. J Immunol *192*, 5476-5480.
Bertrand, M.J., Milutinovic, S., Dickson, K.M., Ho, W.C., Boudreault, A., Durkin, J., Gillard, J.W., Jaquith, J.B., Morris, S.J., and Barker, P.A. (2008). cIAP1 and cIAP2 facilitate cancer cell survival by functioning as E3 ligases that promote RIP1 ubiquitination. Mol Cell *30*, 689-700.
Bone, R.C., Balk, R.A., Cerra, F.B., Dellinger, R.P., Fein, A.M., Knaus, W.A., Schein, R.M., and Sibbald, W.J. (1992). Definitions for sepsis and organ failure and guidelines for the use of innovative therapies in sepsis. The ACCP/SCCM Consensus Conference Committee. American College of Chest Physicians/Society of Critical Care Medicine. Chest *101*, 1644-1655.
Brummelkamp, T.R., Nijman, S.M., Dirac, A.M., and Bernards, R. (2003). Loss of the cylindromatosis tumour suppressor inhibits apoptosis by activating NF-kappaB. Nature *424*, 797-801.
Buchrieser, J., Oliva-Martin, M.J., Moore, M.D., Long, J.C.D., Cowley, S.A., Perez-Simon, J.A., James, W., and Venero, J.L. (2018). RIPK1 is a critical modulator of both tonic and TLR-responsive inflammatory and cell death pathways in human macrophage differentiation. Cell Death Dis *9*, 973.
Cai, Z., Jitkaew, S., Zhao, J., Chiang, H.C., Choksi, S., Liu, J., Ward, Y., Wu, L.G., and Liu, Z.G. (2014). Plasma membrane translocation of trimerized MLKL protein is required for TNF-induced necroptosis. Nat Cell Biol *16*, 55-65.
Cargnello, M., and Roux, P.P. (2011). Activation and function of the MAPKs and their substrates, the MAPK-activated protein kinases. Microbiol Mol Biol Rev *75*, 50-83.
Chang, D.W., Xing, Z., Capacio, V.L., Peter, M.E., and Yang, X. (2003). Interdimer processing mechanism of procaspase-8 activation. EMBO J *22*, 4132-4142.
Cho, Y.S., Challa, S., Moquin, D., Genga, R., Ray, T.D., Guildford, M., and Chan, F.K. (2009). Phosphorylation-driven assembly of the RIP1-RIP3 complex regulates programmed necrosis and virus-induced inflammation. Cell *137*, 1112-1123.
Clark, K., Nanda, S., and Cohen, P. (2013). Molecular control of the NEMO family of ubiquitin-binding proteins. Nat Rev Mol Cell Biol *14*, 673-685.
Cougnoux, A., Clifford, S., Salman, A., Ng, S.L., Bertin, J., and Porter, F.D. (2018). Necroptosis inhibition as a therapy for Niemann-Pick disease, type C1: Inhibition of RIP kinases and combination therapy with 2-hydroxypropyl-beta-cyclodextrin. Mol Genet Metab *125*, 345-350.

Cuchet-Lourenco, D., Eletto, D., Wu, C., Plagnol, V., Papapietro, O., Curtis, J., Ceron-Gutierrez, L., Bacon, C.M., Hackett, S., Alsaleem, B.*, et al.* (2018). Biallelic RIPK1 mutations in humans cause severe immunodeficiency, arthritis, and intestinal inflammation. Science *361*, 810-813.
Cusson-Hermance, N., Khurana, S., Lee, T.H., Fitzgerald, K.A., and Kelliher, M.A. (2005). Rip1 mediates the Trif-dependent toll-like receptor 3- and 4-induced NF-{kappa}B activation but does not contribute to interferon regulatory factor 3 activation. J Biol Chem *280*, 36560-36566.
Dannappel, M., Vlantis, K., Kumari, S., Polykratis, A., Kim, C., Wachsmuth, L., Eftychi, C., Lin, J., Corona, T., Hermance, N.*, et al.* (2014). RIPK1 maintains epithelial homeostasis by inhibiting apoptosis and necroptosis. Nature *513*, 90-94.
De, A., Dainichi, T., Rathinam, C.V., and Ghosh, S. (2014). The deubiquitinase activity of A20 is dispensable for NF-kappaB signaling. EMBO Rep *15*, 775-783.
de Almagro, M.C., Goncharov, T., Izrael-Tomasevic, A., Duttler, S., Kist, M., Varfolomeev, E., Wu, X., Lee, W.P., Murray, J., Webster, J.D.*, et al.* (2017). Coordinated ubiquitination and phosphorylation of RIP1 regulates necroptotic cell death. Cell Death Differ *24*, 26-37.
de Almagro, M.C., Goncharov, T., Newton, K., and Vucic, D. (2015). Cellular IAP proteins and LUBAC differentially regulate necrosome-associated RIP1 ubiquitination. Cell Death Dis *6*, e1800.
Degterev, A., Hitomi, J., Germscheid, M., Ch'en, I.L., Korkina, O., Teng, X., Abbott, D., Cuny, G.D., Yuan, C., Wagner, G.*, et al.* (2008). Identification of RIP1 kinase as a specific cellular target of necrostatins. Nat Chem Biol *4*, 313-321.
Degterev, A., Huang, Z., Boyce, M., Li, Y., Jagtap, P., Mizushima, N., Cuny, G.D., Mitchison, T.J., Moskowitz, M.A., and Yuan, J. (2005). Chemical inhibitor of nonapoptotic cell death with therapeutic potential for ischemic brain injury. Nat Chem Biol *1*, 112-119.
Degterev, A., Ofengeim, D., and Yuan, J. (2019). Targeting RIPK1 for the treatment of human diseases. Proc Natl Acad Sci U S A *116*, 9714-9722.
Dillon, C.P., Weinlich, R., Rodriguez, D.A., Cripps, J.G., Quarato, G., Gurung, P., Verbist, K.C., Brewer, T.L., Llambi, F., Gong, Y.N.*, et al.* (2014). RIPK1 blocks early postnatal lethality mediated by caspase-8 and RIPK3. Cell *157*, 1189-1202.
Dondelinger, Y., Aguileta, M.A., Goossens, V., Dubuisson, C., Grootjans, S., Dejardin, E., Vandenabeele, P., and Bertrand, M.J. (2013). RIPK3 contributes to TNFR1-mediated RIPK1 kinase-dependent apoptosis in conditions of cIAP1/2 depletion or TAK1 kinase inhibition. Cell Death Differ *20*, 1381-1392.
Dondelinger, Y., Declercq, W., Montessuit, S., Roelandt, R., Goncalves, A., Bruggeman, I., Hulpiau, P., Weber, K., Sehon, C.A., Marquis, R.W.*, et al.* (2014). MLKL compromises plasma membrane integrity by binding to phosphatidylinositol phosphates. Cell Rep *7*, 971-981.
Dondelinger, Y., Delanghe, T., Priem, D., Wynosky-Dolfi, M.A., Sorobetea, D., Rojas-Rivera, D., Giansanti, P., Roelandt, R., Gropengiesser, J., Ruckdeschel, K.*, et al.* (2019). Serine 25 phosphorylation inhibits RIPK1 kinase-dependent cell death in models of infection and inflammation. Nat Commun *10*, 1729.
Dondelinger, Y., Delanghe, T., Rojas-Rivera, D., Priem, D., Delvaeye, T., Bruggeman, I., Van Herreweghe, F., Vandenabeele, P., and Bertrand, M.J.M. (2017). MK2 phosphorylation of RIPK1 regulates TNF-mediated cell death. Nat Cell Biol *19*, 1237-1247.
Dondelinger, Y., Jouan-Lanhouet, S., Divert, T., Theatre, E., Bertin, J., Gough, P.J., Giansanti, P., Heck, A.J., Dejardin, E., Vandenabeele, P.*, et al.* (2015). NF-kappaB-Independent Role of IKKalpha/IKKbeta in Preventing RIPK1 Kinase-Dependent Apoptotic and Necroptotic Cell Death during TNF Signaling. Mol Cell *60*, 63-76.
Dowling, J.P., Alsabbagh, M., Del Casale, C., Liu, Z.G., and Zhang, J. (2019). TRADD regulates perinatal development and adulthood survival in mice lacking RIPK1 and RIPK3. Nat Commun *10*, 705.
Draber, P., Kupka, S., Reichert, M., Draberova, H., Lafont, E., de Miguel, D., Spilgies, L., Surinova, S., Taraborrelli, L., Hartwig, T.*, et al.* (2015). LUBAC-Recruited CYLD and A20 Regulate Gene Activation and Cell Death by Exerting Opposing Effects on Linear Ubiquitin in Signaling Complexes. Cell Rep *13*, 2258-2272.
Duprez, L., Takahashi, N., Van Hauwermeiren, F., Vandendriessche, B., Goossens, V., Vanden Berghe, T., Declercq, W., Libert, C., Cauwels, A., and Vandenabeele, P. (2011). RIP

kinase-dependent necrosis drives lethal systemic inflammatory response syndrome. Immunity *35*, 908-918.
Dynek, J.N., Goncharov, T., Dueber, E.C., Fedorova, A.V., Izrael-Tomasevic, A., Phu, L., Helgason, E., Fairbrother, W.J., Deshayes, K., Kirkpatrick, D.S.*, et al.* (2010). c-IAP1 and UbcH5 promote K11-linked polyubiquitination of RIP1 in TNF signalling. EMBO J *29*, 4198-4209.
Ea, C.K., Deng, L., Xia, Z.P., Pineda, G., and Chen, Z.J. (2006). Activation of IKK by TNFalpha requires site-specific ubiquitination of RIP1 and polyubiquitin binding by NEMO. Mol Cell *22*, 245-257.
Edgar, R., Domrachev, M., and Lash, A.E. (2002). Gene Expression Omnibus: NCBI gene expression and hybridization array data repository. Nucleic Acids Res *30*, 207-210.
Ehlken, H., Krishna-Subramanian, S., Ochoa-Callejero, L., Kondylis, V., Nadi, N.E., Straub, B.K., Schirmacher, P., Walczak, H., Kollias, G., and Pasparakis, M. (2014). Death receptor-independent FADD signalling triggers hepatitis and hepatocellular carcinoma in mice with liver parenchymal cell-specific NEMO knockout. Cell Death Differ *21*, 1721-1732.
Emmerich, C.H., Bakshi, S., Kelsall, I.R., Ortiz-Guerrero, J., Shpiro, N., and Cohen, P. (2016). Lys63/Met1-hybrid ubiquitin chains are commonly formed during the activation of innate immune signalling. Biochem Biophys Res Commun *474*, 452-461.
Enesa, K., Zakkar, M., Chaudhury, H., Luong le, A., Rawlinson, L., Mason, J.C., Haskard, D.O., Dean, J.L., and Evans, P.C. (2008). NF-kappaB suppression by the deubiquitinating enzyme Cezanne: a novel negative feedback loop in pro-inflammatory signaling. J Biol Chem *283*, 7036-7045.
Estornes, Y., Toscano, F., Virard, F., Jacquemin, G., Pierrot, A., Vanbervliet, B., Bonnin, M., Lalaoui, N., Mercier-Gouy, P., Pacheco, Y.*, et al.* (2012). dsRNA induces apoptosis through an atypical death complex associating TLR3 to caspase-8. Cell Death Differ *19*, 1482-1494.
Feng, L., Yin, Y.Y., Liu, C.H., Xu, K.R., Li, Q.R., Wu, J.R., and Zeng, R. (2020). Proteome-wide Data Analysis Reveals Tissue-specific Network Associated with SARS-CoV-2 Infection. J Mol Cell Biol.
Feoktistova, M., Geserick, P., Kellert, B., Dimitrova, D.P., Langlais, C., Hupe, M., Cain, K., MacFarlane, M., Hacker, G., and Leverkus, M. (2011). cIAPs block Ripoptosome formation, a RIP1/caspase-8 containing intracellular cell death complex differentially regulated by cFLIP isoforms. Mol Cell *43*, 449-463.
Fitzgerald, K.A., McWhirter, S.M., Faia, K.L., Rowe, D.C., Latz, E., Golenbock, D.T., Coyle, A.J., Liao, S.M., and Maniatis, T. (2003). IKKepsilon and TBK1 are essential components of the IRF3 signaling pathway. Nat Immunol *4*, 491-496.
Geng, J., Ito, Y., Shi, L., Amin, P., Chu, J., Ouchida, A.T., Mookhtiar, A.K., Zhao, H., Xu, D., Shan, B.*, et al.* (2017). Regulation of RIPK1 activation by TAK1-mediated phosphorylation dictates apoptosis and necroptosis. Nat Commun *8*, 359.
Gerlach, B., Cordier, S.M., Schmukle, A.C., Emmerich, C.H., Rieser, E., Haas, T.L., Webb, A.I., Rickard, J.A., Anderton, H., Wong, W.W.*, et al.* (2011). Linear ubiquitination prevents inflammation and regulates immune signalling. Nature *471*, 591-596.
Gijbels, M.J., Zurcher, C., Kraal, G., Elliott, G.R., HogenEsch, H., Schijff, G., Savelkoul, H.F., and Bruijnzeel, P.L. (1996). Pathogenesis of skin lesions in mice with chronic proliferative dermatitis (cpdm/cpdm). Am J Pathol *148*, 941-950.
Green, D.R. (2019). The Coming Decade of Cell Death Research: Five Riddles. Cell *177*, 1094-1107.
Grievink, H.W., Heuberger, J., Huang, F., Chaudhary, R., Birkhoff, W.A.J., Tonn, G.R., Mosesova, S., Erickson, R., Moerland, M., Haddick, P.C.G.*, et al.* (2020). DNL104, a Centrally Penetrant RIPK1 Inhibitor, Inhibits RIP1 Kinase Phosphorylation in a Randomized Phase I Ascending Dose Study in Healthy Volunteers. Clin Pharmacol Ther *107*, 406-414.
Haas, T.L., Emmerich, C.H., Gerlach, B., Schmukle, A.C., Cordier, S.M., Rieser, E., Feltham, R., Vince, J., Warnken, U., Wenger, T.*, et al.* (2009). Recruitment of the linear ubiquitin chain assembly complex stabilizes the TNF-R1 signaling complex and is required for TNF-mediated gene induction. Mol Cell *36*, 831-844.
Harris, P.A., Berger, S.B., Jeong, J.U., Nagilla, R., Bandyopadhyay, D., Campobasso, N., Capriotti, C.A., Cox, J.A., Dare, L., Dong, X.*, et al.* (2017). Discovery of a First-in-Class

Receptor Interacting Protein 1 (RIP1) Kinase Specific Clinical Candidate (GSK2982772) for the Treatment of Inflammatory Diseases. J Med Chem *60*, 1247-1261.
Hayden, M.S., and Ghosh, S. (2014). Regulation of NF-kappaB by TNF family cytokines. Semin Immunol *26*, 253-266.
He, S., Liang, Y., Shao, F., and Wang, X. (2011). Toll-like receptors activate programmed necrosis in macrophages through a receptor-interacting kinase-3-mediated pathway. Proc Natl Acad Sci U S A *108*, 20054-20059.
He, S., Wang, L., Miao, L., Wang, T., Du, F., Zhao, L., and Wang, X. (2009). Receptor interacting protein kinase-3 determines cellular necrotic response to TNF-alpha. Cell *137*, 1100-1111.
Heger, K., Wickliffe, K.E., Ndoja, A., Zhang, J., Murthy, A., Dugger, D.L., Maltzman, A., de Sousa, E.M.F., Hung, J., Zeng, Y.*, et al.* (2018). OTULIN limits cell death and inflammation by deubiquitinating LUBAC. Nature *559*, 120-124.
Hemmi, H., Takeuchi, O., Sato, S., Yamamoto, M., Kaisho, T., Sanjo, H., Kawai, T., Hoshino, K., Takeda, K., and Akira, S. (2004). The roles of two IkappaB kinase-related kinases in lipopolysaccharide and double stranded RNA signaling and viral infection. J Exp Med *199*, 1641-1650.
HogenEsch, H., Janke, S., Boggess, D., and Sundberg, J.P. (1999). Absence of Peyer's patches and abnormal lymphoid architecture in chronic proliferative dermatitis (cpdm/cpdm) mice. J Immunol *162*, 3890-3896.
Hsu, H., Huang, J., Shu, H.B., Baichwal, V., and Goeddel, D.V. (1996). TNF-dependent recruitment of the protein kinase RIP to the TNF receptor-1 signaling complex. Immunity *4*, 387-396.
Hsu, H., Xiong, J., and Goeddel, D.V. (1995). The TNF receptor 1-associated protein TRADD signals cell death and NF-kappa B activation. Cell *81*, 495-504.
Huang, D., Zheng, X., Wang, Z.A., Chen, X., He, W.T., Zhang, Y., Xu, J.G., Zhao, H., Shi, W., Wang, X.*, et al.* (2017). The MLKL Channel in Necroptosis Is an Octamer Formed by Tetramers in a Dyadic Process. Mol Cell Biol *37*.
Hughes, M.A., Harper, N., Butterworth, M., Cain, K., Cohen, G.M., and MacFarlane, M. (2009). Reconstitution of the death-inducing signaling complex reveals a substrate switch that determines CD95-mediated death or survival. Mol Cell *35*, 265-279.
Hughes, M.A., Powley, I.R., Jukes-Jones, R., Horn, S., Feoktistova, M., Fairall, L., Schwabe, J.W., Leverkus, M., Cain, K., and MacFarlane, M. (2016). Co-operative and Hierarchical Binding of c-FLIP and Caspase-8: A Unified Model Defines How c-FLIP Isoforms Differentially Control Cell Fate. Mol Cell *61*, 834-849.
Huse, M., and Kuriyan, J. (2002). The conformational plasticity of protein kinases. Cell *109*, 275-282.
Iannielli, A., Bido, S., Folladori, L., Segnali, A., Cancellieri, C., Maresca, A., Massimino, L., Rubio, A., Morabito, G., Caporali, L.*, et al.* (2018). Pharmacological Inhibition of Necroptosis Protects from Dopaminergic Neuronal Cell Death in Parkinson's Disease Models. Cell Rep *22*, 2066-2079.
Ingram, J.P., Thapa, R.J., Fisher, A., Tummers, B., Zhang, T., Yin, C., Rodriguez, D.A., Guo, H., Lane, R., Williams, R.*, et al.* (2019). ZBP1/DAI Drives RIPK3-Mediated Cell Death Induced by IFNs in the Absence of RIPK1. J Immunol *203*, 1348-1355.
Ito, Y., Ofengeim, D., Najafov, A., Das, S., Saberi, S., Li, Y., Hitomi, J., Zhu, H., Chen, H., Mayo, L.*, et al.* (2016). RIPK1 mediates axonal degeneration by promoting inflammation and necroptosis in ALS. Science *353*, 603-608.
Jaco, I., Annibaldi, A., Lalaoui, N., Wilson, R., Tenev, T., Laurien, L., Kim, C., Jamal, K., Wicky John, S., Liccardi, G.*, et al.* (2017). MK2 Phosphorylates RIPK1 to Prevent TNF-Induced Cell Death. Mol Cell *66*, 698-710 e695.
Jiang, Z., Mak, T.W., Sen, G., and Li, X. (2004). Toll-like receptor 3-mediated activation of NF-kappaB and IRF3 diverges at Toll-IL-1 receptor domain-containing adapter inducing IFN-beta. Proc Natl Acad Sci U S A *101*, 3533-3538.
Jinek, M., Chylinski, K., Fonfara, I., Hauer, M., Doudna, J.A., and Charpentier, E. (2012). A programmable dual-RNA-guided DNA endonuclease in adaptive bacterial immunity. Science *337*, 816-821.

Kaiser, W.J., Daley-Bauer, L.P., Thapa, R.J., Mandal, P., Berger, S.B., Huang, C., Sundararajan, A., Guo, H., Roback, L., Speck, S.H.*, et al.* (2014). RIP1 suppresses innate immune necrotic as well as apoptotic cell death during mammalian parturition. Proc Natl Acad Sci U S A *111*, 7753-7758.
Kaiser, W.J., Sridharan, H., Huang, C., Mandal, P., Upton, J.W., Gough, P.J., Sehon, C.A., Marquis, R.W., Bertin, J., and Mocarski, E.S. (2013). Toll-like receptor 3-mediated necrosis via TRIF, RIP3, and MLKL. J Biol Chem *288*, 31268-31279.
Kaiser, W.J., Upton, J.W., and Mocarski, E.S. (2008). Receptor-interacting protein homotypic interaction motif-dependent control of NF-kappa B activation via the DNA-dependent activator of IFN regulatory factors. J Immunol *181*, 6427-6434.
Kanayama, A., Seth, R.B., Sun, L., Ea, C.K., Hong, M., Shaito, A., Chiu, Y.H., Deng, L., and Chen, Z.J. (2004). TAB2 and TAB3 activate the NF-kappaB pathway through binding to polyubiquitin chains. Mol Cell *15*, 535-548.
Kellendonk, C., Opherk, C., Anlag, K., Schutz, G., and Tronche, F. (2000). Hepatocyte-specific expression of Cre recombinase. Genesis *26*, 151-153.
Kelliher, M.A., Grimm, S., Ishida, Y., Kuo, F., Stanger, B.Z., and Leder, P. (1998). The death domain kinase RIP mediates the TNF-induced NF-kappaB signal. Immunity *8*, 297-303.
Kerr, J.F., Wyllie, A.H., and Currie, A.R. (1972). Apoptosis: a basic biological phenomenon with wide-ranging implications in tissue kinetics. Br J Cancer *26*, 239-257.
Kondylis, V., and Pasparakis, M. (2019). RIP Kinases in Liver Cell Death, Inflammation and Cancer. Trends Mol Med *25*, 47-63.
Kondylis, V., Polykratis, A., Ehlken, H., Ochoa-Callejero, L., Straub, B.K., Krishna-Subramanian, S., Van, T.M., Curth, H.M., Heise, N., Weih, F.*, et al.* (2015a). NEMO Prevents Steatohepatitis and Hepatocellular Carcinoma by Inhibiting RIPK1 Kinase Activity-Mediated Hepatocyte Apoptosis. Cancer Cell *28*, 582-598.
Kondylis, V., Polykratis, A., Ehlken, H., Ochoa-Callejero, L., Straub, B.K., Krishna-Subramanian, S., Van, T.M., Curth, H.M., Heise, N., Weih, F.*, et al.* (2015b). NEMO Prevents Steatohepatitis and Hepatocellular Carcinoma by Inhibiting RIPK1 Kinase Activity-Mediated Hepatocyte Apoptosis. Cancer Cell *28*, 830.
Koudstaal, S., Oerlemans, M.I., Van der Spoel, T.I., Janssen, A.W., Hoefer, I.E., Doevendans, P.A., Sluijter, J.P., and Chamuleau, S.A. (2015). Necrostatin-1 alleviates reperfusion injury following acute myocardial infarction in pigs. Eur J Clin Invest *45*, 150-159.
Kovalenko, A., Chable-Bessia, C., Cantarella, G., Israel, A., Wallach, D., and Courtois, G. (2003). The tumour suppressor CYLD negatively regulates NF-kappaB signalling by deubiquitination. Nature *424*, 801-805.
Krysko, D.V., Garg, A.D., Kaczmarek, A., Krysko, O., Agostinis, P., and Vandenabeele, P. (2012). Immunogenic cell death and DAMPs in cancer therapy. Nat Rev Cancer *12*, 860-875.
Kumar, H., Kawai, T., and Akira, S. (2011). Pathogen recognition by the innate immune system. Int Rev Immunol *30*, 16-34.
Kumari, S., Redouane, Y., Lopez-Mosqueda, J., Shiraishi, R., Romanowska, M., Lutzmayer, S., Kuiper, J., Martinez, C., Dikic, I., Pasparakis, M.*, et al.* (2014). Sharpin prevents skin inflammation by inhibiting TNFR1-induced keratinocyte apoptosis. Elife *3*.
Kupka, S., De Miguel, D., Draber, P., Martino, L., Surinova, S., Rittinger, K., and Walczak, H. (2016). SPATA2-Mediated Binding of CYLD to HOIP Enables CYLD Recruitment to Signaling Complexes. Cell Rep *16*, 2271-2280.
Lafont, E., Draber, P., Rieser, E., Reichert, M., Kupka, S., de Miguel, D., Draberova, H., von Massenhausen, A., Bhamra, A., Henderson, S.*, et al.* (2018). TBK1 and IKKepsilon prevent TNF-induced cell death by RIPK1 phosphorylation. Nat Cell Biol *20*, 1389-1399.
Lalaoui, N., Boyden, S.E., Oda, H., Wood, G.M., Stone, D.L., Chau, D., Liu, L., Stoffels, M., Kratina, T., Lawlor, K.E.*, et al.* (2020). Mutations that prevent caspase cleavage of RIPK1 cause autoinflammatory disease. Nature *577*, 103-108.
Lee, T.H., Shank, J., Cusson, N., and Kelliher, M.A. (2004). The kinase activity of Rip1 is not required for tumor necrosis factor-alpha-induced IkappaB kinase or p38 MAP kinase activation or for the ubiquitination of Rip1 by Traf2. J Biol Chem *279*, 33185-33191.

Legarda-Addison, D., Hase, H., O'Donnell, M.A., and Ting, A.T. (2009). NEMO/IKKgamma regulates an early NF-kappaB-independent cell-death checkpoint during TNF signaling. Cell Death Differ *16*, 1279-1288.
Legrand, A.J., Konstantinou, M., Goode, E.F., and Meier, P. (2019). The Diversification of Cell Death and Immunity: Memento Mori. Mol Cell *76*, 232-242.
Li, H., Kobayashi, M., Blonska, M., You, Y., and Lin, X. (2006). Ubiquitination of RIP is required for tumor necrosis factor alpha-induced NF-kappaB activation. J Biol Chem *281*, 13636-13643.
Li, J., McQuade, T., Siemer, A.B., Napetschnig, J., Moriwaki, K., Hsiao, Y.S., Damko, E., Moquin, D., Walz, T., McDermott, A.*, et al.* (2012). The RIP1/RIP3 necrosome forms a functional amyloid signaling complex required for programmed necrosis. Cell *150*, 339-350.
Li, Y., Fuhrer, M., Bahrami, E., Socha, P., Klaudel-Dreszler, M., Bouzidi, A., Liu, Y., Lehle, A.S., Magg, T., Hollizeck, S.*, et al.* (2019). Human RIPK1 deficiency causes combined immunodeficiency and inflammatory bowel diseases. Proc Natl Acad Sci U S A *116*, 970-975.
Liedtke, C., Bangen, J.M., Freimuth, J., Beraza, N., Lambertz, D., Cubero, F.J., Hatting, M., Karlmark, K.R., Streetz, K.L., Krombach, G.A.*, et al.* (2011). Loss of caspase-8 protects mice against inflammation-related hepatocarcinogenesis but induces non-apoptotic liver injury. Gastroenterology *141*, 2176-2187.
Lin, J., Kumari, S., Kim, C., Van, T.M., Wachsmuth, L., Polykratis, A., and Pasparakis, M. (2016). RIPK1 counteracts ZBP1-mediated necroptosis to inhibit inflammation. Nature *540*, 124-128.
Lin, Y., Devin, A., Rodriguez, Y., and Liu, Z.G. (1999). Cleavage of the death domain kinase RIP by caspase-8 prompts TNF-induced apoptosis. Genes Dev *13*, 2514-2526.
Linkermann, A., Brasen, J.H., Himmerkus, N., Liu, S., Huber, T.B., Kunzendorf, U., and Krautwald, S. (2012). Rip1 (receptor-interacting protein kinase 1) mediates necroptosis and contributes to renal ischemia/reperfusion injury. Kidney Int *81*, 751-761.
Liu, S., Zhang, H., and Duan, E. (2013). Epidermal development in mammals: key regulators, signals from beneath, and stem cells. Int J Mol Sci *14*, 10869-10895.
Liu, Y., Fan, C., Zhang, Y., Yu, X., Wu, X., Zhang, X., Zhao, Q., Zhang, H., Xie, Q., Li, M.*, et al.* (2017). RIP1 kinase activity-dependent roles in embryonic development of Fadd-deficient mice. Cell Death Differ *24*, 1459-1469.
Luedde, T., Beraza, N., Kotsikoris, V., van Loo, G., Nenci, A., De Vos, R., Roskams, T., Trautwein, C., and Pasparakis, M. (2007). Deletion of NEMO/IKKgamma in liver parenchymal cells causes steatohepatitis and hepatocellular carcinoma. Cancer Cell *11*, 119-132.
Luedde, T., Kaplowitz, N., and Schwabe, R.F. (2014). Cell death and cell death responses in liver disease: mechanisms and clinical relevance. Gastroenterology *147*, 765-783 e764.
Madison, B.B., Dunbar, L., Qiao, X.T., Braunstein, K., Braunstein, E., and Gumucio, D.L. (2002). Cis elements of the villin gene control expression in restricted domains of the vertical (crypt) and horizontal (duodenum, cecum) axes of the intestine. J Biol Chem *277*, 33275-33283.
Mahoney, D.J., Cheung, H.H., Mrad, R.L., Plenchette, S., Simard, C., Enwere, E., Arora, V., Mak, T.W., Lacasse, E.C., Waring, J.*, et al.* (2008). Both cIAP1 and cIAP2 regulate TNFalpha-mediated NF-kappaB activation. Proc Natl Acad Sci U S A *105*, 11778-11783.
Martens, S., Hofmans, S., Declercq, W., Augustyns, K., and Vandenabeele, P. (2020). Inhibitors Targeting RIPK1/RIPK3: Old and New Drugs. Trends Pharmacol Sci *41*, 209-224.
McQuade, T., Cho, Y., and Chan, F.K. (2013). Positive and negative phosphorylation regulates RIP1- and RIP3-induced programmed necrosis. Biochem J *456*, 409-415.
Meng, H., Liu, Z., Li, X., Wang, H., Jin, T., Wu, G., Shan, B., Christofferson, D.E., Qi, C., Yu, Q.*, et al.* (2018). Death-domain dimerization-mediated activation of RIPK1 controls necroptosis and RIPK1-dependent apoptosis. Proc Natl Acad Sci U S A *115*, E2001-E2009.
Menon, M.B., Gropengiesser, J., Fischer, J., Novikova, L., Deuretzbacher, A., Lafera, J., Schimmeck, H., Czymmeck, N., Ronkina, N., Kotlyarov, A.*, et al.* (2017). p38(MAPK)/MK2-dependent phosphorylation controls cytotoxic RIPK1 signalling in inflammation and infection. Nat Cell Biol *19*, 1248-1259.
Meylan, E., Burns, K., Hofmann, K., Blancheteau, V., Martinon, F., Kelliher, M., and Tschopp, J. (2004). RIP1 is an essential mediator of Toll-like receptor 3-induced NF-kappa B activation. Nat Immunol *5*, 503-507.

Micheau, O., and Tschopp, J. (2003). Induction of TNF receptor I-mediated apoptosis via two sequential signaling complexes. Cell *114*, 181-190.
Mifflin, L., Ofengeim, D., and Yuan, J. (2020). Receptor-interacting protein kinase 1 (RIPK1) as a therapeutic target. Nat Rev Drug Discov *19*, 553-571.
Newton, K. (2020). Multitasking Kinase RIPK1 Regulates Cell Death and Inflammation. Cold Spring Harb Perspect Biol *12*.
Newton, K., Dugger, D.L., Maltzman, A., Greve, J.M., Hedehus, M., Martin-McNulty, B., Carano, R.A., Cao, T.C., van Bruggen, N., Bernstein, L.*, et al.* (2016a). RIPK3 deficiency or catalytically inactive RIPK1 provides greater benefit than MLKL deficiency in mouse models of inflammation and tissue injury. Cell Death Differ *23*, 1565-1576.
Newton, K., Dugger, D.L., Wickliffe, K.E., Kapoor, N., de Almagro, M.C., Vucic, D., Komuves, L., Ferrando, R.E., French, D.M., Webster, J.*, et al.* (2014). Activity of protein kinase RIPK3 determines whether cells die by necroptosis or apoptosis. Science *343*, 1357-1360.
Newton, K., Wickliffe, K.E., Dugger, D.L., Maltzman, A., Roose-Girma, M., Dohse, M., Komuves, L., Webster, J.D., and Dixit, V.M. (2019). Cleavage of RIPK1 by caspase-8 is crucial for limiting apoptosis and necroptosis. Nature *574*, 428-431.
Newton, K., Wickliffe, K.E., Maltzman, A., Dugger, D.L., Strasser, A., Pham, V.C., Lill, J.R., Roose-Girma, M., Warming, S., Solon, M.*, et al.* (2016b). RIPK1 inhibits ZBP1-driven necroptosis during development. Nature *540*, 129-133.
Nolte, H., MacVicar, T.D., Tellkamp, F., and Kruger, M. (2018). Instant Clue: A Software Suite for Interactive Data Visualization and Analysis. Sci Rep *8*, 12648.
O'Donnell, J.A., Lehman, J., Roderick, J.E., Martinez-Marin, D., Zelic, M., Doran, C., Hermance, N., Lyle, S., Pasparakis, M., Fitzgerald, K.A.*, et al.* (2018). Dendritic Cell RIPK1 Maintains Immune Homeostasis by Preventing Inflammation and Autoimmunity. J Immunol *200*, 737-748.
O'Donnell, M.A., Legarda-Addison, D., Skountzos, P., Yeh, W.C., and Ting, A.T. (2007). Ubiquitination of RIP1 regulates an NF-kappaB-independent cell-death switch in TNF signaling. Curr Biol *17*, 418-424.
Oerlemans, M.I., Liu, J., Arslan, F., den Ouden, K., van Middelaar, B.J., Doevendans, P.A., and Sluijter, J.P. (2012). Inhibition of RIP1-dependent necrosis prevents adverse cardiac remodeling after myocardial ischemia-reperfusion in vivo. Basic Res Cardiol *107*, 270.
Ofengeim, D., Ito, Y., Najafov, A., Zhang, Y., Shan, B., DeWitt, J.P., Ye, J., Zhang, X., Chang, A., Vakifahmetoglu-Norberg, H.*, et al.* (2015). Activation of necroptosis in multiple sclerosis. Cell Rep *10*, 1836-1849.
Ofengeim, D., Mazzitelli, S., Ito, Y., DeWitt, J.P., Mifflin, L., Zou, C., Das, S., Adiconis, X., Chen, H., Zhu, H.*, et al.* (2017). RIPK1 mediates a disease-associated microglial response in Alzheimer's disease. Proc Natl Acad Sci U S A *114*, E8788-E8797.
Orozco, S., Yatim, N., Werner, M.R., Tran, H., Gunja, S.Y., Tait, S.W., Albert, M.L., Green, D.R., and Oberst, A. (2014). RIPK1 both positively and negatively regulates RIPK3 oligomerization and necroptosis. Cell Death Differ *21*, 1511-1521.
Paquette, N., Conlon, J., Sweet, C., Rus, F., Wilson, L., Pereira, A., Rosadini, C.V., Goutagny, N., Weber, A.N., Lane, W.S.*, et al.* (2012). Serine/threonine acetylation of TGFbeta-activated kinase (TAK1) by Yersinia pestis YopJ inhibits innate immune signaling. Proc Natl Acad Sci U S A *109*, 12710-12715.
Park, H.S., Liu, G., Liu, Q., and Zhou, Y. (2018). Swine Influenza Virus Induces RIPK1/DRP1-Mediated Interleukin-1 Beta Production. Viruses *10*.
Park, Y.H., Jeong, M.S., Park, H.H., and Jang, S.B. (2013). Formation of the death domain complex between FADD and RIP1 proteins in vitro. Biochim Biophys Acta *1834*, 292-300.
Pasparakis, M., and Vandenabeele, P. (2015). Necroptosis and its role in inflammation. Nature *517*, 311-320.
Patel, S., Webster, J.D., Varfolomeev, E., Kwon, Y.C., Cheng, J.H., Zhang, J., Dugger, D.L., Wickliffe, K.E., Maltzman, A., Sujatha-Bhaskar, S.*, et al.* (2020). RIP1 inhibition blocks inflammatory diseases but not tumor growth or metastases. Cell Death Differ *27*, 161-175.
Peltzer, N., Darding, M., and Walczak, H. (2016). Holding RIPK1 on the Ubiquitin Leash in TNFR1 Signaling. Trends Cell Biol *26*, 445-461.

Peltzer, N., Rieser, E., Taraborrelli, L., Draber, P., Darding, M., Pernaute, B., Shimizu, Y., Sarr, A., Draberova, H., Montinaro, A.*, et al.* (2014). HOIP deficiency causes embryonic lethality by aberrant TNFR1-mediated endothelial cell death. Cell Rep *9*, 153-165.
Peltzer, N., and Walczak, H. (2019). Cell Death and Inflammation - A Vital but Dangerous Liaison. Trends Immunol *40*, 387-402.
Perez-Riverol, Y., Csordas, A., Bai, J., Bernal-Llinares, M., Hewapathirana, S., Kundu, D.J., Inuganti, A., Griss, J., Mayer, G., Eisenacher, M.*, et al.* (2019). The PRIDE database and related tools and resources in 2019: improving support for quantification data. Nucleic Acids Res *47*, D442-D450.
Peterson, L.W., Philip, N.H., DeLaney, A., Wynosky-Dolfi, M.A., Asklof, K., Gray, F., Choa, R., Bjanes, E., Buza, E.L., Hu, B.*, et al.* (2017). RIPK1-dependent apoptosis bypasses pathogen blockade of innate signaling to promote immune defense. J Exp Med *214*, 3171-3182.
Petrie, E.J., Sandow, J.J., Jacobsen, A.V., Smith, B.J., Griffin, M.D.W., Lucet, I.S., Dai, W., Young, S.N., Tanzer, M.C., Wardak, A.*, et al.* (2018). Conformational switching of the pseudokinase domain promotes human MLKL tetramerization and cell death by necroptosis. Nat Commun *9*, 2422.
Pfeffer, K., Matsuyama, T., Kundig, T.M., Wakeham, A., Kishihara, K., Shahinian, A., Wiegmann, K., Ohashi, P.S., Kronke, M., and Mak, T.W. (1993). Mice deficient for the 55 kd tumor necrosis factor receptor are resistant to endotoxic shock, yet succumb to L. monocytogenes infection. Cell *73*, 457-467.
Pobezinskaya, Y.L., Kim, Y.S., Choksi, S., Morgan, M.J., Li, T., Liu, C., and Liu, Z. (2008). The function of TRADD in signaling through tumor necrosis factor receptor 1 and TRIF-dependent Toll-like receptors. Nat Immunol *9*, 1047-1054.
Polykratis, A., Hermance, N., Zelic, M., Roderick, J., Kim, C., Van, T.M., Lee, T.H., Chan, F.K.M., Pasparakis, M., and Kelliher, M.A. (2014). Cutting edge: RIPK1 Kinase inactive mice are viable and protected from TNF-induced necroptosis in vivo. J Immunol *193*, 1539-1543.
Polykratis, A., Martens, A., Eren, R.O., Shirasaki, Y., Yamagishi, M., Yamaguchi, Y., Uemura, S., Miura, M., Holzmann, B., Kollias, G.*, et al.* (2019). A20 prevents inflammasome-dependent arthritis by inhibiting macrophage necroptosis through its ZnF7 ubiquitin-binding domain. Nat Cell Biol *21*, 731-742.
Priem, D., Devos, M., Druwe, S., Martens, A., Slowicka, K., Ting, A.T., Pasparakis, M., Declercq, W., Vandenabeele, P., van Loo, G.*, et al.* (2019). A20 protects cells from TNF-induced apoptosis through linear ubiquitin-dependent and -independent mechanisms. Cell Death Dis *10*, 692.
Rahighi, S., Ikeda, F., Kawasaki, M., Akutsu, M., Suzuki, N., Kato, R., Kensche, T., Uejima, T., Bloor, S., Komander, D.*, et al.* (2009). Specific recognition of linear ubiquitin chains by NEMO is important for NF-kappaB activation. Cell *136*, 1098-1109.
Reddick, L.E., and Alto, N.M. (2014). Bacteria fighting back: how pathogens target and subvert the host innate immune system. Mol Cell *54*, 321-328.
Rickard, J.A., Anderton, H., Etemadi, N., Nachbur, U., Darding, M., Peltzer, N., Lalaoui, N., Lawlor, K.E., Vanyai, H., Hall, C.*, et al.* (2014a). TNFR1-dependent cell death drives inflammation in Sharpin-deficient mice. Elife *3*.
Rickard, J.A., O'Donnell, J.A., Evans, J.M., Lalaoui, N., Poh, A.R., Rogers, T., Vince, J.E., Lawlor, K.E., Ninnis, R.L., Anderton, H.*, et al.* (2014b). RIPK1 regulates RIPK3-MLKL-driven systemic inflammation and emergency hematopoiesis. Cell *157*, 1175-1188.
Robinson, N., McComb, S., Mulligan, R., Dudani, R., Krishnan, L., and Sad, S. (2012). Type I interferon induces necroptosis in macrophages during infection with Salmonella enterica serovar Typhimurium. Nat Immunol *13*, 954-962.
Roderick, J.E., Hermance, N., Zelic, M., Simmons, M.J., Polykratis, A., Pasparakis, M., and Kelliher, M.A. (2014). Hematopoietic RIPK1 deficiency results in bone marrow failure caused by apoptosis and RIPK3-mediated necroptosis. Proc Natl Acad Sci U S A *111*, 14436-14441.
Salvesen, G.S., and Dixit, V.M. (1999). Caspase activation: the induced-proximity model. Proc Natl Acad Sci U S A *96*, 10964-10967.
Sato, S., Sanjo, H., Takeda, K., Ninomiya-Tsuji, J., Yamamoto, M., Kawai, T., Matsumoto, K., Takeuchi, O., and Akira, S. (2005). Essential function for the kinase TAK1 in innate and adaptive immune responses. Nat Immunol *6*, 1087-1095.

Sato, S., Sugiyama, M., Yamamoto, M., Watanabe, Y., Kawai, T., Takeda, K., and Akira, S. (2003). Toll/IL-1 receptor domain-containing adaptor inducing IFN-beta (TRIF) associates with TNF receptor-associated factor 6 and TANK-binding kinase 1, and activates two distinct transcription factors, NF-kappa B and IFN-regulatory factor-3, in the Toll-like receptor signaling. J Immunol *171*, 4304-4310.
Schaeffer, V., Akutsu, M., Olma, M.H., Gomes, L.C., Kawasaki, M., and Dikic, I. (2014). Binding of OTULIN to the PUB domain of HOIP controls NF-kappaB signaling. Mol Cell *54*, 349-361.
Scheidereit, C. (2006). IkappaB kinase complexes: gateways to NF-kappaB activation and transcription. Oncogene *25*, 6685-6705.
Schmidt-Supprian, M., Bloch, W., Courtois, G., Addicks, K., Israel, A., Rajewsky, K., and Pasparakis, M. (2000). NEMO/IKK gamma-deficient mice model incontinentia pigmenti. Mol Cell *5*, 981-992.
Seifert, L., Werba, G., Tiwari, S., Giao Ly, N.N., Alothman, S., Alqunaibit, D., Avanzi, A., Barilla, R., Daley, D., Greco, S.H.*, et al.* (2016). The necrosome promotes pancreatic oncogenesis via CXCL1 and Mincle-induced immune suppression. Nature *532*, 245-249.
Seymour, R.E., Hasham, M.G., Cox, G.A., Shultz, L.D., Hogenesch, H., Roopenian, D.C., and Sundberg, J.P. (2007). Spontaneous mutations in the mouse Sharpin gene result in multiorgan inflammation, immune system dysregulation and dermatitis. Genes Immun *8*, 416-421.
Shalini, S., Dorstyn, L., Dawar, S., and Kumar, S. (2015). Old, new and emerging functions of caspases. Cell Death Differ *22*, 526-539.
Sheridan, C. (2019). Death by inflammation: drug makers chase the master controller. Nat Biotechnol *37*, 111-113.
Shu, H.B., Takeuchi, M., and Goeddel, D.V. (1996). The tumor necrosis factor receptor 2 signal transducers TRAF2 and c-IAP1 are components of the tumor necrosis factor receptor 1 signaling complex. Proc Natl Acad Sci U S A *93*, 13973-13978.
Shutinoski, B., Alturki, N.A., Rijal, D., Bertin, J., Gough, P.J., Schlossmacher, M.G., and Sad, S. (2016). K45A mutation of RIPK1 results in poor necroptosis and cytokine signaling in macrophages, which impacts inflammatory responses in vivo. Cell Death Differ *23*, 1628-1637.
Sun, L., Wang, H., Wang, Z., He, S., Chen, S., Liao, D., Wang, L., Yan, J., Liu, W., Lei, X.*, et al.* (2012). Mixed lineage kinase domain-like protein mediates necrosis signaling downstream of RIP3 kinase. Cell *148*, 213-227.
Sun, X., Yin, J., Starovasnik, M.A., Fairbrother, W.J., and Dixit, V.M. (2002). Identification of a novel homotypic interaction motif required for the phosphorylation of receptor-interacting protein (RIP) by RIP3. J Biol Chem *277*, 9505-9511.
Takahashi, N., Duprez, L., Grootjans, S., Cauwels, A., Nerinckx, W., DuHadaway, J.B., Goossens, V., Roelandt, R., Van Hauwermeiren, F., Libert, C.*, et al.* (2012). Necrostatin-1 analogues: critical issues on the specificity, activity and in vivo use in experimental disease models. Cell Death Dis *3*, e437.
Takahashi, N., Vereecke, L., Bertrand, M.J., Duprez, L., Berger, S.B., Divert, T., Goncalves, A., Sze, M., Gilbert, B., Kourula, S.*, et al.* (2014). RIPK1 ensures intestinal homeostasis by protecting the epithelium against apoptosis. Nature *513*, 95-99.
Takeuchi, O., and Akira, S. (2010). Pattern recognition receptors and inflammation. Cell *140*, 805-820.
Tang, Y., Tu, H., Zhang, J., Zhao, X., Wang, Y., Qin, J., and Lin, X. (2019). K63-linked ubiquitination regulates RIPK1 kinase activity to prevent cell death during embryogenesis and inflammation. Nat Commun *10*, 4157.
Tao, P., Sun, J., Wu, Z., Wang, S., Wang, J., Li, W., Pan, H., Bai, R., Zhang, J., Wang, Y.*, et al.* (2020). A dominant autoinflammatory disease caused by non-cleavable variants of RIPK1. Nature *577*, 109-114.
Ting, A.T., and Bertrand, M.J.M. (2016). More to Life than NF-kappaB in TNFR1 Signaling. Trends Immunol *37*, 535-545.
Tokunaga, F., and Iwai, K. (2009). [Involvement of LUBAC-mediated linear polyubiquitination of NEMO in NF-kappaB activation]. Tanpakushitsu Kakusan Koso *54*, 635-642.
Tracey, K.J., Beutler, B., Lowry, S.F., Merryweather, J., Wolpe, S., Milsark, I.W., Hariri, R.J., Fahey, T.J., 3rd, Zentella, A., Albert, J.D.*, et al.* (1986). Shock and tissue injury induced by recombinant human cachectin. Science *234*, 470-474.

Uchiyama, Y., Kim, C.A., Pastorino, A.C., Ceroni, J., Lima, P.P., de Barros Dorna, M., Honjo, R.S., Bertola, D., Hamanaka, K., Fujita, A.*, et al.* (2019). Primary immunodeficiency with chronic enteropathy and developmental delay in a boy arising from a novel homozygous RIPK1 variant. J Hum Genet *64*, 955-960.
Van Hauwermeiren, F., Armaka, M., Karagianni, N., Kranidioti, K., Vandenbroucke, R.E., Loges, S., Van Roy, M., Staelens, J., Puimege, L., Palagani, A.*, et al.* (2013). Safe TNF-based antitumor therapy following p55TNFR reduction in intestinal epithelium. J Clin Invest *123*, 2590-2603.
Varfolomeev, E., Blankenship, J.W., Wayson, S.M., Fedorova, A.V., Kayagaki, N., Garg, P., Zobel, K., Dynek, J.N., Elliott, L.O., Wallweber, H.J.*, et al.* (2007). IAP antagonists induce autoubiquitination of c-IAPs, NF-kappaB activation, and TNFalpha-dependent apoptosis. Cell *131*, 669-681.
Varfolomeev, E., Goncharov, T., Fedorova, A.V., Dynek, J.N., Zobel, K., Deshayes, K., Fairbrother, W.J., and Vucic, D. (2008). c-IAP1 and c-IAP2 are critical mediators of tumor necrosis factor alpha (TNFalpha)-induced NF-kappaB activation. J Biol Chem *283*, 24295-24299.
Varfolomeev, E., and Vucic, D. (2018). Intracellular regulation of TNF activity in health and disease. Cytokine *101*, 26-32.
Varfolomeev, E.E., Schuchmann, M., Luria, V., Chiannilkulchai, N., Beckmann, J.S., Mett, I.L., Rebrikov, D., Brodianski, V.M., Kemper, O.C., Kollet, O.*, et al.* (1998). Targeted disruption of the mouse Caspase 8 gene ablates cell death induction by the TNF receptors, Fas/Apo1, and DR3 and is lethal prenatally. Immunity *9*, 267-276.
Vereecke, L., Beyaert, R., and van Loo, G. (2011). Genetic relationships between A20/TNFAIP3, chronic inflammation and autoimmune disease. Biochem Soc Trans *39*, 1086-1091.
Vince, J.E., Pantaki, D., Feltham, R., Mace, P.D., Cordier, S.M., Schmukle, A.C., Davidson, A.J., Callus, B.A., Wong, W.W., Gentle, I.E.*, et al.* (2009). TRAF2 must bind to cellular inhibitors of apoptosis for tumor necrosis factor (tnf) to efficiently activate nf-{kappa}b and to prevent tnf-induced apoptosis. J Biol Chem *284*, 35906-35915.
Vlantis, K., Wullaert, A., Polykratis, A., Kondylis, V., Dannappel, M., Schwarzer, R., Welz, P., Corona, T., Walczak, H., Weih, F.*, et al.* (2016). NEMO Prevents RIP Kinase 1-Mediated Epithelial Cell Death and Chronic Intestinal Inflammation by NF-kappaB-Dependent and -Independent Functions. Immunity *44*, 553-567.
Wallach, D., Kang, T.B., and Kovalenko, A. (2014). Concepts of tissue injury and cell death in inflammation: a historical perspective. Nat Rev Immunol *14*, 51-59.
Wang, C., Deng, L., Hong, M., Akkaraju, G.R., Inoue, J., and Chen, Z.J. (2001). TAK1 is a ubiquitin-dependent kinase of MKK and IKK. Nature *412*, 346-351.
Wang, L., Du, F., and Wang, X. (2008). TNF-alpha induces two distinct caspase-8 activation pathways. Cell *133*, 693-703.
Wang, W., Marinis, J.M., Beal, A.M., Savadkar, S., Wu, Y., Khan, M., Taunk, P.S., Wu, N., Su, W., Wu, J.*, et al.* (2018). RIP1 Kinase Drives Macrophage-Mediated Adaptive Immune Tolerance in Pancreatic Cancer. Cancer Cell *34*, 757-774 e757.
Weber, A., Kirejczyk, Z., Besch, R., Potthoff, S., Leverkus, M., and Hacker, G. (2010). Proapoptotic signalling through Toll-like receptor-3 involves TRIF-dependent activation of caspase-8 and is under the control of inhibitor of apoptosis proteins in melanoma cells. Cell Death Differ *17*, 942-951.
Weinlich, R., and Green, D.R. (2014). The two faces of receptor interacting protein kinase-1. Mol Cell *56*, 469-480.
Weisel, K., Scott, N.E., Tompson, D.J., Votta, B.J., Madhavan, S., Povey, K., Wolstenholme, A., Simeoni, M., Rudo, T., Richards-Peterson, L.*, et al.* (2017). Randomized clinical study of safety, pharmacokinetics, and pharmacodynamics of RIPK1 inhibitor GSK2982772 in healthy volunteers. Pharmacol Res Perspect *5*.
Weng, D., Marty-Roix, R., Ganesan, S., Proulx, M.K., Vladimer, G.I., Kaiser, W.J., Mocarski, E.S., Pouliot, K., Chan, F.K., Kelliher, M.A.*, et al.* (2014). Caspase-8 and RIP kinases regulate bacteria-induced innate immune responses and cell death. Proc Natl Acad Sci U S A *111*, 7391-7396.

Wertz, I.E., O'Rourke, K.M., Zhou, H., Eby, M., Aravind, L., Seshagiri, S., Wu, P., Wiesmann, C., Baker, R., Boone, D.L.*, et al.* (2004). De-ubiquitination and ubiquitin ligase domains of A20 downregulate NF-kappaB signalling. Nature *430*, 694-699.
West, A.P., Koblansky, A.A., and Ghosh, S. (2006). Recognition and signaling by toll-like receptors. Annu Rev Cell Dev Biol *22*, 409-437.
Wong, W.W., Gentle, I.E., Nachbur, U., Anderton, H., Vaux, D.L., and Silke, J. (2010). RIPK1 is not essential for TNFR1-induced activation of NF-kappaB. Cell Death Differ *17*, 482-487.
Wu, W., Wang, X., Berleth, N., Deitersen, J., Wallot-Hieke, N., Bohler, P., Schlutermann, D., Stuhldreier, F., Cox, J., Schmitz, K.*, et al.* (2020). The Autophagy-Initiating Kinase ULK1 Controls RIPK1-Mediated Cell Death. Cell Rep *31*, 107547.
Wu, X.N., Yang, Z.H., Wang, X.K., Zhang, Y., Wan, H., Song, Y., Chen, X., Shao, J., and Han, J. (2014). Distinct roles of RIP1-RIP3 hetero- and RIP3-RIP3 homo-interaction in mediating necroptosis. Cell Death Differ *21*, 1709-1720.
Xie, T., Peng, W., Liu, Y., Yan, C., Maki, J., Degterev, A., Yuan, J., and Shi, Y. (2013). Structural basis of RIP1 inhibition by necrostatins. Structure *21*, 493-499.
Xu, D., Jin, T., Zhu, H., Chen, H., Ofengeim, D., Zou, C., Mifflin, L., Pan, L., Amin, P., Li, W.*, et al.* (2018). TBK1 Suppresses RIPK1-Driven Apoptosis and Inflammation during Development and in Aging. Cell *174*, 1477-1491 e1419.
Yatim, N., Cullen, S., and Albert, M.L. (2017). Dying cells actively regulate adaptive immune responses. Nat Rev Immunol *17*, 262-275.
Yeh, W.C., de la Pompa, J.L., McCurrach, M.E., Shu, H.B., Elia, A.J., Shahinian, A., Ng, M., Wakeham, A., Khoo, W., Mitchell, K.*, et al.* (1998). FADD: essential for embryo development and signaling from some, but not all, inducers of apoptosis. Science *279*, 1954-1958.
Yeh, W.C., Itie, A., Elia, A.J., Ng, M., Shu, H.B., Wakeham, A., Mirtsos, C., Suzuki, N., Bonnard, M., Goeddel, D.V.*, et al.* (2000). Requirement for Casper (c-FLIP) in regulation of death receptor-induced apoptosis and embryonic development. Immunity *12*, 633-642.
Yuan, J., Amin, P., and Ofengeim, D. (2019). Necroptosis and RIPK1-mediated neuroinflammation in CNS diseases. Nat Rev Neurosci *20*, 19-33.
Zhang, Q., Lenardo, M.J., and Baltimore, D. (2017a). 30 Years of NF-kappaB: A Blossoming of Relevance to Human Pathobiology. Cell *168*, 37-57.
Zhang, X., Dowling, J.P., and Zhang, J. (2019a). RIPK1 can mediate apoptosis in addition to necroptosis during embryonic development. Cell Death Dis *10*, 245.
Zhang, X., Yin, M., and Zhang, L.J. (2019b). Keratin 6, 16 and 17-Critical Barrier Alarmin Molecules in Skin Wounds and Psoriasis. Cells *8*.
Zhang, X., Zhang, H., Xu, C., Li, X., Li, M., Wu, X., Pu, W., Zhou, B., Wang, H., Li, D.*, et al.* (2019c). Ubiquitination of RIPK1 suppresses programmed cell death by regulating RIPK1 kinase activation during embryogenesis. Nat Commun *10*, 4158.
Zhang, Y., Su, S.S., Zhao, S., Yang, Z., Zhong, C.Q., Chen, X., Cai, Q., Yang, Z.H., Huang, D., Wu, R.*, et al.* (2017b). RIP1 autophosphorylation is promoted by mitochondrial ROS and is essential for RIP3 recruitment into necrosome. Nat Commun *8*, 14329.
Zhao, Q., Yu, X., Zhang, H., Liu, Y., Zhang, X., Wu, X., Xie, Q., Li, M., Ying, H., and Zhang, H. (2017). RIPK3 Mediates Necroptosis during Embryonic Development and Postnatal Inflammation in Fadd-Deficient Mice. Cell Rep *19*, 798-808.

6. Acknowledgement

First of all, I would like to thank Prof. Dr. Manolis Pasparakis for providing me with the opportunity to work on this important and exciting project. I am grateful for his constant scientific guidance and encouragement and always believing in my work. I consider myself very lucky for having had a supervisor who has constantly shown great interest in my project and was always available for questions and discussions. He has throughout this time not only been a scientific advisor, but also a mentor to me.

Second, I would like to express my gratitude to all collaborators in this project: Dr. Masahiro Nagata for his reliable and precise working style and crucial help with revision experiments, Hannah Schünke for her experimental as well as mental support, Tom Delanghe and Prof. Dr. Mathieu Bertrand for their outstanding willingness to help with experiments and scientific questions, Janica L. Wiederstein and Prof. Dr. Marcus Krüger for their perseverance in challenging mass-spec experiments, Dr. Robin Schwarzer for his gut and Dr. Snehlata Kumari for her skin expertise, Dr. Teresa Corona for generation of *Ripk1*$^{S166/S166A}$ mice and Dr. Vangelis Kondylis for contribution of important in-vivo data.

Furthermore, I would like to thank Jennifer Kuth, Claudia Uthoff-Hachenberg, Elza Gareus, Edeltraud Stade and Julia von Rhein for excellent technical assistance, Lisa Hohorst for great experimental support and Huipeng Jiao for proofreading this thesis. Additionally, my thank goes to all former and present lab members of the Pasparakis lab for inspiring scientific discussions, a great working atmosphere as well as non-scientific exchange and friendships.

Last but not least I would like to express my deep gratitude to my family and my friends for their endless support. This work would have not been possible without them.

7. Erklärung zur Dissertation

„Hiermit versichere ich an Eides statt, dass ich die vorliegende Dissertation selbstständig und ohne die Benutzung anderer als der angegebenen Hilfsmittel und Literatur angefertigt habe. Alle Stellen, die wörtlich oder sinngemäß aus veröffentlichten und nicht veröffentlichten Werken dem Wortlaut oder dem Sinn nach entnommen wurden, sind als solche kenntlich gemacht. Ich versichere an Eides statt, dass diese Dissertation noch keiner anderen Fakultät oder Universität zur Prüfung vorgelegen hat; dass sie - abgesehen von unten angegebenen Teilpublikationen und eingebundenen Artikeln und Manuskripten - noch nicht veröffentlicht worden ist sowie, dass ich eine Veröffentlichung der Dissertation vor Abschluss der Promotion nicht ohne Genehmigung des Promotionsausschusses vornehmen werde. Die Bestimmungen dieser Ordnung sind mir bekannt. Darüber hinaus erkläre ich hiermit, dass ich die Ordnung zur Sicherung guter wissenschaftlicher Praxis und zum Umgang mit wissenschaftlichem Fehlverhalten der Universität zu Köln gelesen und sie bei der Durchführung der Dissertation zugrundeliegenden Arbeiten und der schriftlich verfassten Dissertation beachtet habe und verpflichte mich hiermit, die dort genannten Vorgaben bei allen wissenschaftlichen Tätigkeiten zu beachten und umzusetzen. Ich versichere, dass die eingereichte elektronische Fassung der eingereichten Druckfassung vollständig entspricht."

Teilpublikation:

Laurien, L., Nagata, M., Schunke, H., Delanghe, T., Wiederstein, J.L., Kumari, S., Schwarzer, R., Corona, T., Kruger, M., Bertrand, M.J.M.*, et al.* (2020). Autophosphorylation at serine 166 regulates RIP kinase 1-mediated cell death and inflammation. Nat Commun *11*, 1747.

25.03.21, L. Laurien

Datum, Name und Unterschrift

nature COMMUNICATIONS

ARTICLE

https://doi.org/10.1038/s41467-020-15466-8 OPEN

Autophosphorylation at serine 166 regulates RIP kinase 1-mediated cell death and inflammation

Lucie Laurien[1], Masahiro Nagata[1], Hannah Schünke[1], Tom Delanghe[2,3], Janica L. Wiederstein[1], Snehlata Kumari[1], Robin Schwarzer[1], Teresa Corona[1], Marcus Krüger[1], Mathieu J.M. Bertrand[2,3], Vangelis Kondylis[1] & Manolis Pasparakis[1,4]✉

Receptor interacting protein kinase 1 (RIPK1) regulates cell death and inflammatory responses downstream of TNFR1 and other receptors, and has been implicated in the pathogenesis of inflammatory and degenerative diseases. RIPK1 kinase activity induces apoptosis and necroptosis, however the mechanisms and phosphorylation events regulating RIPK1-dependent cell death signaling remain poorly understood. Here we show that RIPK1 autophosphorylation at serine 166 plays a critical role for the activation of RIPK1 kinase-dependent apoptosis and necroptosis. Moreover, we show that S166 phosphorylation is required for RIPK1 kinase-dependent pathogenesis of inflammatory pathologies in vivo in four relevant mouse models. Mechanistically, we provide evidence that trans autophosphorylation at S166 modulates RIPK1 kinase activation but is not by itself sufficient to induce cell death. These results show that S166 autophosphorylation licenses RIPK1 kinase activity to induce downstream cell death signaling and inflammation, suggesting that S166 phosphorylation can serve as a reliable biomarker for RIPK1 kinase-dependent pathologies.

[1] Institute for Genetics, Cologne Excellence Cluster on Cellular Stress Responses in Aging-Associated Diseases (CECAD), University of Cologne, Cologne, Germany. [2] VIB Center for Inflammation Research, Technologiepark-Zwinjaarde 71, 9052 Zwinjaarde-Ghent, Belgium. [3] Department of Biomedical Molecular Biology, Ghent University, Technologiepark-Zwinjaarde 71, 9052 Zwinaarde-Ghent, Belgium. [4] Center for Molecular Medicine Cologne, University of Cologne, Cologne, Germany. ✉email: pasparakis@uni-koeln.de